Engineering Osteoclasts to Prevent Diseases Caused by Osteoclast Deficiency

Worakanya Buranaphatthana

A dissertation

submitted in partial fulfillment of the

requirements for the degree of

Doctor of Philosophy

University of Washington

2017

Reading Committee:

Cecilia M. Giachelli, Chair

Marta Scatena

Tracy Popowics

Hai Zhang

Program Authorized to Offer Degree:

Oral Biology

University of Washington

Abstract

Engineering Osteoclasts to Prevent Diseases Caused by Osteoclast Deficiency

Worakanya Buranaphatthana

Chair of the Supervisory Committee:
Professor Cecilia M. Giachelli
Bioengineering

Osteoclasts are bone-resorbing cells that bind to mineralized surfaces and resorb calcification via formation of resorption lacunae. However, their ability to prevent calcification via elaboration of anticalcific factors has not been investigated. To test this, RAW264.7 murine monocytic cells were engineered with an inducible receptor activator of nuclear factor kappa-B (iRANK) construct to induce differentiation into osteoclasts under the control of a chemical inducer of dimerization (CID). iRANK cells treated with CID formed TRAP-positive multi-nucleated osteoclasts that were capable of mineral resorption. We demonstrated that iRANK osteoclasts could inhibit mineralization of C2C12 myoprogenitor cells and bovine aortic valve interstitial cells in a co-culture system. Analyses of candidate anticalcific proteins identified osteopontin (OPN) in the culture media of CID-treated iRANK cells at significantly higher levels compared to untreated cells. Immunodepletion of OPN from the media conditioned by CID-

treated iRANK cells significantly reduced its ability to inhibit C2C12 calcification, as well as progressive mineralization of human heterotopic ossification samples *in vitro*. These data suggest that engineered osteoclasts may be useful for preventing ectopic calcification through elaboration of potent anticalcific factors. Both anticalcific and bone resorptive functions of osteoclasts could thus prove useful as therapeutic tools for the treatment of heterotopic ossification and other ectopic calcification disorders.

One such disorder, medication-related osteonecrosis of the jaw or MRONJ, stems from a serious side effect of treatment with antiresorptive medications (such as denosumab) used in patients with cancer and metastatic bone disease. It often occurs after dental-related interventions such as tooth extraction, and is thought to occur due to inhibition of osteoclastic bone resorption. In this study, we showed that iRANK cells are resistant to inhibition by anti-mouse RANKL antibody, a mouse analog of denosumab. Thus, we proposed to utilize the engineered cells to elucidate the role of osteoclasts in MRONJ development and subsequently use these cells to prevent this disease. In this study, we developed a mouse model of MRONJ in nude mice and validated cell delivery method and osteoclast induction *in vivo*. These techniques will be used in future studies to test the hypothesis that MRONJ occurs as a result of impaired osteoclasts due to the inhibition by antiresorptive drugs such as denosumab. Thus, delivering engineered osteoclasts, resistant to this inhibition, may prevent the development of MRONJ after dental-related trauma.

TABLE OF CONTENTS

LIST OF FIGURES

LIST OF ABBREVIATIONS

α-MEM	minimum essential medium eagle - alpha modification
ALP	alkaline phosphatase
BMP	bone morphogenetic protein
BPs	bisphosphonates
BVIC	bovine aortic valve interstitial cell
CAII	carbonic anhydrase II
CAM	cell adhesion molecule
CAVD	calcific aortic valve disease
CID	chemical inducer of dimerization
CKD	chronic kidney disease
DMEM	dulbecco's modified eagle's medium
DNA	deoxyribonucleic acid
EC	ectopic calcification
EDTA	ethylenediaminetetraacetic acid
ELISA	enzyme-linked immunosorbent assay
EtOH	ethanol
EVs	extracellular vesicles
FACS	fluorescence-activated cell sorting
FBS	fetal bovine serum
FOP	fibrodysplasia ossificans progressiva
GFP	green fluorescent protein

HCl	hydrochloric acid
H&E	hematoxylin and eosin
HO	heterotopic ossification
HSMC	human aortic smooth muscle cell
iRANK	inducible receptor activator of nuclear factor kappa-B
M-CSF	macrophage-colony stimulating factor
MGP	matrix Gla protein
miRNA	microRNA
MMP	matrix metalloproteinase
mRNA	messenger RNA
MRONJ	medication-related osteonecrosis of the jaw
microCT	microcomputed tomography
MuNC	multinucleated cell
NaCl	sodium chloride
NaOH	sodium hydroxide
NDS	normal donkey serum
NF-κB	nuclear factor kappa-light-chain-enhancer of activated B cells
NSAIDs	non-steroidal anti-inflammatory drugs
OCN	osteocalcin
ONJ	osteonecrosis of the jaw
OPN	osteopontin
OPG	osteoprotegerin
Pi	inorganic phosphate

pNPP	p-nitrophenyl phosphatase
POH	progressive ossific heteroplasia
P/S	penicillin/streptomycin
PTH	parathyroid hormone
PBS	phosphate buffered saline
RANK	receptor activator of nuclear factor kappa-B
RANKL	receptor activator of nuclear factor kappa-B ligand
RNA	ribonucleic acid
SREs	skeletal-related events
TRAP	tartrate resistant acid phosphatase
TBS	TRIS-buffered saline
VC	vascular calcification
VSMC	vascular smooth muscle cell
ZOL	zoledronic acid

ACKNOWLEDGEMENTS

First and foremost, I would like to express my deepest gratitude to the Anandamahidol foundation for providing me a great opportunity to pursue my PhD studies in the United States and for providing me both financial and individual support throughout my doctoral study. I am very honored and humbled to receive the scholarship. This dissertation is dedicated to His Majesty King Bhumibol Adulyadej of Thailand, who founded the foundation, and Her Royal Highness Princess Maha Chakri Sirindhorn, the president of the Anandamahidol foundation. I am forever grateful and perpetually under an obligation to both His Majesty and Her Royal Highness's philanthropy.

This degree would not have been possible without significant guidance, encouragement and support from many individuals including my family and friends who have accompanied me on this journey, and the mentors I have privilege to work with in the past 5 years.

I would like to thank my advisor, Dr. Cecilia Giachelli, for her enormous support, guidance, encouragement and suggestion for my work from the very beginning of my doctoral study. She provides me the entitlement to pursue my own research interests. I am a better research scientist today than I was 5 years ago because of her. I would like to also thank my supervisory committee members, Dr. Marta Scatena, Dr. Tracy Popowics and Dr. Hai Zhang, for their valuable time, suggestion and support. They are never hesitant to reach out and help me when I need their help. They always support and encourage me both physically and emotionally to never give up. I am privileged to study in a superb environment with many marvelous people.

Without questions, I am very grateful to have had an opportunity to work with wonderful people in the Giachelli lab. I would like to thank Dr. Mei Speer for her immeasurable help in

planning and troubleshooting my experiments. Many thanks are owed to Liz Soberg, who has shared her experience and expertise with me and helped me with animal experiments. Without her help, I would not be able to finish all the animal work mentioned in this thesis. Additionally, Mandy Lund and Cameron Rementer collaborated endlessly with me to advance our research project. I am also very fortunate to have met work friends who also become my real, rest-of-life friends, Jia Jun Chia, Jenna Kita and Ted Chen. I am grateful for our friendship and time we spent together outside the lab. I also would like to thank Meiting Wu, Ninghua Kong, Melissa Jackson, Shunsuke Yamada, Nick Chavkin, and Mary Wallingford for providing a wealth of scientific knowledge and technical expertise and for all the help they have provided me during the past 5 years.

Many thanks to my classmates in the Oral Biology program, especially Kajohnkiart Janebodin, Tom Kantrong, Anusha Reddy Etikala, Wenjie Li, Sara Parent, Sanaz Sadaat, Atriya Salamati, Ana Chang and Jonathan An, and friends whom I met in Seattle for their emotional support and arrangement of enjoyable extracurricular activities. They have been a steady source of encouragement, empathy, and escape. Importantly, they become my family here in Seattle and have made my journey all worthwhile.

On top of that, I am in debt to the faculties and staffs in the department of Oral Biology and Diagnostic Sciences, Faculty of Dentistry, Chiang Mai University, especially Dr. Suttichai Krisanaprakornkit who taught me the vast knowledge and techniques before entering graduate school. This made my life much easier to get going with my doctoral study.

Last but not least, I would like to acknowledge my family who have been my biggest support throughout my life. I would not be where I am today without their support, understanding and unconditional love.

DEDICATION

To His Majesty King Bhumibol Adulyadej of Thailand

To the Kingdom of Thailand

To my beloved parents, brother and sister

CHAPTER 1.
INTRODUCTION

Bone homeostasis is maintained by bone forming cells ("osteoblasts") and bone resorbing cells ("osteoclasts"). An imbalance between these two cell types can negatively impact overall bone mass. Increased numbers and/or excessive activity of osteoclasts will result in bone loss. On the other hand, reduction or lack of osteoclasts will result in the presence of too much bone, as observed in ectopic calcification (EC).[1,2] Moreover, some antiresorptive medications can affect osteoclast formation and function, thus resulting in the development of disorders such as medication-related osteonecrosis of the jaw (MRONJ).[3]

Osteoclasts are multinucleated bone resorbing cells that differentiate from hematopoietic cells of the monocyte lineage under the influence of the cytokines, macrophage colony stimulating factor (M-CSF) and receptor activator of nuclear factor kappa-B ligand (RANKL).[4] Osteoprotegerin (OPG) is a potent inhibitor of osteoclast survival and differentiation and acts as a decoy receptor for RANKL, thus preventing interaction with its membrane receptor, RANK.[5]

The best known function of osteoclasts is their ability to bind to bone surfaces and resorb mineralized matrices via the formation of resorption lacunae and secretion of an acid- and protease-rich milieu in a protected environment.[4] However, little is known about their ability to prevent calcification. In previous studies, we developed a novel bioengineered system to conditionally regulate osteoclast differentiation from monocytic precursors to facilitate mechanistic and translational studies of this unique cell type. RAW264.7 murine monocytic cells were engineered with an inducible receptor activator of nuclear factor kappa-B (iRANK) construct to induce differentiation into osteoclasts under the control of a chemical inducer of dimerization (CID).[6] This differentiation was independent of

RANKL and M-CSF, and resistant to OPG.[6] Moreover, CID-induced osteoclasts could functionally resorb mineral from two dimensional mineralized discs and three dimensional mineralized microporous fibrin scaffolds *in vitro.*[6]

In this study, we hypothesized that engineered osteoclasts may be therapeutically useful not only to physically resorb pre-existing mineral, but also to release factors that may prevent mineralization. To test this, we investigated whether engineered osteoclasts could inhibit ectopic mineralization using *in vitro* model systems of EC. Then, we further identified potential mechanisms of EC prevention by engineered osteoclasts.

We previously showed that engineered osteoclasts are resistant to inhibition by OPG which is a natural analogue of denosumab, a drug that induces MRONJ.[7] Therefore, we hypothesized that MRONJ occurs as a result of impaired osteoclast differentiation and function due to the inhibition by antiresorptive drugs such as denosumab. Thus, delivering engineered osteoclasts resistant to this inhibition may prevent the development of MRONJ after dental-related trauma.

1.1 BACKGROUND

1.1.1 *Osteoclasts and osteoclast-related diseases*

Osteoclasts are multinucleated bone resorbing cells that comprise 1-2% of bone cells.[8] They differentiate from hematopoietic precursor cells under the influence of cytokines secreted by osteoblasts and/or osteocytes –M-CSF and RANKL (**Figure 1.1**).[4,9] M-CSF, synthesized by bone marrow stromal cells, binds to its receptor c-Fms to activate distinct signaling pathways to stimulate the proliferation and survival of osteoclast precursors and the mature cell.[10] RANKL, however, is the primary osteoclast differentiation factor, and promotes osteoclast differentiation mainly through controlling gene expression by activating its receptor, RANK.[8,10] RANKL acts via several downstream signaling

molecules, including c-fos, NF-κB, NFATc1, MAPK and TRAF6.[8,10–12] RANKL also induces expression of the $\alpha_v\beta_3$ integrin in osteoclast precursor cells, which signals via c-src to induce the activation of small GTPases that are critical for formation of the actin ring sealing zone and osteoclast migration and survival. In addition to RANKL, osteoblasts and bone marrow stromal cells also express OPG,[8] a secreted decoy receptor for RANKL which functions as the physiological inhibitor of RANK–RANKL signaling (**Figure 1.1**).[5] Thus, the ratio of RANKL to OPG expressed by osteoblasts determines osteoclast differentiation and activity. This ratio is determined by systemic hormones and local cytokines that regulate bone remodeling, which include estrogen, parathyroid hormone (PTH), glucocorticoids, thyroid hormone, TNF-α, IL-1 and prostaglandin E_2.[13]

The main function of osteoclasts is to bind to mineralized surfaces and resorb calcification via formation of resorption lacunae and secretion of an acid- and protease-rich milieu in a protected environment (**Figure 1.2**).[4] Attachment of osteoclasts to bone is mediated by $\alpha_v\beta_3$ integrins expressed on the surface of filamentous actin-containing podosomes.[14] $\alpha_v\beta_3$ integrins interact with bone matrix proteins that include osteopontin (OPN) and vitronectin.[8] These interactions lead to development of an actin ring and sealing zone with polarization of the osteoclast into functionally distinct ruffled border and basolateral membrane regions.[15] Carbonic anhydrase II (CAII) generates protons (H^+) and bicarbonate (HCO_3^-) within the osteoclast cytoplasm and the HCO_3^- is exchanged for extracellular chloride at the basolateral membrane by a specific Cl^-/HCO_3^-channel.[14] Protons are transported across the ruffled border into resorption lacunae by an osteoclast-specific H^+-ATPase pump, while chloride ions are transported simultaneously to balance the ionic charge through the CLCN7 chloride channel.[8,12,14] Within the resorption lacuna, the resultant acidic environment facilitates dissolution of bone mineral to release Ca^{2+}, HPO_4^{2-} and H_2O, while organic matrix is degraded by cathepsin K, a secreted cysteine protease, and degradation products are transported across the cytoplasm in tartrate

resistant acid phosphatase (TRAP)-containing vesicles and exocytosed at the basolateral membrane.[8,14,15]

Balance within the osteoblast-osteoclast relationship is essential for the maintenance of skeletal integrity, where bone resorption is equaled by bone formation.[1] Any alteration in formation or function within either cell type has the potential to offset this equilibrium and negatively impact overall bone mass. With regard to osteoclasts, it is unsurprising that elevated numbers and/or excessive activity will result in bone loss, as seen in osteoporosis and Paget's disease.[1,2] On the other hand, reduction or lack of osteoclasts will result in the presence of too much bone, as observed in osteopetrosis, pycnodysostosis as well as ectopic bone formation.[1,2] Moreover, some antiresorptive medications, including bisphosphonates (BPs) and denosumab, can affect osteoclast formation and function, thus resulting in the development of disorders such as medication-related osteonecrosis of the jaw (MRONJ).[3]

1.1.2 *Ectopic calcification (EC)*

EC is defined as an abnormal deposition of mineral in soft tissues as a result of genetic mutation, trauma, disease, aging or metabolic imbalance.[16,17] It is typically composed of calcium phosphate mineral, most often hydroxyapatite, but can also consist of calcium oxalates and octacalcium phosphate as seen in kidney stones.[16,18] Although most soft tissues can undergo calcification, kidney, blood vessels, heart valves, and tendons, are particularly susceptible to developing this pathology.[16,17] As a result, EC often occurs in certain parts of the body including heart valves as in calcific aortic valve disease (CAVD), blood vessels as in vascular calcification (VC), joints, tendons and amputation sites as in heterotopic ossification (HO).[16,19] EC can lead to clinical symptoms and is particular destructive to mechanical functions of organs where it occurs.[16,19]

1.1.2.1 Calcific aortic valve disease (CAVD)

CAVD is the most prevalent form of valvular heart disease, affecting 2% of adults over 65 years of age.[20–22] CAVD affected 2.5 million people in 2000 and this number is expected to increase to 4.5 million in 2030.[21] CAVD is characterized by a range of disease from aortic valve leaflet thickening (aortic valve sclerosis) to severe mineralization of valve leaflets with impaired leaflet motion (aortic valve stenosis)[20], as shown in **Figure 1.3**[23]. If not treated, aortic valve stenosis can lead to heart failure and death. The identified cardiovascular risk factors involved in the development of aortic valve disease from sclerosis to stenosis include metabolic syndrome, obesity, hypertension, smoking, renal failure, hyperlipidemia, male gender, oxidative stress and older age (**Figure 1.3**).[23] Calcification seen in CAVD, accumulated in the setting of fibro-inflammatory lesions and cell death, are largely driven by osteochondrogenic cells, apoptosis, and extracellular matrix mineralization process.[24–26] While mineral deposition is triggered, there is also mounting evidence that mineral resorption is deficient in CAVD, since few osteoclasts have been observed in these lesions.[27–29] Additionally, many studies suggest that inflammation in CAVD patients favors inhibition of osteoclasts, since OPG, a potent osteoclast inhibitor, is upregulated early in the disease progression.[30] The major treatment for CAVD is surgical aortic valve replacement with a mechanical or bioprosthetic valve.[21] However, this treatment is associated with considerable morbidity and mortality, as well as a significant reoperation rate.[21] Moreover, the major cause of failure of valve replacement is also calcification.[31]

1.1.2.2 Vascular calcification (VC)

VC is the pathological deposition of calcium/phosphate crystals in the vascular system.[32] It is a common complication seen in patients with atherosclerosis, diabetes, certain heredity conditions, and kidney disease, especially chronic kidney disease (CKD).[33] VC is an active process initiated and regulated by a variety of molecular signaling pathways.[34] There are mainly two types of vascular

calcification – intimal and medial calcification – differentiated according to the arterial layer that is affected by mineral deposition (**Figure 1.4**).[35,36] Intimal calcification is associated with macrophages, lipids, and vascular smooth muscle cells (VSMC) as seen in classical atherosclerosis.[37] In atherosclerosis, the intima becomes profoundly inflamed, thickened and eventually calcified.[33] Calcification of coronary arteries is an excellent predictor of atherosclerotic plaque burden and may contribute to atherosclerotic plaque rupture.[33] However, the connection between atherosclerotic plaque calcification and plaque rupture is heavily argued.[38] Medial calcification is characterized by the deposition of hydroxyapatite along the elastic lamina and extracellular matrix, as a result of elastin fiber mineralization, VSMC degeneration, and upregulation of osteogenic programs as seen in CKD or diabetes.[32,33,37] The result of medial calcification is a stiffening of the artery wall, with the associated rise in blood pressure, and a higher risk of cardiovascular mortality.[33] The current major mechanisms of vascular calcification include (1) failed anticalcific processes (2) induction of osteochondrogenesis (3) cell death (4) abnormal calcium/phosphate homeostasis (5) circulating calciprotein particles and (6) matrix degradation/modification.[33]

1.1.2.3 Heterotopic ossification (HO)

HO is a type of ectopic calcification in which calcified bone is formed outside of the skeleton (**Figure 1.5**). HO can be either acquired or hereditary, as in fibrodysplasia ossificans progressiva (FOP) and progressive ossific heteroplasia (POH).[39,40] Acquired HO is more common, whereas the hereditary condition is rare but life threatening. The development of acquired HO is predominantly associated with severe trauma, particularly to muscle or neuronal tissues, such as traumatic brain injury, spinal cord injury, joint arthroplasty, severe burns or combat blast wounds and amputations.[40] Due to the mechanical effects of hard tissue formation in non-skeletal sites, patients with HO experience a wide range of problems including pain, loss of joint mobility, skin ulceration, overlying skin graft failure,

muscle and neurovascular entrapment, and prosthetic limb fitting difficulties.[40] The mechanisms underlying the development of trauma-related HO are not well-understood. Inflammation appears to be a major contributor potentially by elevating cytokines that facilitate the recruitment of mesenchymal precursors locally and/or systemically that undergo chondrogenic and osteoblastic differentiation to form HO.[40–42] Traumatic injury may also lead to the upregulation of factors that inhibit mineral formation, such as OPG, or downregulation of factors that inhibit mineral formation, such as OPN, thereby shifting the balance towards bone forming pathway.

1.1.3 *Medication-related osteonecrosis of the jaw (MRONJ)*

MRONJ, which was first described in 2003, is clinically defined as an area of exposed and necrotic bone that has persisted more than eight weeks with no history of radiation therapy (**Figure 1.6**).[43,44] Initially the lesions are asymptomatic, but may become symptomatic when the surrounding tissues become inflamed. It is a potentially serious side effect of treatment with antiresorptive and antiangiogenic medications that often occurs in the oral cavity after dental-related interventions such as tooth extraction.[3,43] These antiresorptive medications, BPs and denosumab, are used to decrease the risk of skeletal-related events (SREs) in patients with cancer and metabolic bone disease, such as osteoporosis.[3] MRONJ incidence in patients with cancer receiving intravenous BPs is reported to range from 2% to 15%[45,46], whereas MRONJ development in osteoporotic patients still remains controversial. Two recent randomized clinical trials showed that the incidences of BP-related and denosumab-related ONJ were comparable in cancer patients, suggesting that ONJ induced by both drugs adversely affects patients' quality of life and produces significant morbidity.[45,46]

BPs are synthetic analogues of the naturally occurring pyrophosphate and have high affinity to hydroxyapatite, allowing them to bind to the bone surfaces and exert suppressive effects on osteoclast

functions.[47] BPs also reduce osteoclast activity by decreasing osteoclast progenitors and by promoting osteoclast apoptosis.[48] Zoledronic acid (ZOL), a third generation, nitrogen-containing BP, is one of the most potent available.[49] Denosumab is a fully human monoclonal antibody (IgG_2) with a high affinity and specificity for human RANKL.[50] Denosumab inhibits osteoclast formation, differentiation, survival and bone resorptive function by reducing RANKL binding to RANK in a manner similar to native osteoclast inhibitor, OPG.[7] In 2010, Denosumab was approved by the U.S. Food and Drug Administration for use in postmenopausal women with risk of osteoporosis under the trade name Prolia® and as Xgeva® for the prevention of SREs in patients with bone metastases from solid tumors.[51]

Despite the fact that the first case of MRONJ was described over a decade ago, the mechanism and pathophysiology of MRONJ still remain elusive. Proposed hypotheses that attempt to explain the unique localization of MRONJ exclusively to the jaw include altered bone remodeling or oversuppression of bone resorption, angiogenesis inhibition, constant microtrauma, suppression of innate or acquired immunity, vitamin D deficiency, soft tissue toxicity, and inflammation or infection.[3] Moreover, the management of MRONJ remains a significant clinical challenge, with little progress having been made on treatment.[52] Most patients with MRONJ are treated conservatively with rinses, antibiotics, oral analgesics or surgical debridement.[3,53] Thus, given the significant morbidity attributable to MRONJ and the challenges associated with its management, new therapies aimed at preventing MRONJ are greatly needed.

1.2 SIGNIFICANCE

Ectopic calcification (EC) is the abnormal biomineralization occurring in soft tissues including heart valves, blood vessels, joints, tendons and amputation sites.[16,17] EC can lead to clinical symptoms

and is particularly destructive to mechanical functions of organs where it occurs.[16,19] Current treatments for EC include surgical excision of the calcified soft tissue, radiation therapy, and treatment with drugs. However, these therapies cannot effectively treat EC. Usually, there is no treatment for mild calcification. Moreover, surgical approaches, such as bioprosthetic valve replacement in CAVD patients, have had limited efficacy.[31] Drugs used to treat vascular inflammatory conditions, such as statins, have been largely ineffective in clinical trials.[54] Additionally, radiation therapy is not effective once calcification is formed.[55] Thus, new therapies specifically aimed at preventing and/or regressing calcification are greatly needed. EC is believed to occur as a result of an imbalance between bone forming and bone resorbing pathways, in which there is an induction of osteochondrogenesis and reduction of factors that inhibit mineral formation. Furthermore, osteoclast deficiency is considered as one potential cause of EC.[2] Thus, we propose to utilize osteoclasts as a potential cell therapy to prevent and/or regress EC. Osteoclasts are bone-resorbing cells whose main function is to bind to mineralized surfaces and resorb mineral via formation of resorption lacunae. In addition, osteoclasts also secrete proteins, such as OPN, bone morphogenetic protein 3 (BMP-3) and sclerostin, that have anticalcific functions.[56–58] However, whether osteoclasts can prevent calcification through elaboration (defined as secretion or other mechanisms of release) of calcification inhibitors has not been investigated. *In this study, we hypothesize that osteoclasts may be therapeutically useful not only to physically resorb pre-existing mineral, but also to release factors, such as OPN, that may prevent mineralization.* This is the first report describing a role for osteoclasts in inhibiting mineralization through the elaboration of anticalcific factors.

Medication-related osteonecrosis of the jaw (MRONJ) is a potentially serious side effect of treatment with antiresorptive and antiangiogenic medications that often occurs in the oral cavity after dental-related interventions such as tooth extraction.[3,43] These antiresorptive medications, BPs and

denosumab, are used to decrease the risk of SREs in patients with cancer and metabolic bone disease, such as osteoporosis.[3] Even though the first case of MRONJ was described over 10 years ago, the mechanism and pathophysiology of MRONJ still remain elusive. One proposed mechanism is due to the lack of osteoclasts' bone resorptive function. Moreover, the management of MRONJ is mostly conservative with rinses, antibiotics, oral analgesics or surgical debridement.[3,53] Thus, given the significant morbidity attributable to MRONJ and the challenges associated with its management, new therapies aimed at preventing MRONJ are greatly needed. We previously engineered RAW264.7 murine monocytic cells with an inducible RANK (iRANK) construct to differentiate into osteoclasts under the control of a CID drug. This differentiation is independent of RANKL and M-CSF, and also resistant to OPG, a natural analogue of denosumab. In this thesis, we hypothesize that *the development of MRONJ is caused by the loss of osteoclasts' bone resorptive function due to antiresorptive drugs, and that delivering engineered osteoclasts resistant to inhibition by this drug may promote the bone healing process after tooth extraction*. This study provides a novel paradigm for the mechanism and pathophysiology of MRONJ. Moreover, this study is the first to provide proof of concept data that osteoclast cell therapy might be a unique strategy for solving this debilitating disease in patients. Finally, it provides a novel paradigm for the mechanism and pathophysiology of MRONJ which may serve as the basis for a NIH/NIDCR grant submission in the near future.

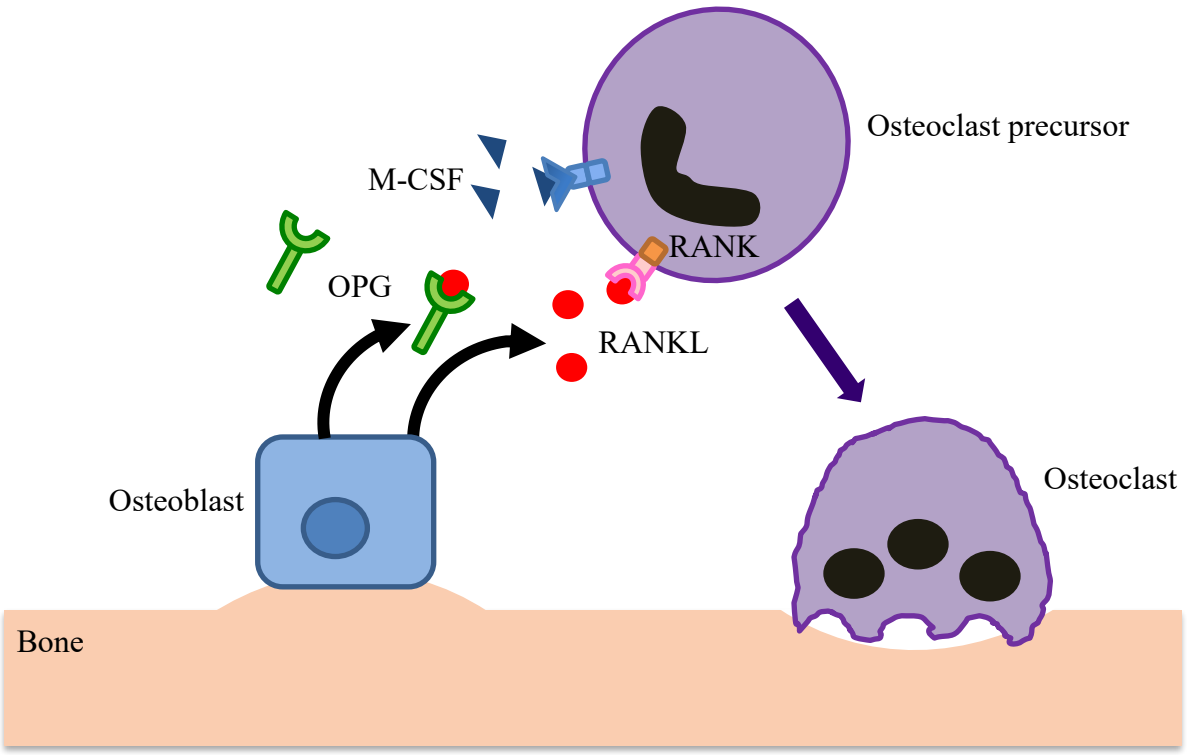

Figure 1.1. Factors that regulate osteoclast differentiation

Macrophage-colony stimulating factor (M-CSF) and receptor activator of nuclear factor kappa-B ligand (RANKL), synthesized by osteoclasts, induce osteoclast formation through M-CSF receptor and RANK expressed on osteoclast precursors. On the other hand, osteoprotegerin (OPG) counteracts this effect by competing for and neutralizing RANKL.

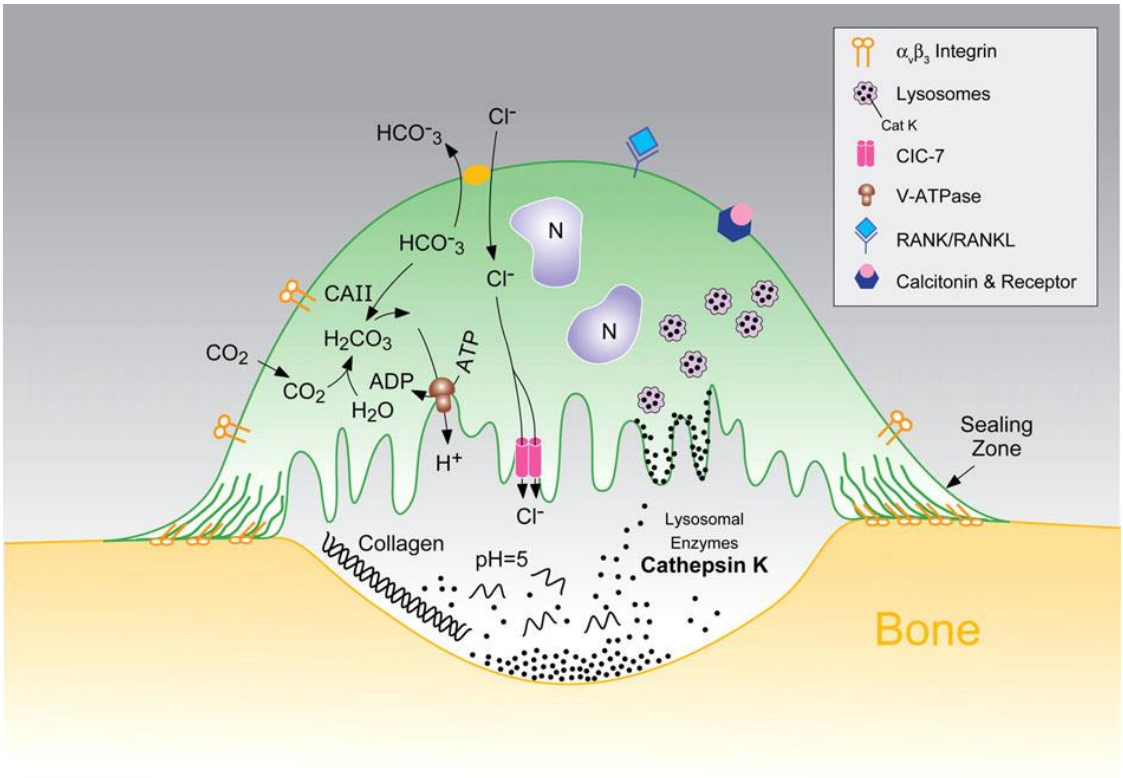

Figure 1.2. Mechanism of osteoclastic bone resorption [59]

Osteoclasts attach to bone via podosomes containing filamentous actin and αvβ3 integrin. Carbonic anhydrase II (CAII) generates H^+ and HCO^-_3 from CO_2 and H_2O. Protons (H^+) and chloride ions (Cl^-) are transported across the ruffled border into resorption lacunae by an osteoclast-specific H^+-ATPase pump and the CLCN7 chloride channel. The chloride–bicarbonate exchanger facilitates the balance of ionic charge across the basolateral cell membrane. The acidic environment facilitates dissolution of bone mineral to release Ca^{2+}, HPO_4^{3-} and H_2O. Organic matrix is degraded by cathepsin K and degradation products are transported across the cytoplasm in TRAP-containing vesicles and exocytosed at the basolateral membrane.

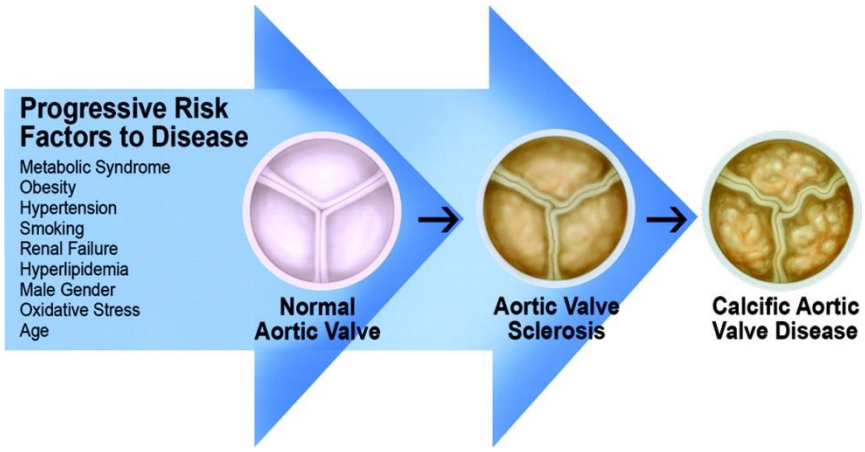

Figure 1.3. CAVD progression from aortic valve sclerosis to aortic valve stenosis [23]

The identified atherosclerotic cardiovascular risk factors involved in the development of aortic valve disease from aortic valve stenosis to severe mineralization in calcific aortic valve disease are metabolic syndrome, obesity, hypertension, smoking, renal failure, hyperlipidemia, gender, oxidative stress and age.

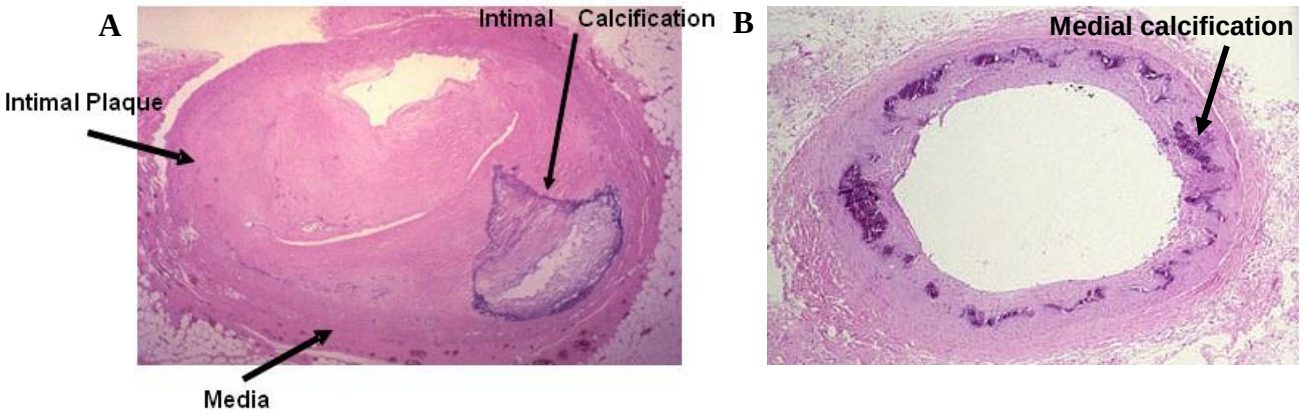

Figure 1.4. Two types of vascular calcification [60]

(A) Intimal calcification is characterized by lipid deposition, inflammation, and plaque formation in the subintima, ultimately resulting in obstruction of the arterial lumen. It is strongly associated with atherosclerosis and the development of plaques containing a fibrous cap enclosing a lipid-rich necrotic core.

(B) Medial calcification is characterized by arterial stiffening and calcium phosphate deposition within the elastin layers of the medial layer and without any form of lumen obstruction. This is often seen in aging patients, and is especially severe in patients with diabetes or CKD.

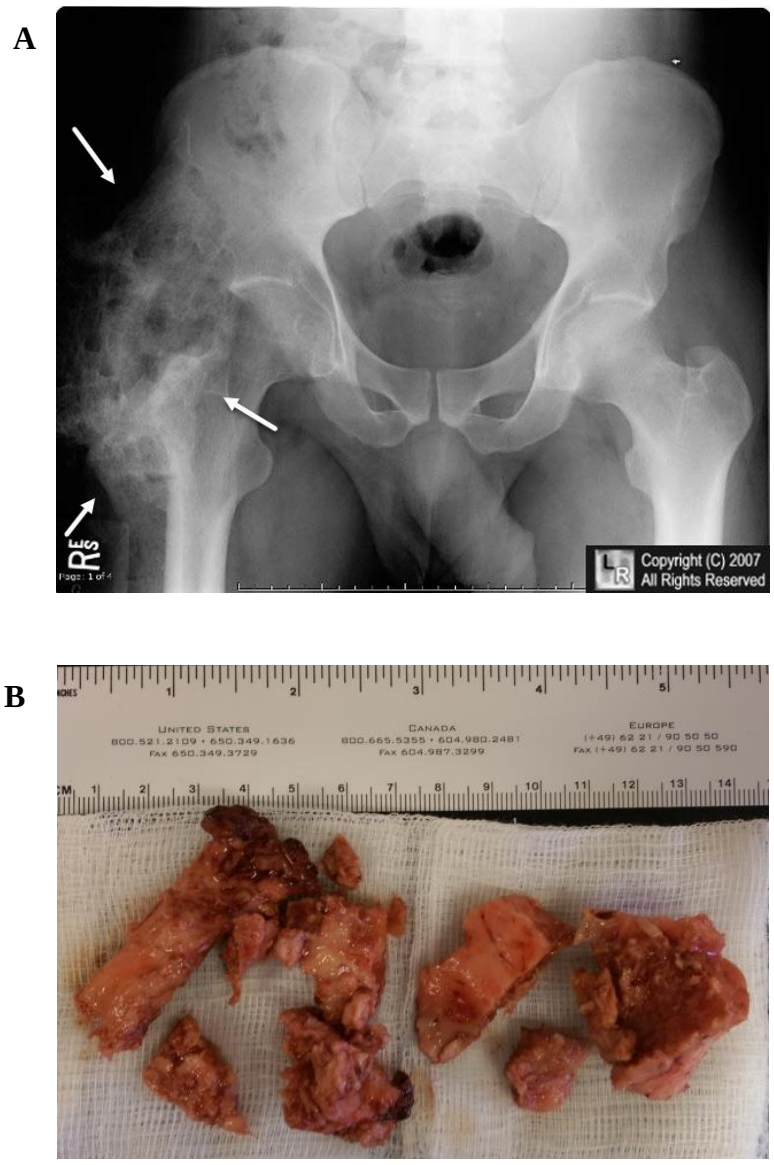

Figure 1.5. Development of HO in patients

(A) Radiograph shows HO formation after traumatic brain injury.[61] White arrows point to ossification with trabeculae and cortex surrounding the right hip joint in a patient with traumatic spinal cord injury several months earlier.

(B) Human HO samples were obtained after surgical explantation from an orthopedic surgeon at Harborview Medical Center, Seattle, WA.

A

B

Figure 1.6. Medication-related osteonecrosis of the jaw [62]

(A) Clinical presentation of BP-related osteonecrosis of the jaw at extraction site of tooth #18. Necrotic, nonhealing exposed bone extends up the ramus and to the buccal aspect of tooth #19.

(B) Radiograph of BP-related osteonecrotic lesion at extraction site of tooth #18. Lesion extends to the apices of adjacent tooth #19.

CHAPTER 2.

DEVELOPMENT OF ENGINEERED OSTEOCLAST SYSTEM

2.1 INNOVATION

Our lab has been using chemical inducer of dimerization (CID) technology to control monocyte differentiation to osteoclasts for use as bioengineered cell therapy to treat or prevent ectopic calcification. The idea that controlled differentiation of autologous monocytes to osteoclasts can prevent and/or regress calcification is innovative and has not yet been investigated. In addition to being the first to demonstrate dimerizer regulated osteoclast formation from monocytic precursors, ours are the first studies to utilize this technology to control cell differentiation in general, as this system has been previously used only for control of cell proliferation or apoptosis. Moreover, this study is the first to show that osteoclasts can prevent calcification by secreting calcification inhibitors. Additionally, this work is the first to use this system to turn on osteoclastogenesis in a mouse model of MRONJ and prove whether controlled osteoclast formation and function can prevent the development of this disease. It also elucidates the role of osteoclasts in the pathophysiology of MRONJ which has not been fully understood. Finally and most importantly, it provides a new door for innovative prevention/treatment for dental-related disease using engineered cell delivery.

2.2 DEVELOPMENT OF ENGINEERED OSTEOCLAST SYSTEM

Over the past several years, our lab has developed a system for conditional differentiation of monocytic precursors into osteoclasts for potential application in prevention and treatment of ectopic calcification. Our approach relies on the principle that protein interactions are at the heart of many signaling pathways controlling cell death, proliferation and differentiation.[63] The system has two components: a fusion protein and a drug (**Figure 2.1**).[64] In our case, the fusion protein contains the

intracellular portion of the osteoclast differentiation receptor, RANK, linked to two binding site for a drug called a chemical inducer of dimerization (CID). The prototypical CID is FK1012 that is comprised of 2 covalently linked molecules of the commonly used immunosuppressive drug, FK506, and binds to the naturally occurring immunophilin, FKBP12.[63] The fusion protein is functionally inert unless directed to dimerize, and dimerization is enforced through addition of the CID. This approach has been used extensively in the past to regulate growth and apoptosis of genetically modified cells[65–71], but to our knowledge, has not yet been used to successfully control osteoclastogenesis in any system.

In our studies, we used an optimized immunophilin analogue of FKBP12, F36V, that permits specific binding to second generation CIDs (e.g. AP1903, AP20187 or AP23510) that are not immunosuppressive and have a markedly reduced affinity for endogenous FKBP12.[72] The specific CID-iRANK construct to be used in our studies is shown in **Figure 2.2A**. Since RANK requires trimerization for effective signaling[73], we utilized two F36V domains fused to the RANK intracellular domain in order to ensure successful oligomerization. In addition, a myristoylation signal was added to direct the protein to the cell membrane to maximize interaction with downstream signaling molecules. An illustration of the trimerized fusion protein following CID treatment compared to RANKL induced trimerization of RANK is show in **Figure 2.2B**. Trimerization is critical for CID-induced osteoclastogenesis, since a construct mediating simple dimerization was not effective in promoting multi-nucleated osteoclast formation.[74] Moreover, the construct also contained the gene for green fluorescent protein (GFP), which allowed cell sorting to be performed. Cells were sorted twice by fluorescence-activated cell sorting (FACS) to obtain a purified (>98% GFP-positive) population for *in vitro* characterization.

As shown in our previously published work, we have engineered a murine monocytic cell line, RAW264.7, to express the iRANK construct.[6] Virally infected cells containing these constructs were

treated with the CID (AP20187) and dose-dependent induction of TRAP activity as well as formation of multi-nucleated osteoclasts were observed (**Figure 2.3**). In addition to expressing TRAP, the cells were positive for cathepsin consistent with an osteoclast lineage. Furthermore, NF-κB signaling was upregulated in a CID-dependent fashion, demonstrating effective RANK intracellular signaling (**Figure 2.4**). Functionally, *in vitro* mineral resorption data showed that CID-induced osteoclasts had better resorption activity than RANKL-induced osteoclasts (**Figure 2.5**). In addition, CID-induced osteoclasts could resorb a mineralized three-dimensional matrix in a CID-dependent fashion. Importantly, the CID-induced osteoclasts died when the CID was withdrawn (**Figure 2.6**), giving us an efficient on/off switch required to control extent of mineral resorption. Finally, and most critically, CID-induction of osteoclastogenesis occurred even in the presence of OPG (**Figure 2.7A**), in contrast to RANKL-mediated osteoclastogenesis that was completely inhibited by OPG (**Figure 2.7B**). Besides being the first demonstration of small molecule controlled osteoclast differentiation, to our knowledge, this is the first use of CID technology to control any type of cellular differentiation.

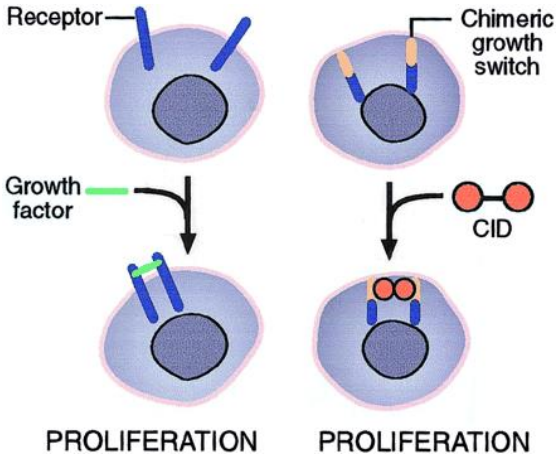

Figure 2.1. Chemical Inducer of Dimerization (CID) system [64]

CID system entails a conditional fusion protein that can oligomerize and initiate signaling in the presence of a small molecule CID.

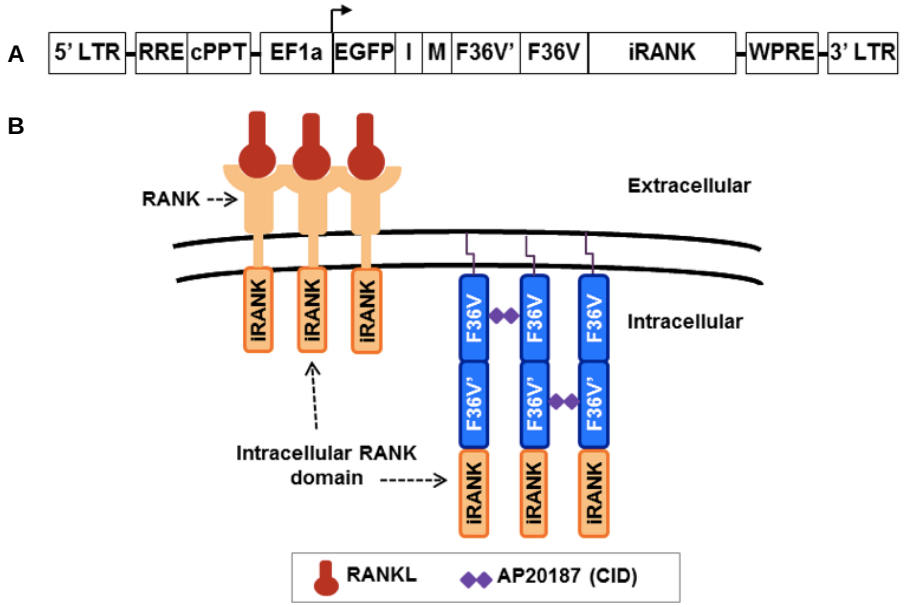

Figure 2.2. CID-iRANK lentiviral construct and comparison of RANKL-mediated trimerization of RANK and CID-mediated iRANK trimerization.

(A) Schematic representation of CID-inducible intracellular RANK (iRANK) construct. LTR=long terminal repeat; RRE=rev response element; cPPT=central polypurine tract; EF1a=elongation factor 1-Alpha; EGFP=green fluorescent protein; I=IRES; M=myristoylation; F36V=FKBP12; F36V'=modified FKBP12; iRANK=intracellular domain of RANK; WPRE=WHP posttranscriptional regulatory element.

(B) RANK signaling is initiated by trimerization of the RANK receptor in the presence of RANKL. The fusion protein consists of the intracellular RANK domain linked to two F36V binding sites, which allows for trimerization of the protein in the presence of the CID, AP20187.

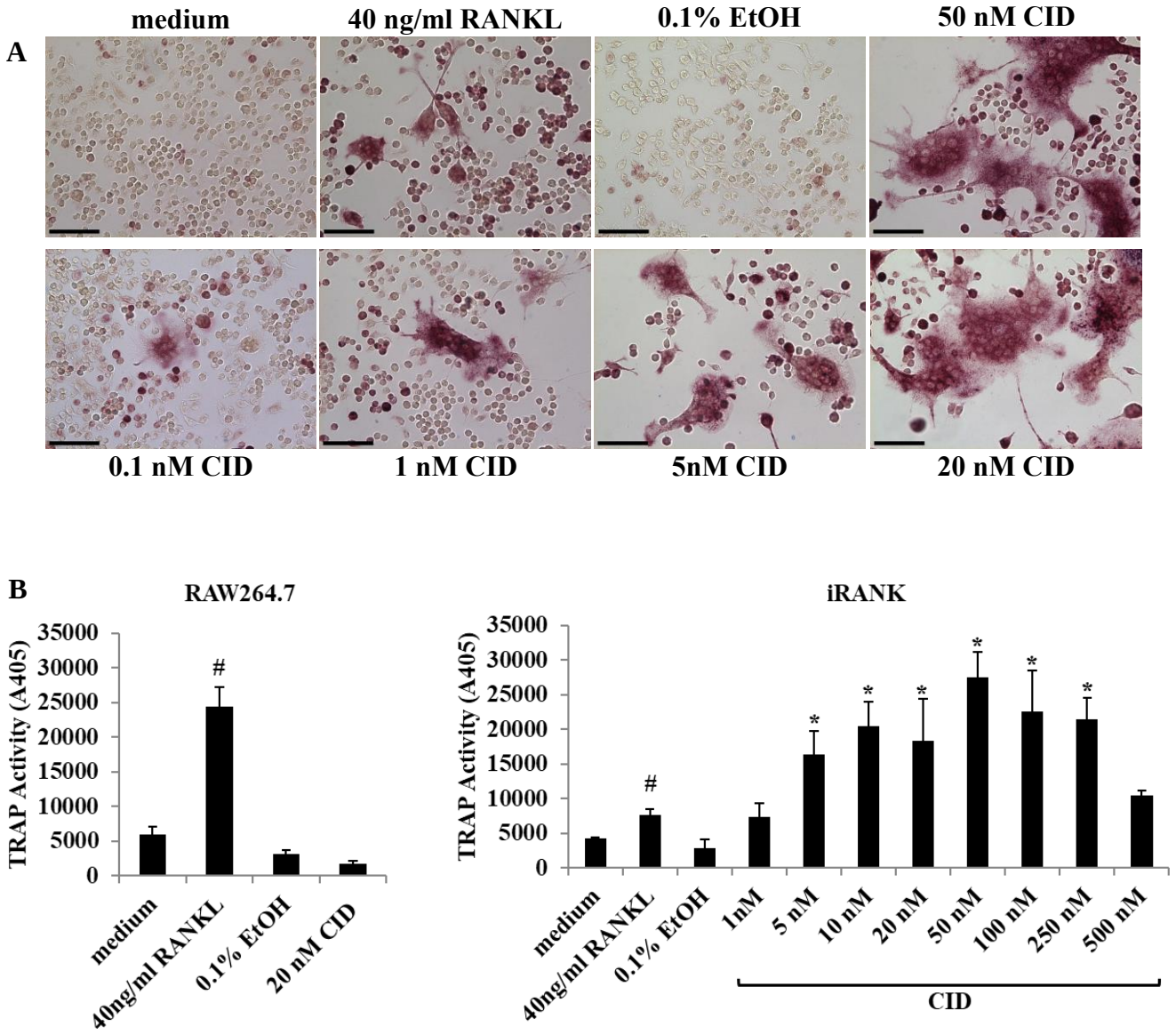

Figure 2.3. CID-responsiveness of the iRANK construct

iRANK cells were cultured in medium containing vehicle (EtOH), RANKL, or 0.1-50 nM CID for 5 days and then stained with TRAP solution. (A) iRANK cells responded to increasing doses of CID by forming more and larger TRAP-positive cells. Scale bar = 100 μm (B) Dose-dependent induction of TRAP activity in iRANK cells following CID treatment. #p<0.05 compared to medium, *p<0.05 compared to 0.1% EtOH

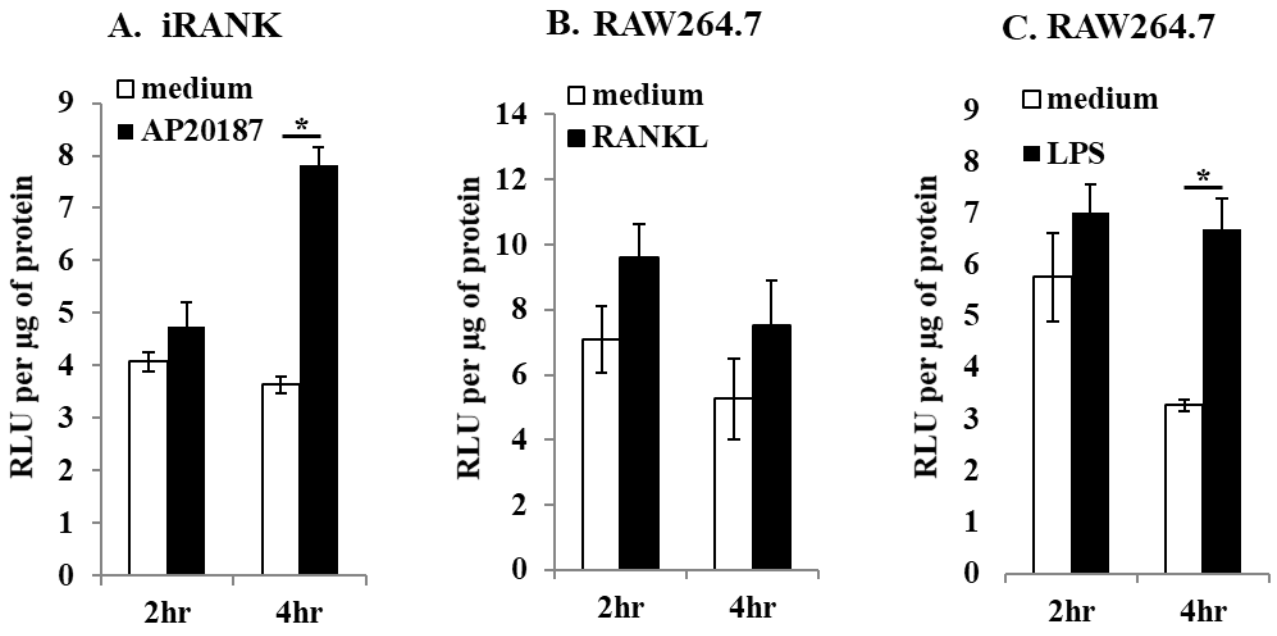

Figure 2.4. NF-κB dependent signaling in engineered osteoclasts.

NF-κB activation was observed in CID-treated iRANK cells (A) and was comparable to the effect of RANKL **(**B) and lipopolysaccharide (LPS) (C) on RAW264.7 cells. RLU = relative light units, *p<0.05

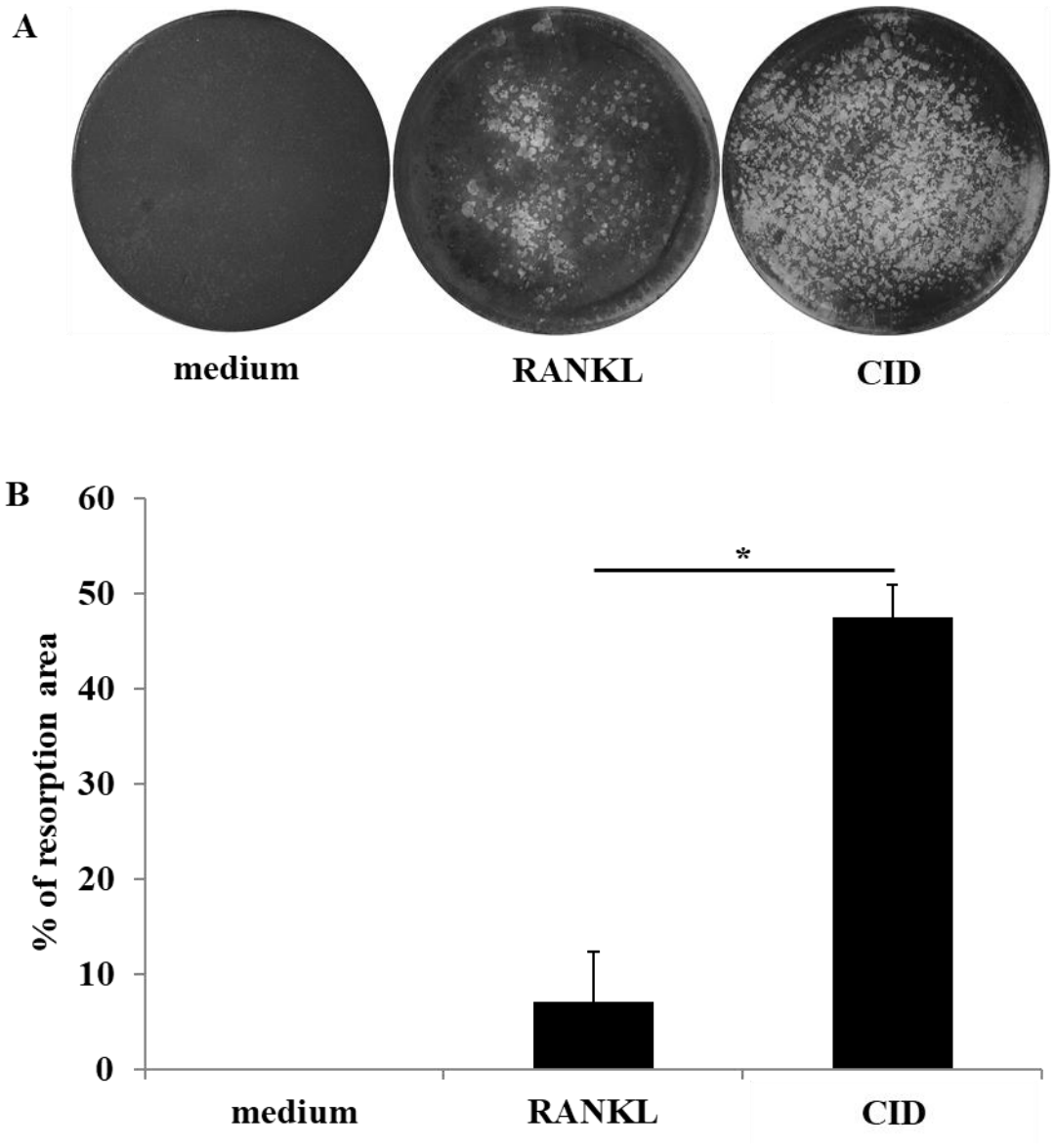

Figure 2.5. CID-induced osteoclasts resorbed a two-dimensional mineralized substrate.

(A) iRANK cells were treated with either RANKL (100 ng/ml) or CID (50 nM) on Osteologic discs. After 10 days, resorption lacunae were visualized by von Kossa staining. (B) The percentage of resorption area per disc was measured and analyzed using ImageJ. The resorption area in CID-treated iRANK cells was significantly higher than the cells treated with RANKL. *p<0.05

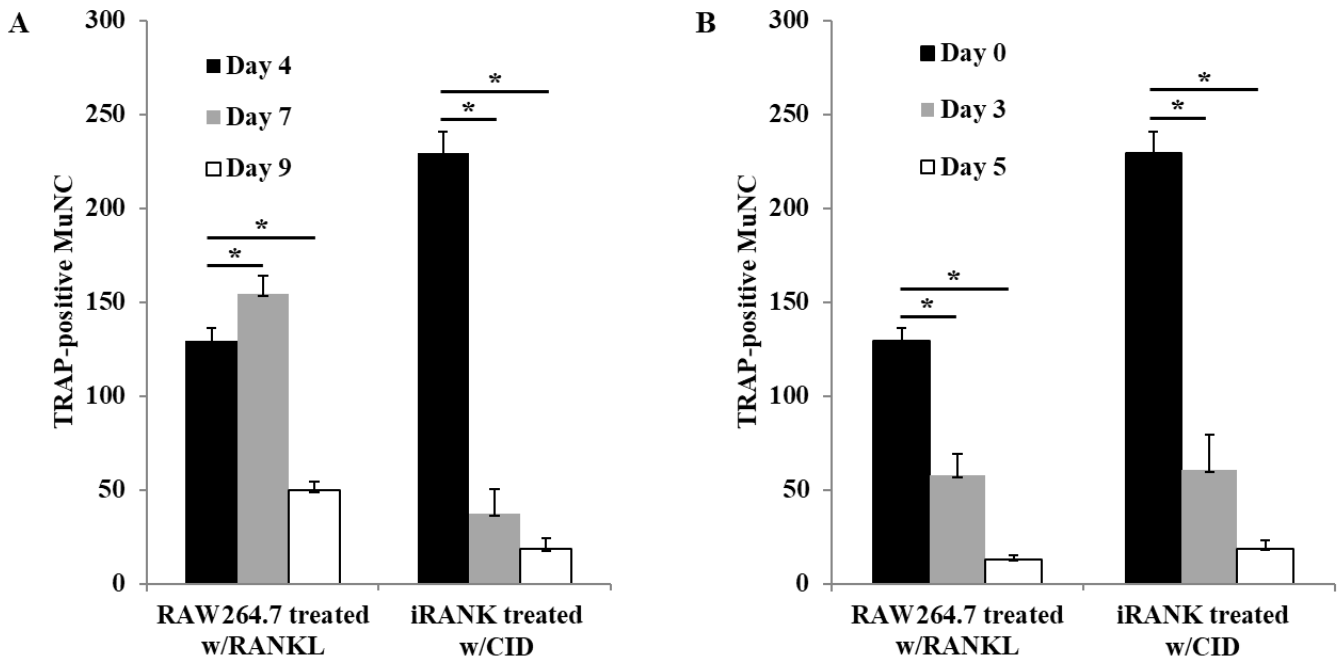

Figure 2.6. RAW264.7 and iRANK cell survival study.

(A) In RANKL-treated RAW264.7 cells, the number of osteoclasts increased with time and attained a maximum at day 7 followed by a large decline in osteoclast number by day 9. In contrast, CID-treated iRANK cells achieved maximal osteoclast numbers by day 4, followed by large declines at days 7 and 9. *p<0.05

(B) RAW264.7 and iRANK cells were treated with 40 ng/ml RANKL or 50 nM CID, respectively, for 4 days after which the drug was withdrawn (day 0) and the cells were cultured in media alone for another 3 or 5 days. CID-induced osteoclasts had a similar life span compared to RANKL-induced osteoclasts, and the lifespan was not altered by CID treatment. *p<0.05

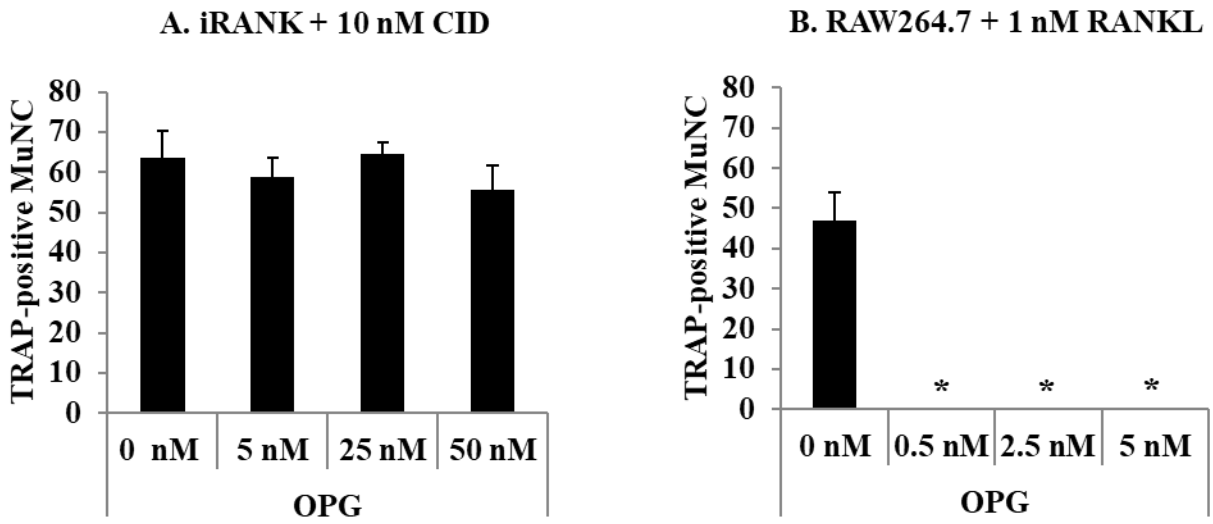

Figure 2.7. CID-induced osteoclastogenesis in iRANK cells was OPG-independent.

In the presence of OPG, a potent osteoclast inhibitor, iRANK cells exhibited no change in osteoclast formation (A) whereas RANKL-stimulated RAW264.7 cells had osteoclast formation completely blocked by OPG (B). *p<0.05 compared to 0 nM OPG

CHAPTER 3.
RESEARCH GOALS

The goals of this dissertation are first to determine the ability of osteoclasts to prevent calcification by releasing anticalcific factors, then to determine the role of osteoclasts in the development of medication-related osteonecrosis of the jaw (MRONJ) and finally to utilize engineered osteoclasts as a local cell therapy to prevent the development of MRONJ after dental interventions.

Osteoclast deficiency is involved in the pathogenesis of many diseases including ectopic calcification (EC) and MRONJ. Osteoclasts are bone-resorbing cells derived from hematopoietic cells. Their main function is to bind to mineralized surfaces and resorb calcification via formation of resorption lacunae.[4] Osteoclasts also secrete many proteins during their differentiation and some of these proteins, such as OPN, have inhibitory effect on calcification.[75] However, whether osteoclasts can prevent calcification through elaboration of calcification inhibitors has not been investigated. In addition to developing a cell therapy whereby osteoclasts resorb mineral, we also aim to use them to prevent calcification. In this study, we hypothesize that osteoclasts are therapeutically useful not only to physically resorb pre-existing mineral, but also to release factors, such as OPN, that may prevent mineralization. We previously engineered RAW264.7 murine monocytic cells with an inducible RANK (iRANK) construct to differentiate into osteoclasts under the control of a CID drug.[6] This differentiation is independent of cytokines, RANKL and M-CSF, and also resistant to osteoclast inhibitor, OPG. OPG is a physiological analogue of denosumab, a drug that induces MRONJ.[7] Therefore, we hypothesize that MRONJ occurs as a result of impaired osteoclast differentiation and function due to the inhibition by antiresorptive drugs such as denosumab. Thus, delivering engineered osteoclasts resistant to this inhibition may prevent the development of MRONJ after dental-related trauma.

This study is the first to demonstrate the ability of osteoclasts in preventing calcification by secreting anticalcific factors. Moreover, this work elucidates the role of osteoclasts in the development of MRONJ. Importantly, this study develops proof-of-concept data for using engineered osteoclasts as a local cell therapy to prevent MRONJ, potentially paving the way for clinical use in patients to improve outcome and mortality of MRONJ.

Aim 1: To determine the ability of engineered osteoclasts to prevent calcification *in vitro* using co-culture system.

We hypothesize that engineered osteoclasts not only physically resorb mineral, but also release factors that may prevent mineralization. First, we developed two models of *in vitro* ectopic calcification (EC), heterotopic ossification (HO) and valvular calcification. We first developed a model of HO, in which C2C12 mouse myoblast cells were cultured in the presence of bone morphogenetic protein 2 (BMP-2) or high inorganic phosphate (Pi) for 5 days. To develop a model of valvular calcification, bovine aortic valve interstitial cells (BVICs) were cultured in the presence of high Pi conditions for 7 days. Finally, we developed a co-culture system and determine whether engineered osteoclasts can prevent BVIC and C2C12 calcification.

Aim 2: To identify mechanisms used by osteoclasts to prevent calcification.

We hypothesize that a mechanism by which osteoclasts might prevent mineral accumulation is by elaborating anticalcific factors, such as OPN. First, we used ELISA (enzyme-linked immunosorbent assay) to determine levels of OPN secreted by engineered osteoclasts in culture media. To further verify whether the ability of engineered osteoclasts to prevent calcification is due to the accumulation of OPN, we use an immunodepletion technique to remove OPN from iRANK osteoclast conditioned media. We then used OPN-depleted conditioned media to culture C2C12 in the presence of high Pi and human HO

samples. We hypothesize that conditioned media from iRANK osteoclasts lacking OPN could not inhibit C2C12 calcification and passive mineralization of human HO samples. Using Western blot analysis, we also identified different forms of OPN present in iRANK osteoclast conditioned media. Furthermore, we demonstrated that osteoclasts secreted exosomes and OPN present in iRANK osteoclast-derived exsosomes is unique and different than OPN present in conditioned media.

Aim 3: To develop a mouse model of MRONJ to determine the role of osteoclasts in MRONJ development and prevention *in vivo.*

We hypothesize that MRONJ occurs as a result of impaired osteoclast differentiation and function due to the inhibition by antiresorptive drugs such as denosumab. Thus, delivering engineered osteoclasts resistant to this inhibition may prevent the development of MRONJ after dental-related trauma. We first determined whether engineered murine osteoclasts are resistant to the inhibition by anti-mouse RANKL antibody, a mouse analogue of denosumab, *in vitro*. Then, we developed a model of MRONJ in nude mice and validated a cell delivery method and osteoclast induction *in vivo*. Finally, we will utilize this model to determine whether engineered osteoclasts can prevent the development of MRONJ after tooth extraction in the future.

CHAPTER 4.

ABILITY OF ENGINEERED OSTEOCLASTS TO PREVENT ECTOPIC CALCIFICATION

In previous studies, we utilized CID technology to control monocytic precursor differentiation into functional osteoclasts, which is independent of RANKL and M-CSF and also resistant to OPG, a potent natural inhibitor of osteoclast differentiation. In this chapter, we propose that osteoclasts not only physically resorb bone, but also prevent mineral accumulation by secreting anticalcific factors. To test this hypothesis, we developed a co-culture system in which engineered osteoclasts were cultured with calcifying cells in media containing high inorganic phosphate (Pi) using Transwell inserts. Two *in vitro* models of ectopic calcification (EC) – HO and valvular calcification – were used to verify osteoclasts' preventive ability.

4.1 INTRODUCTION

4.1.1 *Heterotopic ossification (HO)*

HO is a type of ectopic calcification in which calcified bone is formed outside of the skeleton. HO can be either hereditary or acquired. Hereditary HO occurs in fibrodysplasia ossificans progressiva (FOP) and progressive ossific heteroplasia (POH).[39,40] Acquired HO is more common and occurs as a result of severe trauma, particularly to muscle or neuronal tissues, including traumatic brain and spinal cord injuries, severe burns, and combat blast wounds.[40,76] Additionally, acquired HO is a common complication following limb amputation, orthopedic fractures, and joint arthroplasty.[77–79] Approximately 10-20% of patients within the civilian population suffering traumatic brain and spinal cord injuries develop HO, while in the military population up to 63% of soldiers with these type of injuries develop HO.[80,81] Due to nerve impingements and/or the mechanical effects of hard tissue formation in non-

skeletal sites, patients with symptomatic HO experience pain and loss of mobility which can lead to dramatic impairment of function and ability to perform daily activities.[40,82] Once HO has developed and restricted motion, it is nearly impossible to regain the lost motion with conservative measures. At the moment, there are no definitive therapies for HO. Current prophylactic treatments include non-steroidal anti-inflammatory drugs (NSAIDs) and radiation therapy, while the only treatment for established HO is surgical removal.[40] However, NSAIDs have adverse drug reactions and can impair bone healing.[83,84] Moreover, radiotherapy increases risk of malignancy, genetic mutations, and gonadal effects.[85] Finally, surgical approaches have had limited efficacy and are associated with a significant recurrent rate of 20%.[6,86] Thus, new therapies specifically aimed at preventing and/or regressing calcification in the setting of HO are greatly needed.

Presently, it is believed that HO occurs as a result of the synergistic effects of local inflammation, hypoxia, neovascularization, the presence of osteogenic factors, and the potential interplay between local and systemic cell types.[40,84,87] Inflammation appears to be a major contributor potentially by elevating cytokines that facilitate the recruitment of mesenchymal precursors that undergo chondrogenic and osteoblastic differentiation to form HO.[40,41,88] Traumatic injury may also lead to the upregulation of factors that promote mineral formation, thereby shifting the balance towards bone forming pathways. HO is typically a heterogeneous mixture of cortical and cancellous bone with distinct regions of fibrocartilage.[89] Importantly, bone marrow elements tend to form late in these lesions and little if any osteoclastic activity has been observed. Together, these data indicate that the development of HO may be due to a deficit in osteoclast formation that leaves ossification unopposed. This is a novel paradigm for the pathology of HO and suggests that osteoclasts and/or osteoclast-derived factors may be unique treatment strategies for HO.

HO models have been developed both *in vitro* and *in vivo* by the induction of intramuscular ectopic ossification using BMPs. Mishra S. *et al* developed a myoprogenitor (C2C12) cell-based pathological *in vitro* model of HO. They showed that exogenously administering human recombinant BMP-2 could induce C2C12 mouse myoblast cells to differentiate into an osteoblastic cell lineage, as determined by an increased alkaline phosphatase (ALP) activity.[90] In addition to BMPs, high Pi was also used to induce calcification of C2C12 cells *in vitro*. Kikkawa N. *et al* cultured C2C12 myoblasts under high Pi conditions and found that myogenic markers, such as myogenin and fusion index, were down-regulated, while osteogenic markers, such as osteocalcin and Runx2, were upregulated.[91] This was followed by the initiation of calcium deposit. Thus, we used BMP-2 and high Pi to develop an *in vitro* model of HO.

4.1.2 *Vascular calcification (VC)*

The normal serum phosphate level in adult ranges from 1.0 to 1.5 mM.[18] Several studies have shown a correlation between high serum Pi level (>1.5 mM; hyperphosphatemia) and a tendency toward vascular calcification.[18,92,93] Our group previously developed an *in vitro* model for vascular and valvular calcification and determined the effect of elevated Pi on calcification in various types of cells including human aortic smooth muscle cells (HSMCs), mouse vascular smooth muscle cells (VSMCs), and bovine valve interstitial cells (BVICs). In the presence of 2 mM Pi, calcium deposition of HSMC dramatically increased in a time- and dose-dependent manner.[18] In addition, significant mouse VSMC matrix mineralization was observed at 2.4 mM Pi or higher.[94] Addition of 2.4 mM Pi to the culture media promoted matrix calcification of BVIC.[95] Valve interstitial cells are heterogeneous cell populations mainly composed of fibroblasts, myofibroblasts and smooth muscle cells.[93] The fibroblast-like VIC subpopulation has been shown to undergo phosphate-induced calcification in the setting of inflammation.[95] These data suggest that cells cultured under high Pi conditions undergo osteogenesis

and form calcium deposition *in vitro*. Thus, we cultured BVICs in the presence of high Pi (2.4 mM) to induce calcification.

In this chapter, the ability of engineered osteoclasts to prevent *in vitro* HO and VC model was determined by using a co-culture system.

4.2 MATERIALS AND METHODS

4.2.1 *Osteoclast differentiation of RAW264.7 and iRANK cells*

RAW264.7 and iRANK cells were cultured in Minimum Essential Medium Eagle – alpha modification (α-MEM) containing 10% heat-inactivated fetal bovine serum (FBS) and 100 U/mL of penicillin/streptomycin (P/S) and incubated at 37°C with 5% CO_2. Cells were plated at 50,000 cells/well in 6-well Transwell inserts (Corning). Four hours after seeding, RAW 264.7 and iRANK cells were induced to differentiate into osteoclasts with 40 ng/mL recombinant human RANKL (hRANKL) (R&D Systems) or 50 nM CID (AP20187; Clontech Laboratories), respectively. The supplemented media was changed every 2 days for 4 days.

4.2.2 *TRAP staining of multinucleated osteoclasts*

Cells were washed with phosphate buffered saline (PBS) twice and fixed with 10% buffered formalin for 10 minutes. After fixing, cells were washed with Milli-Q water twice and subjected to TRAP staining following the manufacturer's instructions (Sigma-Aldrich). Cells were kept in Milli-Q water. Images were taken using a stereomicroscope (Nikon SMZ1500). Multinucleated TRAP-positive osteoclasts (≥3 nuclei) were quantified.

4.2.3 *BMP-2 induced HO model of C2C12 cells*

C2C12 mouse myoblast cell lines from ATCC were cultured on 6-well plates at a density of 38,000 cells/well. Cells were maintained in Dulbecco's Modified Eagle's Medium (DMEM) supplemented with 10% FBS and 100 U/mL of P/S. At 24 hours after seeding, the media was replaced with fresh media containing 100 ng/mL of human recombinant BMP-2 (hrBMP-2) to induce osteochondrogenic differentiation for 5 days. Incubation was performed at 37°C in a humidified atmosphere containing 95% air/5% CO_2 and the media was replaced with fresh supplemented media every other day.

4.2.4 *Detection of alkaline phosphatase (ALP)*

For the histochemical detection of ALP expression, cells were washed with PBS and fixed with 10% formalin for 15 minutes at room temperature. Then, cells were washed with washing buffer (0.05% Tween 20 in PBS). Next, cells were stained with ImmPACT™ Vector® Red working solution and incubated for 30 minutes in the dark at room temperature. Images were taken using an inverted microscope (Nikon TE200).

Quantitative analysis of ALP activities was assessed by using QuantiChrom™ Alkaline Phosphatase Assay. First, cells were washed with PBS and lysed in 0.5 mL 0.2% Triton X-100 in distilled water by shaking for 20 minutes at room temperature. Then, cell lysate was collected and stored in Eppendorf tubes at -20^{o}C. Twenty microliters of cell lysate were reacted with working solution containing p-nitrophenyl phosphatase (pNPP) in 96-well plate in triplicates. The absorbance was measured at 405 nm at t = 0 minute and t = 4 minutes. ALP activity was normalized by total protein content, which was determined by using Pierce micro-BCA Protein Assay Kit (Thermo Fisher Scientific).

4.2.5 *Pi induced HO model of C2C12 cells*

C2C12 mouse myoblast cell lines from ATCC were cultured on gelatin coated 6-well plates at a density of 12,500 cells/well. Cells were maintained in DMEM supplemented with 10% FBS and 100 U/mL of P/S. At 24 hours after seeding, the media was replaced with calcification media that consisted of DMEM, 3% FBS, and 100 U/mL P/S supplemented with Na_2PO_4/$NaPO_4$ (pH=7.4) to obtain 3.2 mM final concentration of Pi for 5 days to induce calcification. Incubation was performed at 37°C in a humidified atmosphere containing 95% air/5% CO_2 and the media was replaced with fresh media every other day. At day 5, calcium content of C2C12 cells was detected and quantified.

4.2.6 *Detection of calcification*

Calcium deposition was evaluated by staining the cell-matrix monolayer with Alizarin Red S. Cells were washed three times with PBS, fixed in 10% formaldehyde for 45 minutes at 4°C, and washed with distilled water three times. Then, cells were incubated with a 2% Alizarin Red S (pH 4.1-4.3) solution at room temperature in the dark for 45 minutes and rinsed with distilled water. Images were obtained using an inverted microscope (Nikon TE200).

Quantification of calcification was assessed by using the *O*-cresolphthalein complexone method as previously described.[17] Briefly, the cultures were decalcified with 0.6 N HCl overnight. Calcium content in HCl supernatant was determined colorimetrically by the *O*-cresolphthalein complexone method (Teco Diagnostics). After removing the HCl supernatant, the cultures were washed with PBS and solubilized with 0.2 N NaOH. Total protein content was measured with the Micro BCA Protein Assay Kit (Thermo Fisher Scientific). The calcium content in individual wells was normalized to protein content.

4.2.7 *Co-culture of C2C12 and RAW264.7 or iRANK cells*

Prior to the co-culture, RAW264.7 and iRANK cells were cultured on Transwell insert (Corning) and induced with either 40 ng/mL hRANKL or 50 nM CID for 4 days to differentiate into osteoclasts, while unstimulated RAW264.7 and iRANK cells were cultured for 1 day. Then, Transwell inserts were transferred to a 6-well containing C2C12 cells as shown in **Figure 4.1A**. These two cells were co-cultured for 5 days in the presence of 100 ng/mL hrBMP-2 to induce osteochondrogenic differentiation or 3.2 mM Pi to induce calcification. The culture media was changed every other day. At day 5, C2C12 cells were measured for ALP activity or calcium content as described above.

4.2.8 *BVIC cell culture as an in vitro model of valvular calcification*

BVICs were obtained as previously described[96] and seeded in collagen type I coated 6-well plates at a density of 12,500 cells/well. Cells were maintained DMEM supplemented with 10% FBS and 100 U/mL of P/S. At 24 hours after seeding, the media was replaced with calcification media that consisted of DMEM, 7% FBS, and 100 U/mL P/S supplemented with $Na_2PO_4/NaPO_4$ (pH=7.4) to obtain 2.4 mM final concentration of Pi for 7 days to induce calcification. Incubation was performed at 37°C in a humidified atmosphere containing 95% air/5% CO_2 and the media was replaced with fresh media every other day.

4.2.9 *Co-culture of BVICs with RAW264.7 or iRANK cells*

Prior to the co-culture, RAW264.7 and iRANK cells were cultured on Transwell insert and induced with either 40 ng/mL hRANKL or 50 nM CID for 4 days to differentiate into osteoclasts, while unstimulated RAW264.7 and iRANK cells were cultured for 1 day. Then, Transwell inserts were transferred to a 6-well containing BVICs as shown in **Figure 4.1B**. These two cells were co-cultured for 7 days in DMEM supplemented with 7% FBS and 100 U/mL of P/S in the presence of 2.4 mM Pi to

induce calcification. The bottom of the insert is composed of polyester with 0.4 µM pore size which permits the passage of small soluble factors. The culture media was changed every other day. At day 5, new osteoclasts from RAW264.7 and iRANK cells were replaced, since the induced osteoclasts have a lifespan of about 5 days after the drug is withdrawn.[6] At day 7, calcium content of BVICs was quantified as described above.

4.2.10 *Statistical analysis*

Results are expressed as mean ± SEM, n=3 for all experiments unless otherwise indicated. SPSS software v16.0 was used to perform Student's *t*-test to compare means of two individual groups, and one-way ANOVA with post-hoc Tukey test to compare means of three or more individual groups. A value of $p<0.05$ was considered statistically significant.

4.3 RESULTS

4.3.1 *Seeding iRANK cells at a density of 50,000 cells/well resulted in optimal osteoclast formation.*

To optimize osteoclast formation for co-culture studies, three densities of iRANK cells (25,000, 50,000 and 100,000 cells) were cultured on the top surface of Transwell inserts (0.4 µM pore size) in 6-well plates, and treated with CID 4 hours after seeding. As shown in **Figure 4.2A**, when seeding cells at 50,000 cells/well more TRAP-positive multinucleated cells were found at 5 days after induction than any other seeding density. Quantitatively, seeding iRANK cells at a density of 50,000 cells/well also resulted in significantly higher numbers of TRAP-positive multinucleated cells compared to other cell densities (**Figure 4.2B**). Therefore, iRANK cells were seeded at a density of 50,000 cells/well and treated with CID to induce osteoclast differentiation in further studies. As expected, no mononuclear or TRAP-positive cells were observed in the lower compartment of the well (data not shown).

4.3.2 *Pi and hrBMP-2 induced C2C12 cells were used as an in vitro model of HO*

To determine the mechanism by which osteoclasts might prevent HO, we utilized an established *in vitro* cell model of HO.[90,91] hrBMP-2 induced a significant increase of ALP activity both quantitatively and qualitatively in C2C12 cell culture as shown in **Figure 4.3**. Moreover, significant calcification was observed when C2C12 cells were cultured in the media containing 3.2 mM Pi for 5 days (**Figure 4.4A**). Alizarin Red S staining also showed calcium deposition in Pi-induced C2C12 culture (**Figure 4.4B**). These data suggest that C2C12 cells cultured in the presence of hrBMP-2 and under high Pi conditions underwent osteochondrogenesis and formed calcium deposition *in vitro.* Thus, these cells were chosen for further studies to examine the anticalcific effects of osteoclasts in a contact-independent, Transwell co-culture system.

4.3.3 *Osteoclasts prevented calcification of C2C2 cells in a contact-independent co-culture model.*

To test the hypothesis that osteoclasts could prevent calcification by elaborating anticalcific factors, we utilized the Transwell co-culture model shown in **Figure 4.1A**. RAW264.7 and iRANK cells were cultured on the Transwell inserts and were induced to differentiate into osteoclasts for 4 days with the inducers, 40 ng/mL hRANKL and 50 nM CID, respectively. Then, Transwell inserts containing osteoclasts differentiated from RAW264.7 or iRANK cells were moved to new plates containing C2C12 cells in media containing high Pi (3.2 mM Pi) for 5 days to induce calcification. The calcium content in individual wells was normalized to protein content. As shown in **Figure 4.5**, treating C2C12 cells with 3.2 mM Pi dramatically increased calcification compared to normal phosphate treatment. In the presence of high Pi, calcium deposition by C2C12 cells co-cultured with untreated RAW264.7 or iRANK cells was not statistically different compared to Pi-induced C2C12 cell calcification. On the other hand, hRANKL-induced RAW264.7 and CID-induced iRANK cells significantly decreased C2C12 cell calcification compared to Pi-induced C2C12 cell calcification and their precursor cells. This data

demonstrates that osteoclasts could inhibit calcification of C2C12 cells *in vitro* without physical contact through secreted factors.

Interestingly, ALP activity was not detected when C2C12 cells were co-cultured with hRANKL-induced osteoclasts and CID-induced osteoclasts in the presence of hrBMP-2 (**Figure 4.6**). Co-culture of precursor cells with C2C12 had significantly lower ALP activity compared to the positive control (C2C12+hrBMP-2).

4.3.4 *Pi induced BVICs were used as an in vitro model of valvular calcification*

Significant calcification was induced when BVICs were cultured in the media containing 2.4 mM Pi for 7 days (**Figure 4.7A**). At day 7, Alizarin Red S staining confirmed the deposition of calcium as shown in **Figure 4.7B**. These results indicate that BVIC cultures were susceptible to calcification when cultured in media containing high Pi concentrations.

4.3.5 *Osteoclasts prevented BVIC calcification in a contact-independent manner*.

As shown in **Figure 4.8**, inducing BVIC with 2.4 mM Pi dramatically increased calcification compared to normal phosphate. The culture experienced significantly less calcification when RAW264.7 and iRANK cells were pretreated with inducers (40 ng/mL hRANKL or 50 nM CID) before co-culture compared to Pi-induced BVIC calcification. Interestingly, co-culture of BVIC and CID-induced iRANK osteoclasts had the lowest calcification levels, although this was not statistically significant compared to RANKL-induced osteoclasts. On the other hand, untreated RAW264.7 and iRANK cells could not prevent BVIC calcification. The calcium deposition of BVIC co-cultured with untreated RAW264.7 and iRANK cells was not statistically different than Pi-induced BVIC calcification. The co-culture result of osteoclasts and BVIC was similar to the result observed in C2C12 calcification. These data suggest that

osteoclasts differentiated either from RAW264.7 or iRANK cells had a contact-independent ability to prevent both BVIC and C2C12 calcifications *in vitro*.

4.4 DISCUSSION

In a previous study, we developed a CID-based system to control monocytic precursor differentiation into functional osteoclasts, which was independent of RANKL and M-CSF, and also resistant to OPG, a potent natural inhibitor of osteoclast differentiation.[6] To test whether engineered osteoclasts could prevent mineral accumulation of HO by elaborating anticalcific factors, we first developed an *in vitro* model of HO and showed that C2C12 cells did not deposit calcium under normal Pi conditions, while they calcified when cultured in high Pi (3.2 mM) media. This data is similar to previous findings by Kikkawa N. *et al* in which they found that C2C12 cells cultured in media containing 3 mM Pi or higher deposited calcium.[91]

We developed a co-culture system in which RAW264.7 and iRANK cells were cultured with C2C12 cells in high Pi media, in the presence and absence of osteoclast inducers (hRANKL and CID) using Transwell inserts. The treatment of RAW264.7 and iRANK cells with inducers led to the inhibition of C2C12 cell calcification demonstrating that osteoclasts can inhibit C2C12 cell calcification *in vitro* without physical contact. Interestingly, CID-induced iRANK cells tended to perform better than RANKL-induced cells, suggesting that our engineered cells, which can be differentiated without the use of costly cytokines (M-CSF and RANKL), have an advantage over existing RAW264.7 cell lines. These data support our hypothesis that osteoclasts can prevent mineral accumulation by releasing anticalcific factors that may bind to calcium phosphate mineral and prevent crystal growth.

Co-culture studies suggest that osteoclasts could be used as a cell therapy to not only treat but also prevent EC. To determine their potential for use as a preventive therapy, we need to further identify the mechanism(s) by which osteoclasts prevent mineral accumulation. Potential mechanisms may

include elaboration of anticalcific factors into the media. Our current studies do not look at contact-dependent mechanisms for osteoclastic prevention of mineral deposition or potential interactions with other cell types *in vivo*. Further studies to determine the full extent of the role of osteoclasts *in vivo* for prevention and treatment of EC are needed.

In conclusion, our studies are the first to demonstrate the contact-independent ability of osteoclasts to prevent EC *in vitro*. Our studies suggest that further research is warranted to determine additional osteoclastic therapeutic strategies.

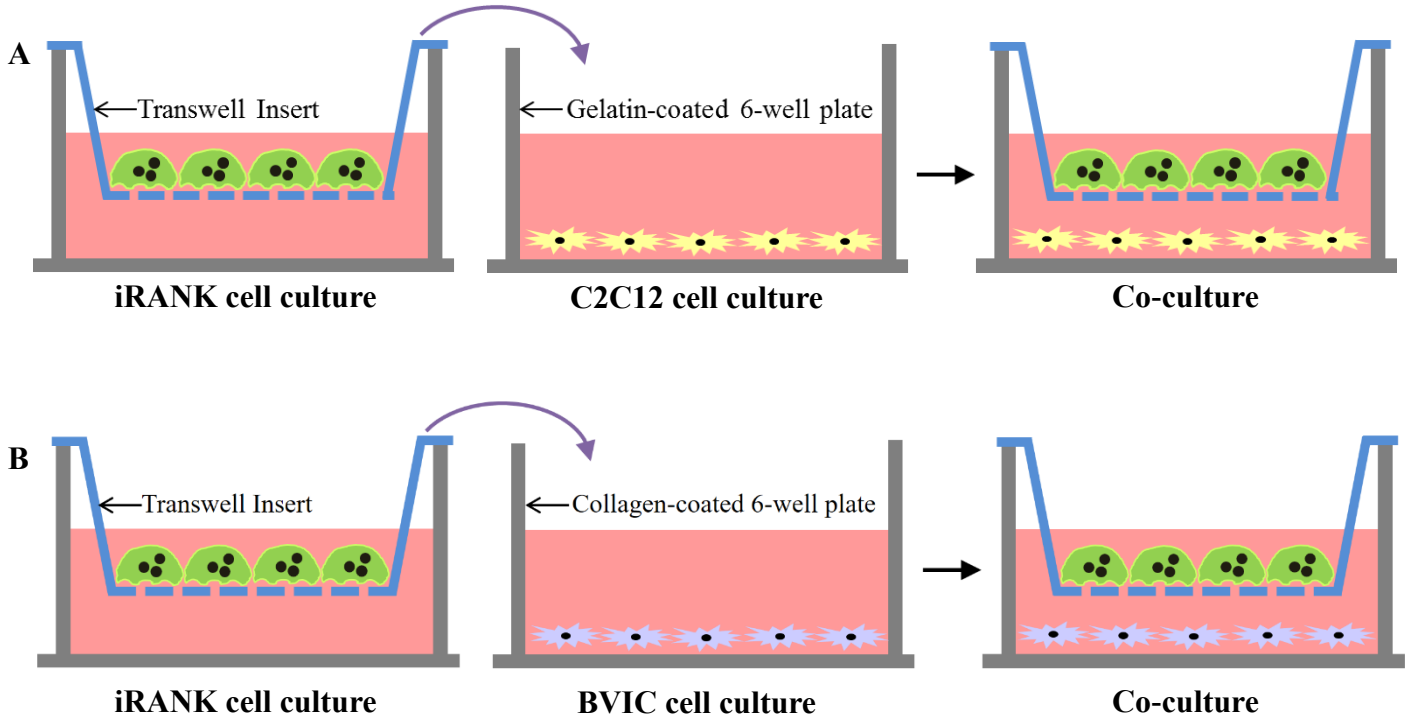

Figure 4.1. Co-culture of osteoclasts with C2C12 cells or BVICs

(A) iRANK or RAW264.7 cells were cultured on polyester Transwell inserts, induced to become osteoclasts, and transferred into plates containing C2C12 cells under high Pi condition.

(B) iRANK or RAW264.7 cells were cultured on polyester Transwell inserts, induced to become osteoclasts, and transferred into plates containing BVICs under high Pi condition.

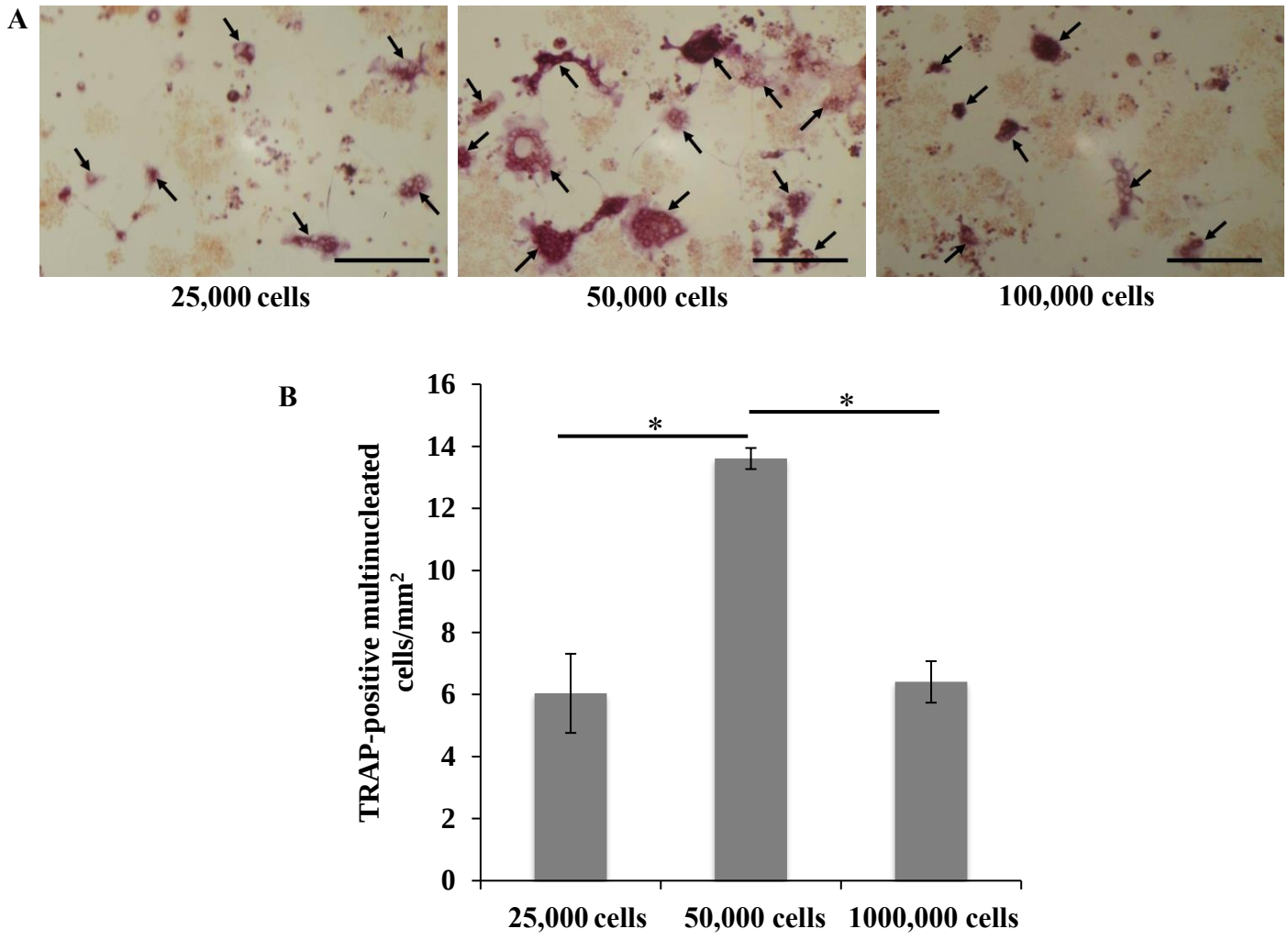

Figure 4.2. CID-induced iRANK cells formed osteoclasts on Transwell inserts.

Three different densities of iRANK cells (25,000, 50,000 and 100,000 cells/Transwell) were cultured and induced with CID. (A) More TRAP-positive multinucleated cells (arrows) were observed when seeding cells at 50,000 cells/well. Scale bar = 200 μm (B) Quantification of TRAP staining showed that cells seeded at 50,000 cells/well had the highest number of TRAP-positive multinucleated cells compared to other seeding densities. *p<0.05

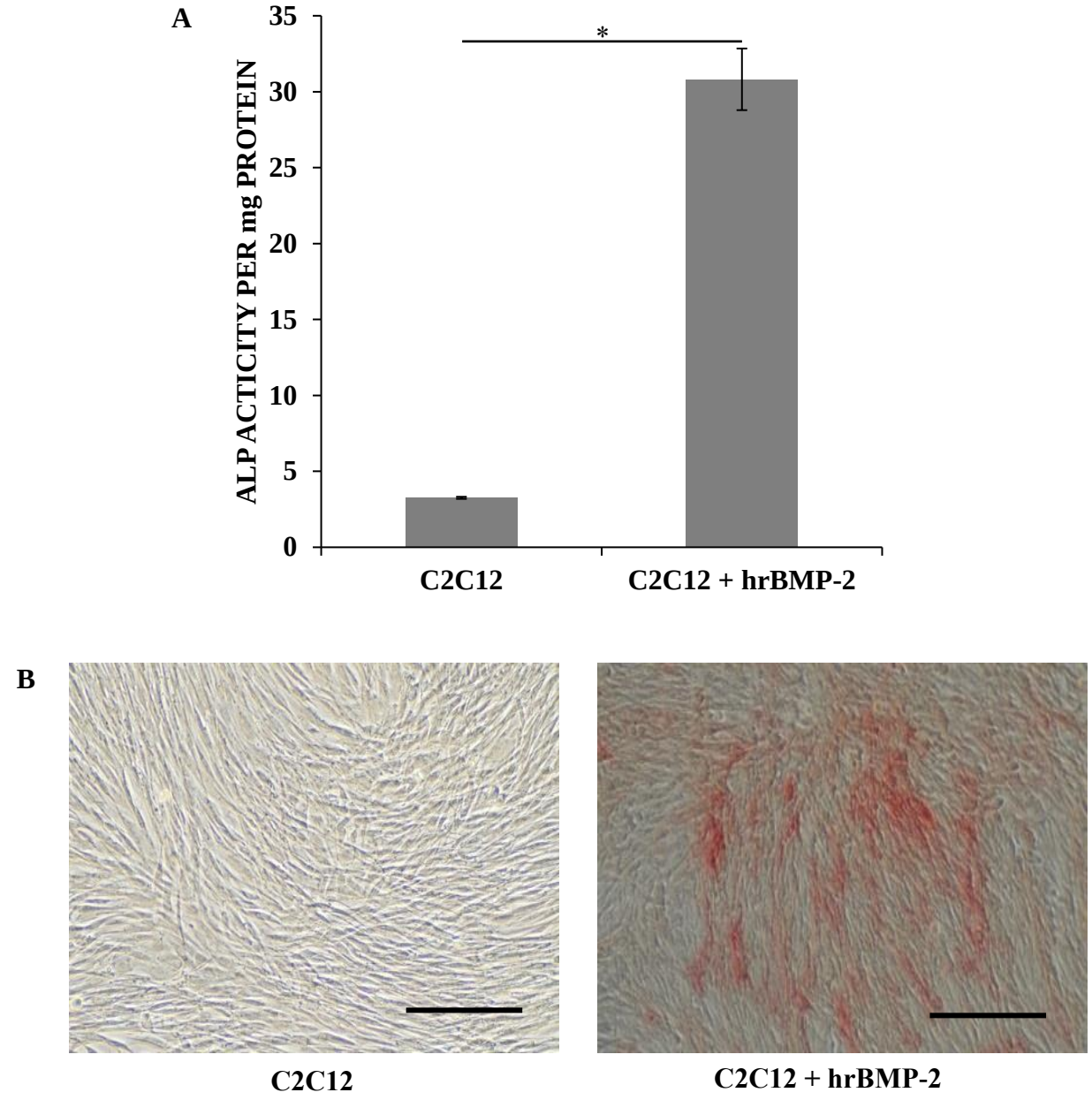

Figure 4.3. hrBMP-2 induced ALP expression in C2C12 cells.

ALP activity was significantly induced by hrBMP-2 in C2C12 culture both quantitatively (A) and qualitatively (B). *p<0.05, scale bar = 200 µm

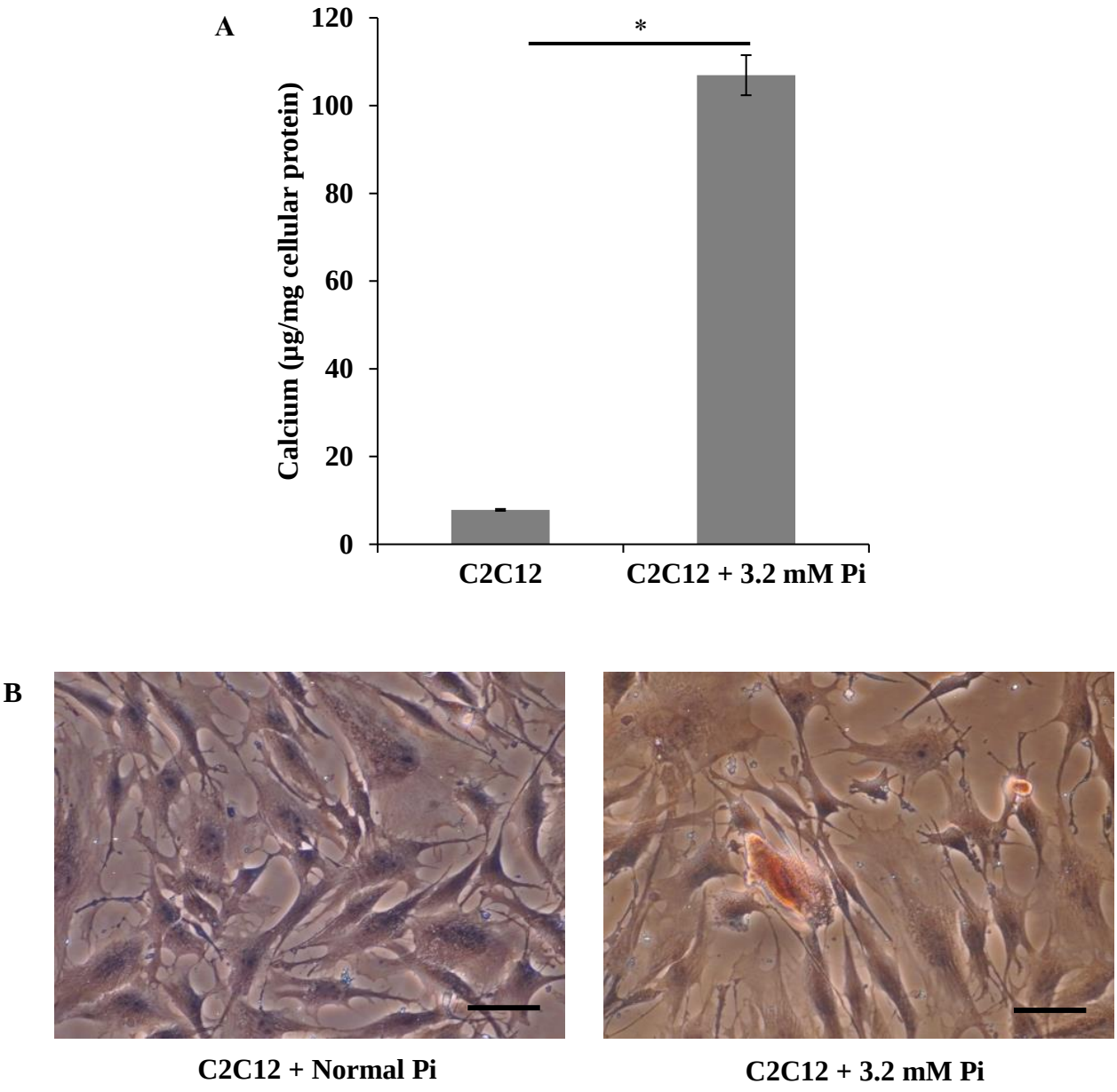

Figure 4.4. High Pi induced calcium deposition in C2C12 culture.

(A) Significant calcification was induced when C2C12 cells were cultured in the media containing 3.2 mM Pi for 5 days. *p<0.001

(B) Alizarin Red S staining showed calcium deposition in C2C12 cells cultured for 5 days in the presence of 3.2 mM Pi. Scale bar = 400 µm

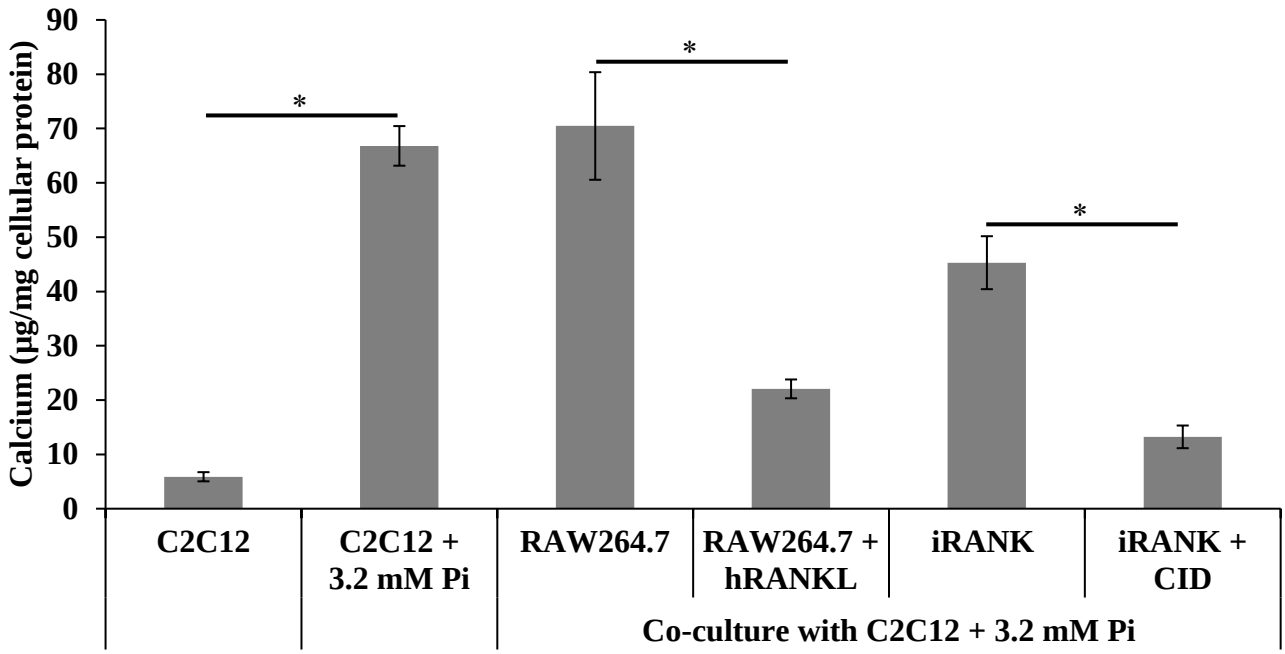

Figure 4.5. Engineered osteoclasts inhibited C2C12 calcification in co-culture.

C2C12 cells experienced significantly less calcification when co-cultured with CID-induced iRANK (iRANK+CID) or hRANKL-induced RAW264.7 cells (RAW264.7+hRANKL). *p<0.001

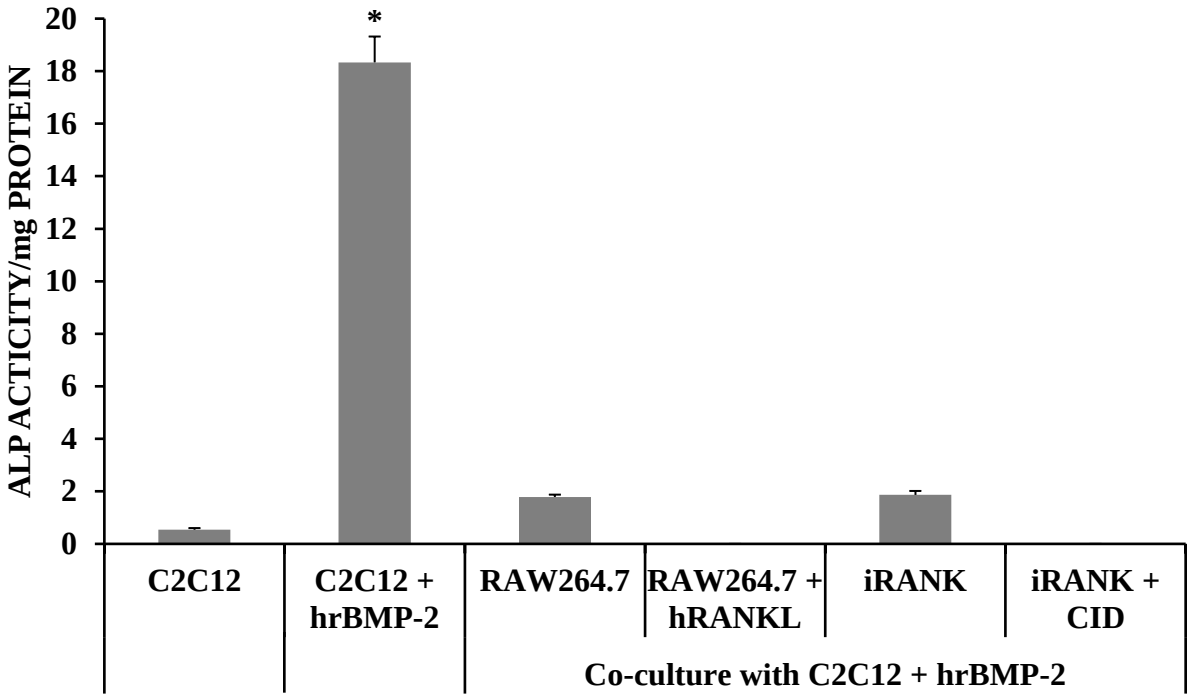

Figure 4.6. C2C12 cells had lower ALP activity when co-cultured with precursor cells or osteoclasts.

ALP activity was not detected when C2C12 cells were co-cultured with osteoclasts in the presence of 100 ng/mL hrBMP-2. Co-culture of precursor cells with C2C12 had significantly lower ALP activity compared to the positive control (C2C12+hrBMP-2). *p<0.001

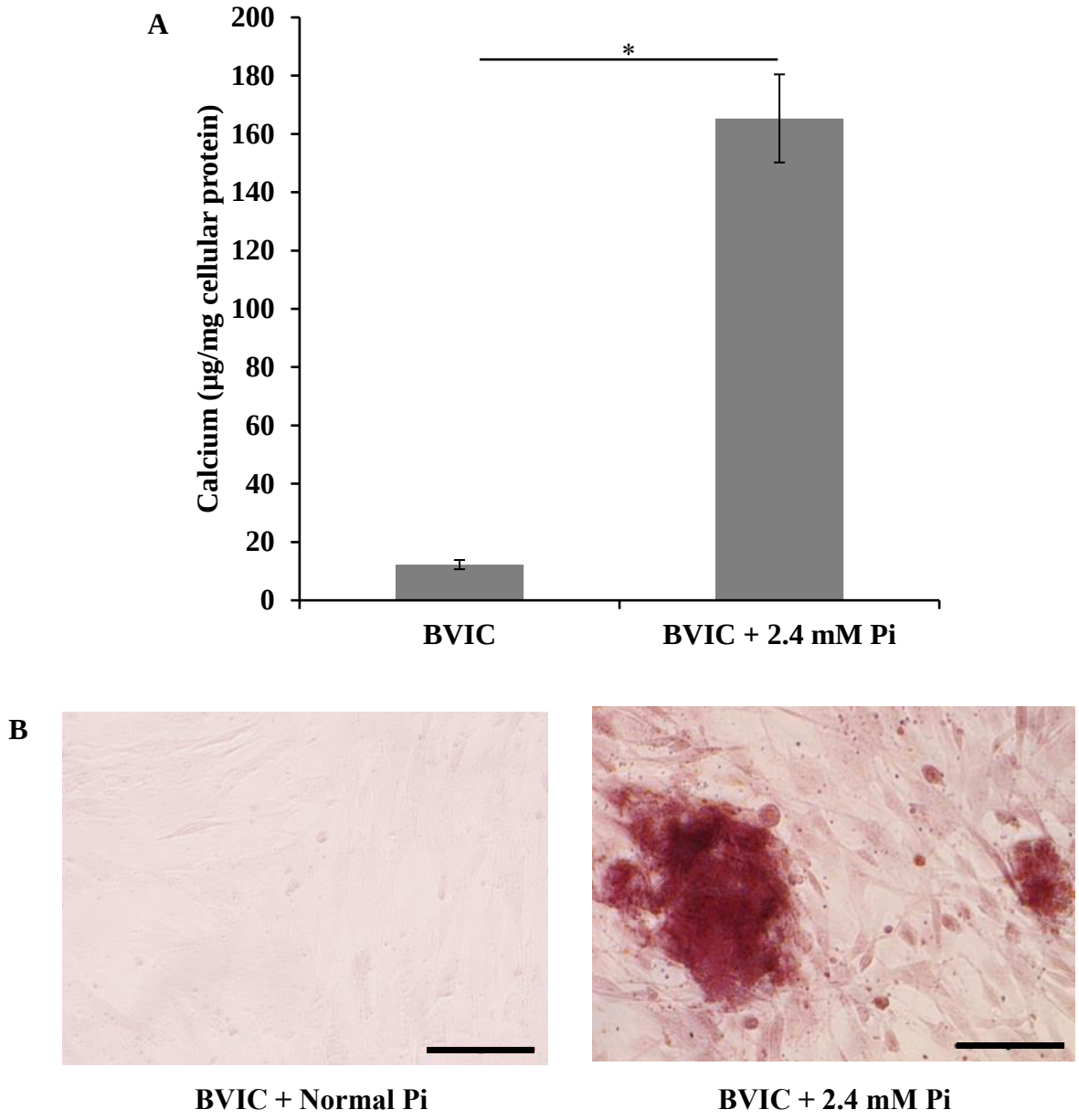

Figure 4.7. High Pi induced calcium deposition in BVIC culture.

(A) Significant calcification was induced when BVICs were cultured in the media containing 2.4 mM Pi for 7 days. *p<0.001.

(B) Alizarin Red S staining showing calcium deposition in BVICs cultured for 7 days in the presence of 2.4 mM Pi. Scale bar = 400 µm

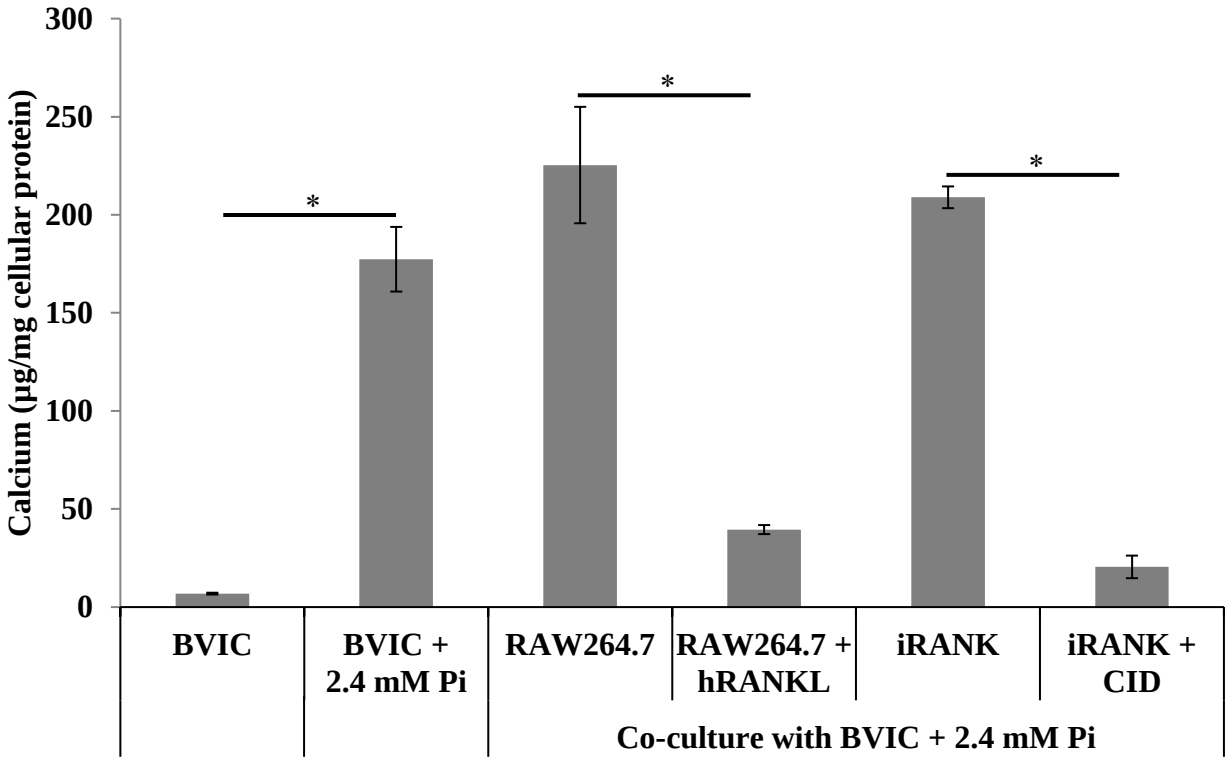

Figure 4.8. Engineered osteoclasts inhibited BVIC calcification in co-culture.

The BVIC culture experienced significantly less calcification when co-cultured with CID-induced iRANK (iRANK+CID) or hRANKL-induced RAW264.7 cells (RAW264.7+hRANKL). *p<0.001

CHAPTER 5.
ROLE OF OSTEOCLAST-DERIVED OSTEOPONTIN IN PREVENTING CALCIFICATION

We proposed that osteoclasts not only physically resorb pre-existing mineral, but also actively prevent calcification by elaborating anticalcific factors. In chapter 4, we showed that engineered osteoclasts could prevent high Pi-induced calcification of both C2C12 cells and BVICs without cell contact. In this chapter, we hypothesize that a mechanism by which osteoclasts could prevent mineral accumulation is by releasing anticalcific factors that bind to calcium phosphate mineral and prevent crystal growth.

5.1 INTRODUCTION

5.1.1 *Osteopontin (OPN)*

Possible calcification inhibitory molecules secreted from osteoclasts include OPN, BMP-3 and sclerostin.[56–58] The candidate molecule secreted by osteoclasts to prevent mineralization is OPN, a secreted non-collagenous phosphorylated glycoprotein involved in the regulation of bone development and pathological calcification.[17] The function of OPN as a potent inhibitor for mineral deposition is well studied both *in vitro* and *in vivo*. OPN is secreted by many cell types including osteoblasts, osteoclasts and macrophages[97], and is a potent inhibitor of mineralization, ectopic calcification, and vascular calcification.[17,58,98] OPN regulates mineralization by binding to hydroxyapatite and calcium ions thereby physically inhibiting crystal formation and growth.[99] OPN also plays a role in osteoclast differentiation and osteoblast recruitment and function.[99] In addition, OPN appears to promote osteoclast function through the ligation of the $\alpha_v\beta_3$ integrin.[99,100] Proteomic analysis of secreted proteins during osteoclast differentiation showed the

upregulation of OPN in two-dimensional gel electrophoresis.[75] This suggests that during osteoclast differentiation, OPN secretion is induced by osteoclasts themselves to help bone resorption. Moreover, previous studies by our group have shown that OPN dose-dependently inhibited calcification of bovine aortic SMC and HSMC cultures.[101,102] Our group also demonstrated that phosphorylation is required for the inhibitory effect of OPN.[102] Furthermore, OPN was shown to inhibit ectopic calcification *in vivo*.[17] Mice deficient in both OPN and matrix Gla protein (MGP) had 2 to 3 times higher arterial calcification than MGP knockout mice, suggesting an inhibitory effect of OPN in vascular calcification.[103] Additionally, many studies have reported that OPN is abundant at sites of calcification in human atherosclerotic plaques and in calcified aortic valves.[100]

5.1.2 *Exosomes*

Exosomes belong to a large family of membrane vesicles referred to as extracellular vesicles (EVs), which generally include microvesicles (100–350 nm), apoptotic blebs (500–1000 nm) and exosomes (30–150 nm).[104] These extracellular vesicles are believed to be involved in many biological processes and play major roles in intercellular communication.[105] As shown in **Figure 5.1**, exosomes have a characteristic lipid bilayer which has an average thickness of ~5 nm.[104] The lipid components of exosomes include ceramide, cholesterol, sphingolipids, and phosphoglycerides with long and saturated fatty-acyl chains. The outer surface of exosomes is rich in saccharide chains, such as mannose, polylactosamine, alpha-2,6 sialic acid, and N-linked glycans.[104]

Proteins found on the surface and in the core of exosomes are one of the most important cargoes that exosomes carry. Exosomal surface markers include TSG101, Alix, flotillin 1, tetraspanins (CD9, CD63, CD81), integrins, and cell adhesion molecules (CAM). Proteins

typically found in exosomes which serve as good biomarkers for the isolation and quantification of exosomes include platelet derived growth factor receptor, lactadherin, transmembrane proteins and lysosome associated membrane protein-2B, annexins, flotillins, GTPases, heat shock proteins, tetraspanins, as well as lipid-related proteins and phospholipases.[104–107] However, only a small fraction of proteins are cell-specific, reflecting the type and pathophysiological conditions of those secreting cells. Exosomes also carry nucleic acids including deoxyribonucleic acids (DNA), coding and non-coding ribonucleic acid (RNA), messenger RNA (mRNA) and microRNA (miRNA).[104–106,108]

Exosomes have received tremendous attention in recent years due to the fact that the biological fingerprints of exosomes practically mirror those of the parental cells they originate from.[104] Moreover, they provide a valuable tool for both diagnostic and therapeutic purposes.[106] Exosomes have the exceptional ability to interact and deliver their payload to target cells. Additionally, several studies indicate that exosomes can be used to target disease tissues and/or organs.[106]

Osteoclasts are among a variety of cells that are known to secrete exosomes. Common protein markers of exosomes, including CD63, EpCAM, TSG101 and HSP70 and β-actin, have been identified in osteoclast-derived exosomes.[105,107–109] Proteins that are not detected in exosomes are common contamination markers of exosome preparation including TFIIB, lamin A/C, calnexin and GP96.[105,107]

In this chapter, we first measured OPN levels released by engineered osteoclasts in culture media compared to their precursor cells. To further verify whether the ability of engineered osteoclasts to prevent calcification is due to OPN, we depleted OPN from conditioned media of iRANK osteoclasts and used the OPN-depleted media to culture C2C12

cells in the presence of high Pi and to culture human HO samples. We hypothesize that iRANK osteoclast conditioned media lacking OPN could not inhibit C2C12 calcification and could not prevent progressive mineralization of human HO samples. We used Western blot analysis to identify different forms of OPN present in conditioned media from iRANK osteoclasts. Finally, we detected OPN expression in iRANK osteoclast-derived exosomes and compared to OPN present in the conditioned media.

5.2 MATERIALS AND METHODS

5.2.1 *iRANK cell culture*

Engineered iRANK cells were cultured in α-MEM containing 10% FBS and 100 U/mL of P/S in the absence or presence of 50 nM CID to induce osteoclast differentiation. At day 5, media was replaced with DMEM containing 3% FBS and 100 U/mL of P/S. The media was collected, centrifuged to remove cells and filtered through a 0.22 μM filter (Fisher Scientific) every day for 4 days and stored at -20ºC for ELISA.

5.2.2 *Osteopontin enzyme-linked immunosorbent assay (OPN ELISA)*

Culture media of CID-treated and untreated iRANK cells was subjected to OPN ELISA following the manufacturer's instructions (Mouse Osteopontin DuoSet, R&D Systems). Briefly, polystyrene flat-bottomed microtiter plates (Thermo Fisher Scientific) were coated with 0.8 μg/mL of capture antibody (goat anti-mouse OPN antibody) in PBS overnight at room temperature. The wells were washed three times with wash buffer (0.05% Tween 20 in PBS), and were blocked with reagent diluent (1% bovine serum albumin in PBS). After washing the plates three times, two-fold serial dilutions of standard in reagent diluent (15.625-1,000 pg/mL of OPN) and samples (diluted in reagent diluent) were added in duplicate to the wells together with

culture media as the negative control. The microplates were incubated for 2 hours at room temperature. After washing the plates three times, the detection antibody (biotinylated goat anti-mouse OPN) was added to each well and incubated for 2 hours at room temperature. Following the washing step, streptavidin conjugated to horseradish-peroxidase was added and incubated for 20 minutes at room temperature. The wells were washed with wash buffer three times. Substrate solution was added to each well and incubated for 20 minutes in the dark. Stop solution was added to each well and finally the optical density of each well was measured using a microplate reader at 450 nm and 540 nm absorption wavelengths.

5.2.3 *Immunodepletion of OPN from conditioned media*

Dynabeads Protein G (1.5 mg) (Life Technologies) were incubated with OP-199 antibody[101,102] (10 μg) or isotype control antibody (normal goat IgG) with rotation for 30 minutes at room temperature in an Eppendorf tube. The tube was then placed on the magnet and the beads-Ab complex was washed with PBS with Tween 20 twice. Conditioned media from CID-treated iRANK cells (1 mL) was added to the Dynabead-Ab complex and incubated with rotation for 1 hour at room temperature. The tube was placed on the magnet and conditioned media was then transferred to a clean tube and filtered before adding to C2C12 cultures.

5.2.4 *Osteoclast conditioned media and C2C12 culture*

iRANK cells were cultured in α-MEM containing 10% FBS and 100 U/mL of P/S in the absence or presence of 50 nM CID to induce osteoclast differentiation. At day 5, media was replaced with DMEM containing 3% FBS and 100 U/mL of P/S. Conditioned media was collected, centrifuged to remove cells and filtered through a 0.22 μM filter. OPN was then removed from one group of the conditioned media with OP-199 antibody as described above.

Conditioned media was added to C2C12 culture in 1:1 ratio of conditioned media to fresh media. Next, $Na_2PO_4/NaPO_4$ (pH=7.4) was added to C2C12 cultures to obtain 3.2 mM final concentration of Pi. The media was replaced and transferred every day. At day 5 of C2C12 culture, calcium content of C2C12 cells was quantified as previously described in chapter 4.

5.2.5 *Osteoclast conditioned media and human HO model*

Human HO samples were obtained at surgery for excision of clinically significant HO or at secondary surgery for reconstructive procedures required for clinical care. The HO tissues were stored in 70% EtOH before being sectioned into 600 μm slices using a Buehler low speed saw equipped with a diamond wafering blade. A biopsy punch was used to create 6 mm diameter discs, cleaned by sonication in 70% EtOH for 5 minutes, twice, and lyophilized. A baseline bone volume of each disc was measured by microCT before experiment. To determine whether OPN derived from engineered osteoclasts could prevent the progression of passive mineralization of human HO samples, human HO discs were cultured in DMEM supplemented with 10% FBS and 100 U/mL of P/S, conditioned media from iRANK cells, conditioned media from engineered osteoclasts, or OPN-depleted conditioned media from engineered osteoclasts. The media and conditioned media were replaced with fresh media as previously described every day for 5 days. Discs were rinsed with distilled water and lyophilized for measurement of bone volume by microCT. The percent change in bone volume of each HO sample was calculated and analyzed.

5.2.6 *Detection of OPN by Western blotting*

Conditioned media from iRANK and iRANK osteoclasts were collected and spun down at 1,000 rpm for 5 minutes. Conditioned media and recombinant mouse OPN (R&D Systems) were separated via gel electrophoresis on a 10% SDS-PAGE gel and transferred to a PVDF

membrane. Amido black staining was used to confirm equal loading. Membranes were rehydrated in methanol for 1 minute, then washed twice with low salt TRIS-buffered saline (TBS). Membranes were then blocked with 5% normal donkey serum (NDS) (Jackson ImmunoResearch) + 0.1% Tween in low salt TBS at room temperature for 1 hour. Membranes were incubated with 0.1 µg/mL or 0.2 µg/mL goat anti-mouse OPN antibody (R&D Systems) diluted in blocking buffer for 1 hour at room temperature and were washed twice in high salt TBS-Tween/Triton and once in low salt TBS. Next, membranes were incubated with the secondary antibody (Donkey Anti-goat-horse radish peroxidase (HRP) from Jackson ImmunoResearch) diluted 1:40,000 or 1:12,000 in blocking buffer for 1 hour at room temperature. Finally, membranes were washed 4 times in high salt TBS-Tween/Triton. SuperSignal West Dura Extended Duration Substrate (Thermo Fisher Scientific) or Pierce ECL Western blotting substrate (Thermo Fisher Scientific) was used to detect HRP according to manufacturer's protocol. Membranes were finally exposed to X-ray films.

5.2.7 *Isolation of osteoclast-derived exosomes*

iRANK cells were cultured in α-MEM containing 10% FBS and 100 U/mL of P/S and incubated at 37°C with 5% CO_2. Cells were plated at 100,000 cells/well in 6-well plates. Four hours after seeding, iRANK cells were induced to differentiate into osteoclasts with 50 nM CID. The supplemented media was changed every other day. At Day 5, the media was changed to α-MEM containing 10% exosome-depleted FBS and 100 U/mL of P/S. After 24 hours, the culture supernatant was collected and centrifuged for 20 minutes at 2000 x g and 4°C to remove dead cells. The supernatant was then transferred to the Ultra-Clear™ Tube #344058 (Beckman Coulter) and centrifuged at 10,000 x g and 4°C for 30 minutes in the Optima L-100 XP

ultracentrifuge (Beckman Coulter) equipped with an SW 32 Ti rotor to remove cell debris. The supernatant was recovered and spun at 100,000 x g and 4°C for 90 minutes. The supernatant was transferred to the new tubes and the exosome pellets were resuspended in PBS. Nanoparticle tracking analysis was performed using the Nanosight NS300. Exosomes were lysed with 1X modified RIPA buffer and centrifuged at 10,000 x g and 4°C for 5 minutes. Lysed exosomes and culture supernatant recovered after exosome isolation were subjected to OPN ELISA following the manufacturer's instructions.

5.2.8 *Nanoparticle tracking analysis*

Nanoparticle tracking analysis was performed using the light scattering mode of the Nanosight NS300 (Malvern). Samples were diluted with PBS and loaded into the machine. Captured videos and average size distribution graphs were created.

5.2.9 *Statistical analysis*

Results are expressed as mean ± SEM, n=3 for all experiments unless otherwise indicated. SPSS software v16.0 was used to perform Student's *t*-test to compare means of two individual groups, and one-way ANOVA with post-hoc Tukey test to compare means of three or more individual groups. A value of $p<0.05$ was considered statistically significant.

5.2.10 *Ethics statement*

The human tissues were obtained from Harborview Medical Center, Seattle, WA. The explanted HO specimens from patients that would otherwise be surgically discarded were de-identified. The University of Washington (UW) Institutional Review Board (IRB) determined that the project does not involve human subjects whom an investigator conducting research

obtains data through intervention or interaction with the individual or identifiable private information.

5.3 RESULTS

5.3.1 *OPN was secreted at high levels by engineered osteoclasts.*

In an attempt to identify the specific osteoclast-derived inhibitory factors responsible for the observed HO preventative activity, we first examined OPN as a candidate protein. We found that secreted OPN protein levels were significantly elevated (~16 fold) in engineered osteoclasts compared to iRANK cells (**Figure 5.2**). Furthermore, we were able to efficiently deplete OPN from the media using an anti-OPN antibody (**Figure 5.2**, iRANK+CID OPN-depleted).

5.3.2 *Depletion of OPN from conditioned media significantly reduced its ability to inhibit calcification.*

To determine whether OPN is required for the inhibitory effect of osteoclasts on C2C12 calcification, we performed a conditioned media experiment. Conditioned media from iRANK cells and engineered osteoclasts were transferred every day to C2C12 culture in the presence of 3.2 mM Pi. Addition of engineered osteoclast-derived conditioned media to mineralizing C2C12 cells resulted in a significant reduction of C2C12 calcification compared to conditioned media from iRANK precursor cells (**Figure 5.3**, iRANK vs iRANK+CID). This result is similar to the co-culture study of engineered osteoclasts with C2C12 cells (**Figure 4.5**). Engineered osteoclast conditioned media incubated with isotype control antibody also resulted in a reduction of C2C12 calcification (**Figure 5.3**, iRANK+CID + NG IgG). On the other hand, OPN-depleted engineered osteoclast-derived conditioned media could no longer inhibit C2C12 calcification (**Figure 5.3**,

iRANK+CID OPN-depleted). These data suggest that depletion of OPN from the conditioned media negated the inhibitory effect of the conditioned media in C2C12 cultures.

5.3.3 *Depletion of OPN from conditioned media significantly reduced its ability to prevent progressive mineral growth of human HO.*

Our preliminary data showed that human HO samples had increased bone volume when cultured in DMEM containing 10% FBS for 5 days or more (**Figure 5.4**, Control media). This result suggests the passive growth of mineral on nucleation sites present in human HO samples when incubated in physiological solutions containing Ca^{2+} and Pi.[110] In this study, we determined whether engineered osteoclast derived-OPN could block progression of mineralization on pre-nucleated sites of human HO samples. As shown in **Figure 5.4**, human HO samples treated with engineered osteoclast conditioned media showed significantly less bone volume growth compared to samples treated with control media or conditioned media collected from iRANK precursor cells. Importantly, the inhibitory effect of the engineered osteoclast conditioned media in human HO growth was lost when OPN was depleted from the conditioned media (**Figure 5.4**, iRANK+CID OPN-depleted). Together, these data suggest that engineered osteoclast-derived OPN could block cell-mediated osteochondrogenic calcification *in vitro*, as well as prevent the passive progression of mineralization of nucleation sites on human HO samples.

5.3.4 *Specific forms of OPN were present in iRANK osteoclast conditioned media.*

OPN is a multifunctional, phosphorylated glycoprotein that has been intensively investigated by our group and others.[17,58,98,99] OPN is known to be a substrate for proteolytic cleavage by the proteases thrombin[111,112], enterokinase[113], matrix metalloproteinase (MMP)

family (MMP-3, MMP-7 and MMP-12)[114,115]. In addition, functional properties of thrombin-cleaved and MMP-cleaved OPN differ from the intact protein[115], demonstrating that proteolytic cleavage is one mechanism of regulating the bioactivity of OPN. MMP-cleaved OPN and thrombin-cleaved OPN have increased activity in promoting both cell adhesion and migration compared with full-length OPN.[115,116] These data suggest that active forms of OPN and the differences in activity of modified OPN are regulated by the activity of proteases.

To begin to identify the specific forms of OPN present in iRANK osteoclast conditioned media, we performed Western blot analysis with an anti-OPN antibody. As shown in **Figure 5.5**, several OPN peptides of various molecular weights were identified in conditioned media derived from iRANK osteoclasts that were not present in iRANK precursor cells (lane 2 and 3 vs lane 4 to 6). Putative full length OPN was found as a doublet at ~60 and 66 KD.[117] We also found two unique OPN peptides, one <~20 kDa and another between ~20 and ~25 kDa, which are different from MMP generated fragments that were previously identified with molecular weights of ~28, 32, and 40 kDa.[114,115,118] Together, these studies point to unique osteoclast-derived OPN peptides as candidate therapeutic agents to prevent or inhibit progression of HO.

5.3.5 *A unique form of OPN was detected in iRANK osteoclast-derived exosomes.*

In an attempt to identify factors accounting for the inhibitory activity against calcification, we have discovered that osteoclasts release an abundance of exosomes. Media conditioned by iRANK osteoclasts was fractionated by differential centrifugation to isolate nanoparticulate exosomes as previously described.[119] Nanoparticle tracking analysis shown in **Figure 5.6** confirmed abundant exosomes in iRANK osteoclast conditioned media (~15,000 EVs per cell), with particle size mode ~145 ± 1.6 nm. Our lab was also one of the first to identify OPN, as a major component of osteoclast-derived exosome (15.67 ng/mL of exosomes), which

was recently confirmed by second group while our studies were in progress.[120] The presence of OPN on exosomes is of particular interest, since we have shown that OPN has an inhibitory effect against calcification. Furthermore, we identified a unique form of OPN expressed in iRANK osteoclast-derived exosomes at a molecular weight of ~15 kDa which is different than the OPN found in iRANK osteoclast conditioned media (**Figure 5.7**).

5.4 DISCUSSION

OPN is an excellent candidate molecule due to its high levels of secretion by osteoclasts.[97] OPN also regulates mineralization by binding to hydroxyapatite and calcium ions thereby physically inhibiting crystal formation and growth.[99] Moreover, the function of OPN as a potent inhibitor for mineral deposition is well studied both *in vitro* and *in vivo*.[17,101,102] Previous studies have shown that OPN dose-dependently inhibited calcification of bovine aortic SMC and HSMC cultures.[101,102] Jono S. *et al* demonstrated that phosphorylation is required for the inhibitory effect of OPN.[102] Furthermore, OPN was shown to inhibit ectopic calcification *in vivo.*[17] A co-culture study by Li X. *et al* showed that the treatment of macrophages with Vitamin D led to the OPN-dependent inhibition of SMC calcification.[121]

In the present study, we demonstrated that OPN levels secreted from CID-induced osteoclasts were significantly higher than untreated cells. We showed that OPN plays in an important role in inhibiting cell-mediated calcification, as well as preventing passive mineralization of human HO samples. Moreover, we identified specific forms of OPN present in conditioned media from iRANK osteoclasts. Interestingly, a different form of OPN was detected in osteoclast-derived exosomes. Together, these studies point to unique OPN peptides as candidate therapeutic agents to prevent or inhibit calcification and progression of HO. OPN undergoes splicing as well as post-translational modifications, including phosphorylation and

proteolytic cleavage, all of which regulate its activity.[99] Phosphorylation is particularly important for its mineral binding and anticalcific activity.[102] Future studies are needed to identify and characterize the specific OPN peptides that has this inhibitory ability. These studies can lead to a protein therapeutic which has several advantages over a cell therapy for use in battlefield medicine. OPN peptides could be formulated as a lyophilized product resulting in a product with a longer shelf-life, less stringent storage requirements and easier administration compared to a cell-based therapy. Additionally, future studies are needed to identify other potential osteoclast-derived inhibitory factors. Secreted proteins in the conditioned media can be analyzed using mass spectrometry to identify these candidate proteins.[122]

In conclusion, our studies are the first to suggest that osteoclasts function not only to resorb mineralized matrix through physical contact, but also to prevent cell-mediated calcification and progression of mineralization of nucleation sites, at least in part, by elaborating OPN, a potent inhibitor for mineral deposition. Future studies are needed to identify specific forms of OPN that have inhibitory activity and to identify other osteoclast-associated anticalcific molecules that play a role in preventing calcification.

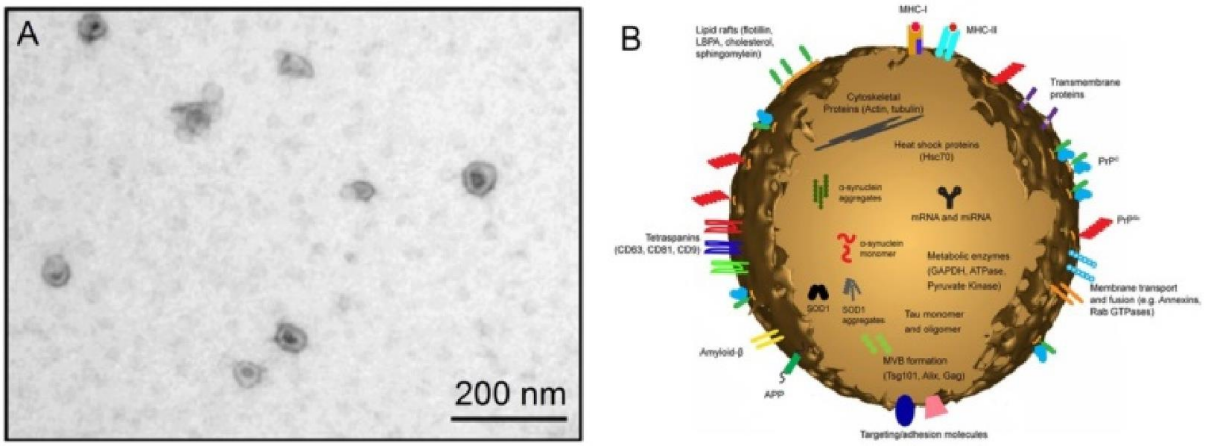

Figure 5.1. Image and diagrammatic representation of exosomes [104]

(A) An electron microscopic image of exosomes and (B) a diagrammatic representation of a medium size exosome

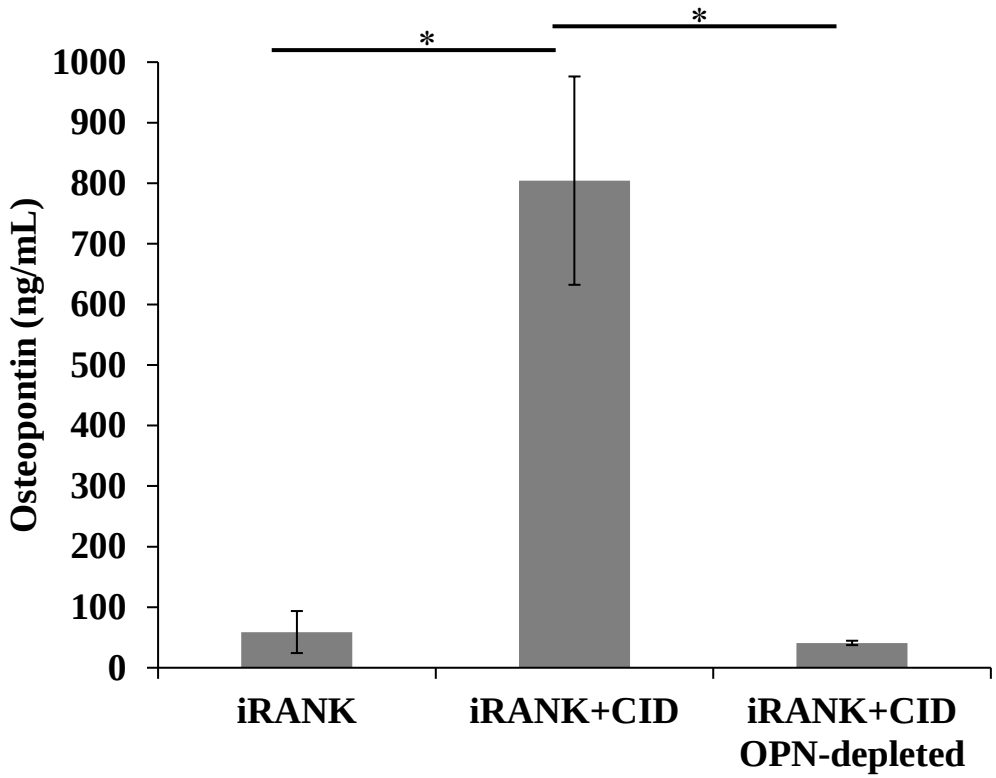

Figure 5.2. Engineered osteoclasts secreted more OPN in culture media than their precursor cells.

Untreated iRANK cells (iRANK) secreted significantly less OPN than CID-induced iRANK cells (iRANK+CID). OPN was depleted from media using OP-199 antibody (iRANK+CID OPN-depleted). *p<0.001

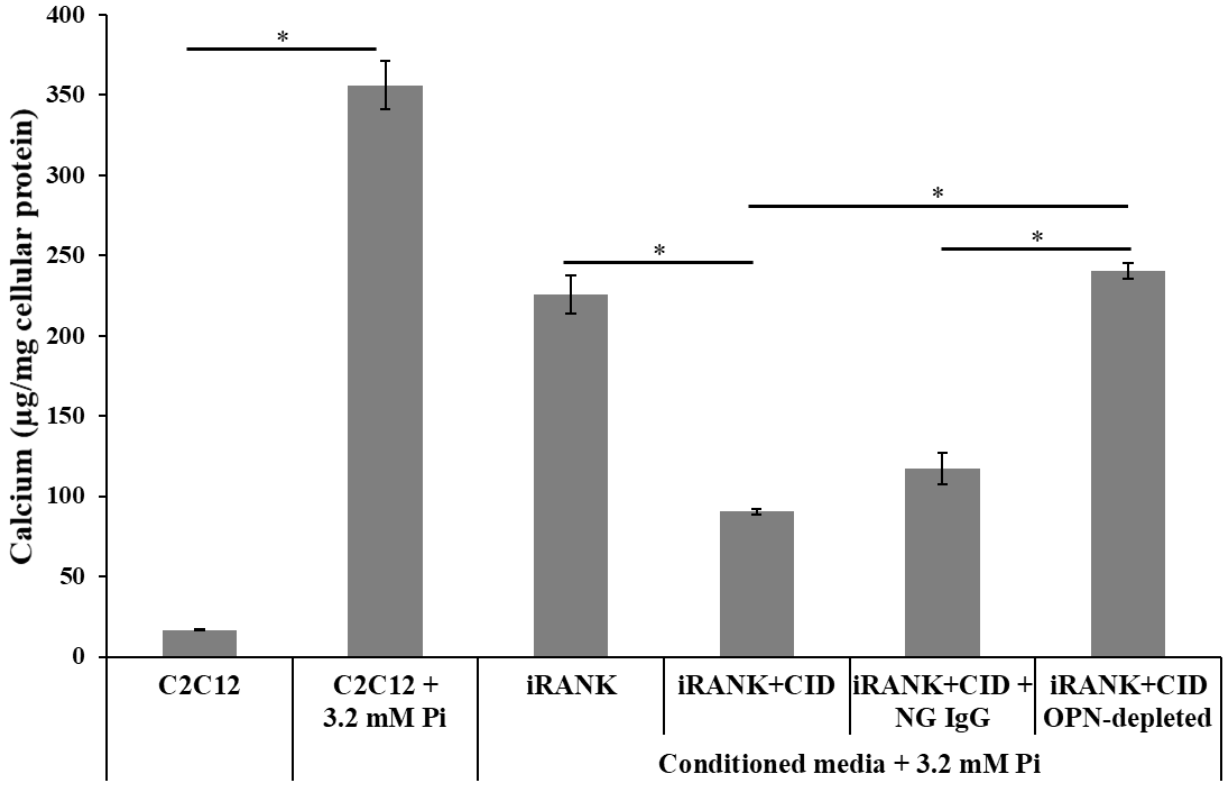

Figure 5.3. Depletion of OPN from conditioned media reduced its ability to inhibit C2C12 calcification.

Conditioned media from CID-induced iRANK cells (iRANK+CID) inhibited C2C12 calcification in a similar manner to previous co-culture experiments. Removal of OPN with OP-199 antibody eliminated the protective effect of engineered osteoclast conditioned media on C2C12 calcification (iRANK+CID OPN-depleted). Normal Goat IgG (NG IgG) was used as an isotype control for OP-199 antibody. *p<0.001

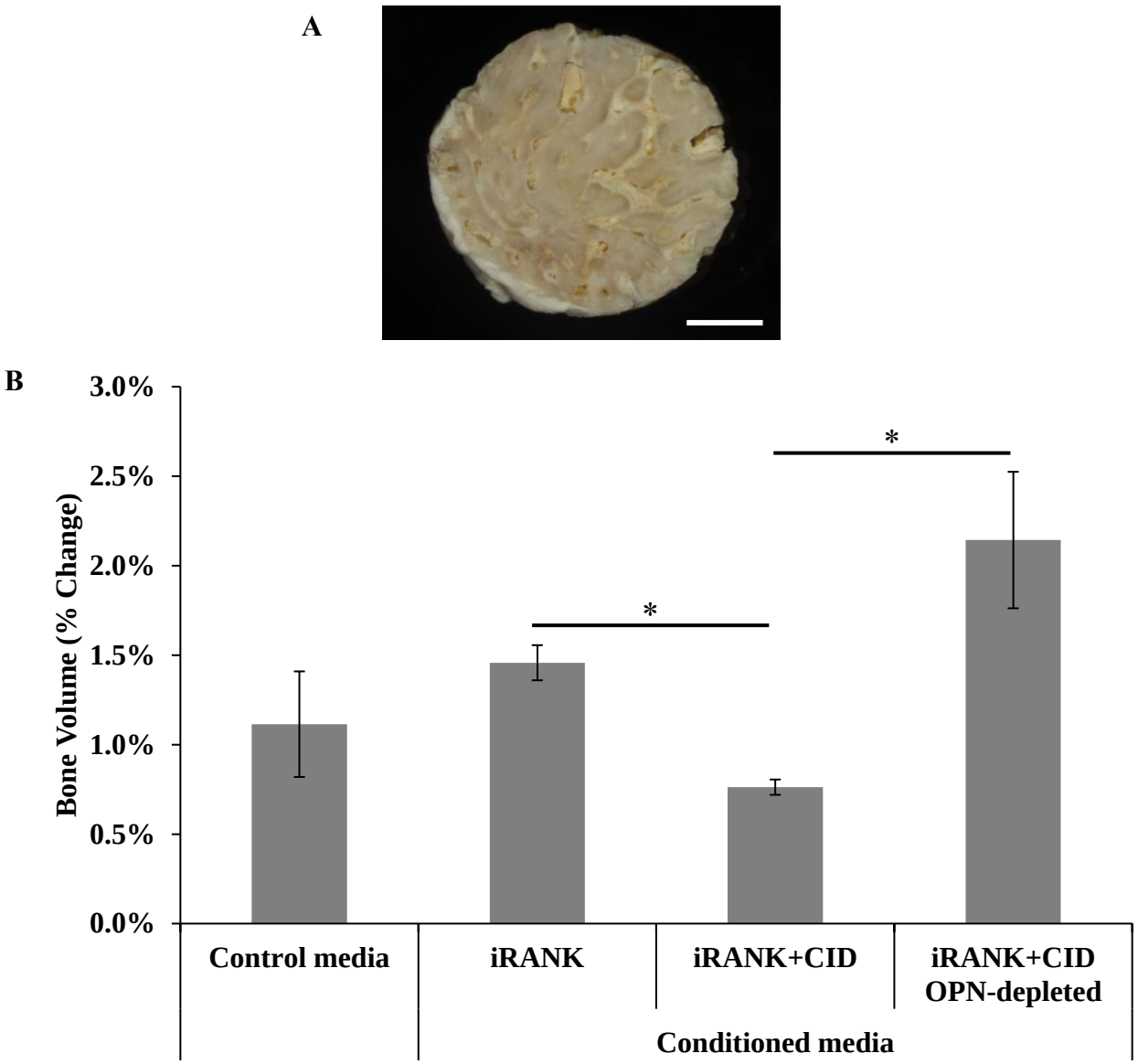

Figure 5.4. OPN secreted by engineered osteoclasts prevented progressive mineral growth of human HO.

(A) Representative image of a 6-mm diameter human HO sample. Scale bar = 2 mm

(B) Similar to C2C12 studies, treatment of human HO discs with conditioned media from CID-induced iRANK cells inhibited bone volume growth, whereas OPN-depletion of conditioned media could not prevent progressive mineralization. n=5; *p<0.05

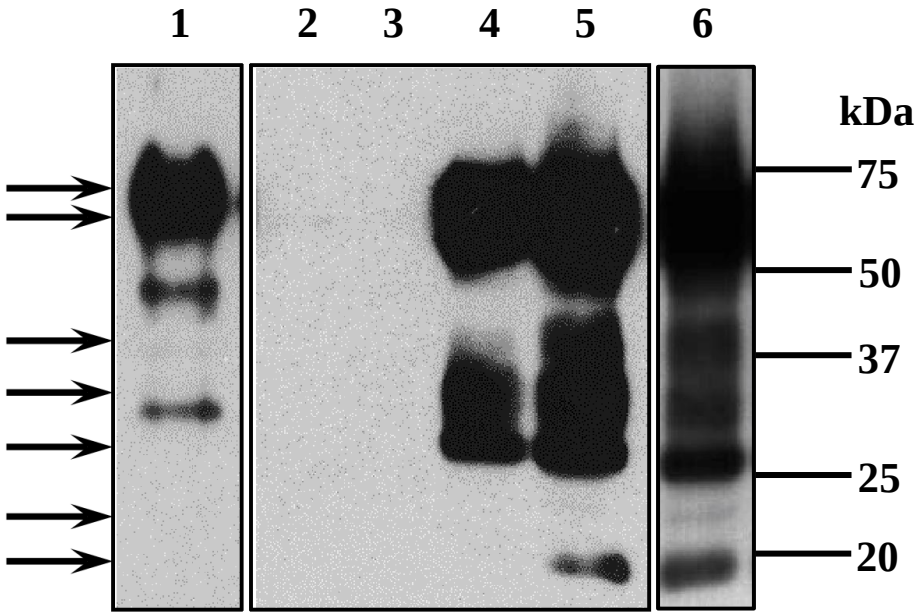

Figure 5.5. Specific forms of OPN were present in iRANK osteoclast conditioned media.

Western blotting of conditioned media collected from iRANK cells (lane 2 and 3) and iRANK osteoclasts (lane 4 to 6). Lane 1 is 2.4 µg of recombinant mouse OPN. Lane 2 and 4 are conditioned media at day 5 with protease and phosphatase inhibitors. Lane 3 and 5 are conditioned media at day 5 without inhibitors. Lane 1 to 5 were detected with more sensitive (femtogram level) SuperSignal West Dura Extended Duration Substrate. Lane 6 is iRANK osteoclast conditioned media at day 5 detected with less sensitive (picogram level) Pierce ECL Western blotting substrate. Arrows designate the unique forms of OPN produced by iRANK osteoclasts.

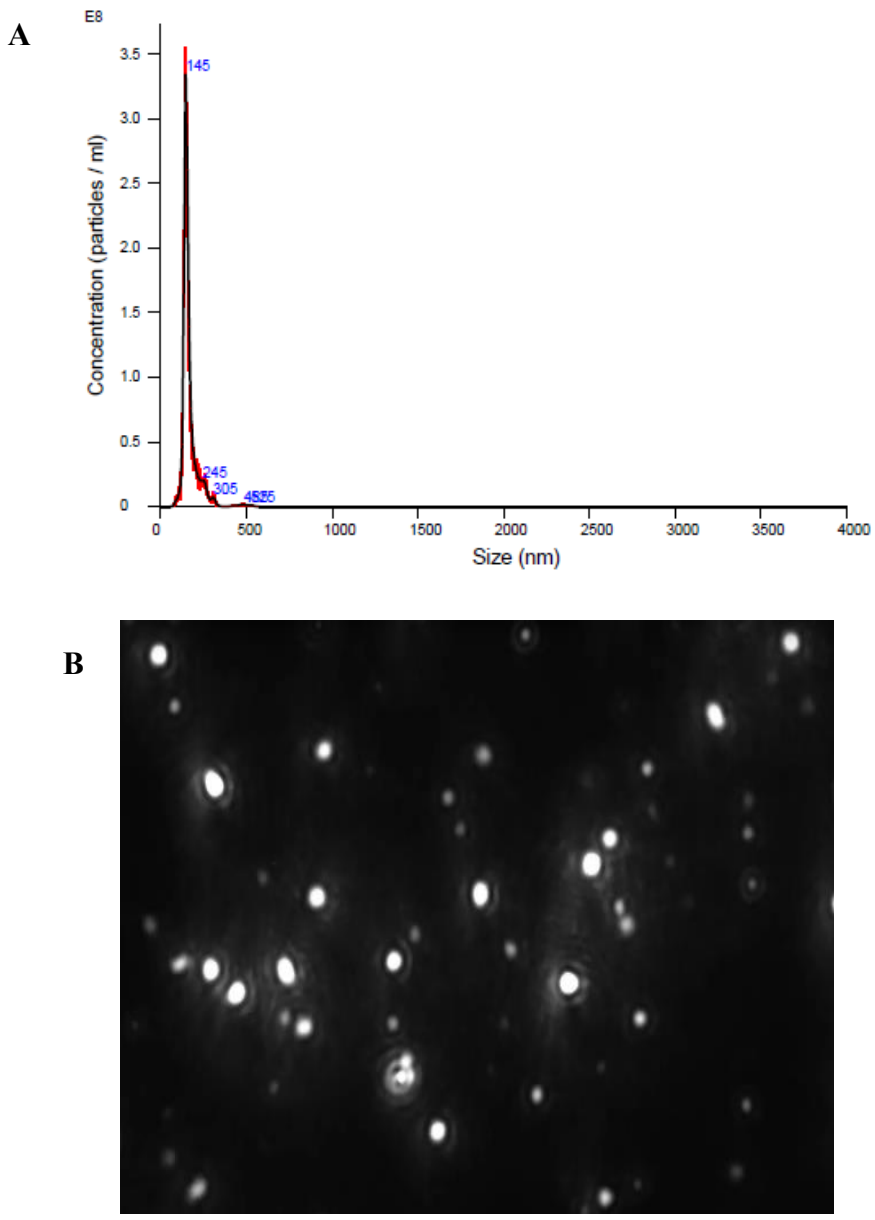

Figure 5.6. Nanoparticle tracking analysis confirmed abundant exosomes derived from iRANK osteoclast conditioned media.

(A) ~15,000 exosomes per iRANK cell with particle size mode ~145 ± 1.6 nm were detected.

(B) A representative image showed exosome particles detected by Nanosight NS300.

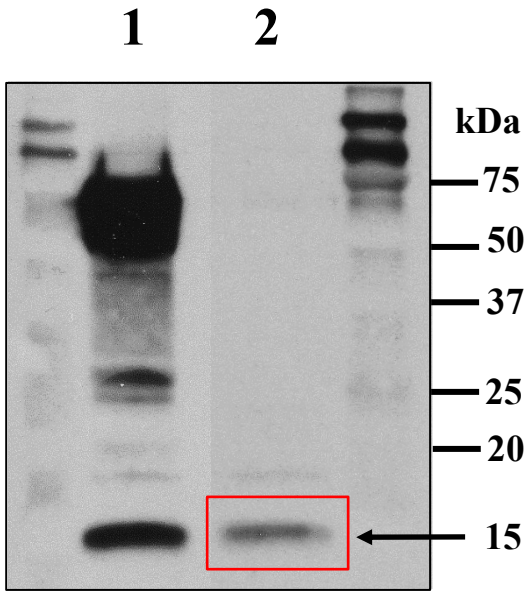

Figure 5.7. A unique form of OPN was detected in iRANK osteoclast-derived exosomes.

One strong band of OPN at ~15 kDa was expressed in iRANK osteoclast-derived exosomes (lane 2). Lane 1 is the positive control (589 pg of recombinant mouse OPN). Chemiluminescent signal was detected with Pierce ECL Western blotting substrate.

CHAPTER 6.
OSTEOCLASTS AND MEDICATION-RELATED OSTEONECROSIS OF THE JAW

In this chapter, we outline the role of osteoclasts in the development of MRONJ, focusing on the loss of their bone resorptive function due to antiresorptive drugs. *We hypothesize that delivering engineered osteoclasts that are resistant to inhibition by antiresorptive drugs may promote the bone healing process following tooth extraction.* This study provides a novel paradigm for the mechanism and pathophysiology of MRONJ. Moreover, this study is the first to provide proof of concept data suggesting that osteoclast cell therapy may be a promising strategy for treatment and/or prevention of this disease in patients.

We first determined whether engineered osteoclasts are resistant to inhibition by anti-mouse RANKL antibody, a mouse analogue of denosumab. Then, we developed an *in vivo* model of MRONJ in nude mice. We also validated methods for delivering iRANK cells and determined whether iRANK cells can form osteoclasts in response to CID *in vivo*. These studies serve as basis for future experiments to determine whether engineered osteoclasts can prevent the development of MRONJ *in vivo* through delivery of engineered cells after tooth extraction in nude mice receiving anti-mouse RANKL antibody treatment.

6.1 INTRODUCTION

6.1.1 *Medication-related osteonecrosis of the jaw (MRONJ)*

MRONJ, which was first described in 2003, is a potentially serious side effect of treatment with antiresorptive and antiangiogenic medications that often occurs in the oral cavity after dental-related interventions such as tooth extraction.[3,43] These antiresorptive medications,

BPs and denosumab, are used to decrease the risk of skeletal-related events (SREs) in patients with cancer and metabolic bone disease, such as osteoporosis.[3] MRONJ is clinically defined as an area of exposed and necrotic bone that has persisted more than eight weeks with no history of radiation therapy.[43,44] Initially, lesions are asymptomatic but may become symptomatic when the surrounding tissues become inflamed. MRONJ incidence in patients with cancer receiving intravenous BPs is reported to range from 2% to 15%[45,46], whereas MRONJ development in osteoporotic patients still remains controversial. Two recent randomized clinical trials showed that the incidences of BP-related and denosumab-related ONJ were comparable in cancer patients, suggesting that ONJ induced by both drugs adversely affects patients' quality of life and produces significant morbidity.[45,46]

6.1.2 *Denosumab and bisphosphonates*

Denosumab is a human monoclonal antibody that binds to RANKL and prevents RANKL from activating its receptor, RANK, on the surface of osteoclasts and their precursors.[7] Prevention of the RANKL/RANK interaction inhibits osteoclast formation, function, and survival, thereby decreasing bone resorption and increasing bone mass and strength in both cortical and trabecular bone.[50,51,123] In contrast to denosumab, many potential mechanisms by which BPs inhibit osteoclastic bone resorption have been proposed. BPs, attached to hydroxyapatite on bony surfaces, are impregnated into osteoclasts when they begin to resorb bone and impair their ability to form the ruffled border, to adhere to the bony surface, and to produce protons necessary for bone resorption.[124,125] Several studies also showed that BPs reduce osteoclast activity by decreasing osteoclast progenitor development and recruitment, and by inducing osteoclast apoptosis via the activation of caspases.[48,126,127] In addition to their inhibitory effect on osteoclasts, BPs appear to have an effect on osteoblasts. An *in vitro* study showed that

zoledronic acid (ZOL) can increase production of OPG in a dose-dependent manner from primary human osteoblasts.[128] OPG then binds to RANKL and blocks the interaction with RANK, thereby inhibiting osteoclastogenesis. Another study also demonstrated that ZOL markedly increased OPG protein secretion and reduced transmembrane RANKL protein expression in osteoblast-like cells.[129]

A key requirement of the osteoclasts to be successfully used in treating MRONJ is that they are resistant to the inhibition by antiresorptive drugs. As shown in **Figure 2.7**, CID-induced osteoclastogenesis of iRANK cells were resistant to the inhibition by OPG, a natural analogue of denosumab. Thus, in this chapter we first determined the effect of denosumab on engineered osteoclast differentiation *in vitro* before we utilized these cells *in vivo.* We hypothesize that engineered osteoclasts form TRAP-positive multinucleated cells in the presence of denosumab, in the similar manner as in the presence of OPG.

6.1.3 *Animal models of MRONJ*

Two animal models for denosumab-related ONJ have been developed. The first study tested the ability of RANKL inhibitors, RANK-Fc and OPG-FC to induce denosumab-related ONJ in mice in the presence of periapical disease, but in the absence of dental extractions.[130] Investigators found that RANK-Fc treatment and OPG-Fc treatment resulted in absence of osteoclasts, periosteal bone formation, empty osteocytic lacunae, osteonecrosis, and bone exposure. Another study is from UCLA scientists who developed *in vivo* models of both BP-related and denosumab-related ONJ by using a tooth-extraction mouse model with intravenous administration of ZOL or mouse anti-RANKL antibody.[45] They showed that after tooth extraction, ONJ-like lesions developed in 50% of anti-RANKL antibody-treated mice and in 30% of ZOL-treated mice. All mice receiving anti-RANKL antibody had undetectable TRAP

levels in the serum and no TRAP-positive osteoclasts at the extracted sockets, whereas ZOL-treated mice had a decreased TRAP levels without altering the numbers of TRAP-positive osteoclasts. These findings suggest that the lack of osteoclasts' bone-resorptive functions by these drugs and suppression of woven bone formation after dental trauma may be associated with ONJ development.

In comparison to denosumab-related ONJ, several animal models have been established for BP-related ONJ but these studies give no clear consensus about whether osteoclasts play a role in ONJ development. The study by Bi Y. *et al* showed that long-term administration of BPs in mice led to an increase in the size and number of osteoclasts and the formation of giant osteoclast-like cells within the alveolar bone[131], whereas the study by Hokugo A. *et al* showed that ONJ lesions were associated with dense accumulation of neutrophils and lymphocytes that appeared to juxtapose apoptotic osteoclasts in a BP-related ONJ rat model.[132] Another study, in which researchers developed a mouse model of BP-related ONJ by injecting animals with ZOL and performing pulpal exposure of mandibular molars, showed no difference in TRAP-positive cell numbers, but cells that were round, detached, and removed from the bone surface were present in animals receiving ZOL.[133] In addition to the aforementioned studies, some studies only focused on osteocytes but not osteoclasts in BP-related ONJ models. Aghaloo T.L. *et al* developed a BP-related ONJ animal model where aggressive periodontal disease was induced by ligature placement around the crown of the right maxillary first molar in the presence of ZOL. They demonstrated that BP-related ONJ was observed as necrotic bone with diffuse loss of osteocytes and empty lacunae, rimming of the necrotic bone by squamous epithelium and inflammation, and exposure to the oral cavity.[134] Another work by Aguirre J.I. *et al* showed that

high dose of ZOL induced ONJ-like lesions and increased osteocyte necrosis/apoptosis in mandibles of rice rat model of periodontitis.[135]

Despite the fact that numerous animal models of BP-related and denosumab-related ONJ have been developed, the role of osteoclasts in the development of MRONJ is still controversial. Direct evidence of osteoclasts' involvement and the extent to which osteoclasts contribute to MRONJ pathogenesis remains elusive. Current literature also remains inconclusive with respect to the presence, numbers, and location of mature osteoclasts.

In this study we propose to utilize engineered osteoclasts that are resistant to inhibition by denosumab in an MRONJ mouse model. This study determines whether the presence of mature osteoclasts can prevent MRONJ development and also provides a new and innovative strategy to intervene and prevent ONJ development. Preliminary data from our lab indicates that engineered osteoclasts can prevent HO formation *in vivo*. In a nude mouse model of BMP2-induced HO, engineered osteoclasts were delivered in collagen hydrogel carrier to retain cells at the site of HO initiation. When cells were activated with CID they fused to form TRAP-positive osteoclasts at the site of HO (**Figure 6.1)**. Importantly, animals receiving engineered osteoclasts with CID had significantly reduced HO lesion volume at 4 weeks compared to the 2-week time point (**Figure 6.2**).

In this chapter, we developed an *in vivo* model of MRONJ in nude mice to determine whether engineered osteoclasts can prevent MRONJ development, and focused on methods for delivering engineered cells and CID drug based on previous studies in an HO model.

6.2 MATERIALS AND METHODS

6.2.1 *Anti-RANKL antibodies and osteoclast differentiation of RAW264.7 and iRANK cells*

To determine whether engineered osteoclasts are resistant to antiresorptive drugs *in vitro*, RAW264.7 and iRANK cells were cultured in α-MEM containing 10% FBS and 100 U/mL of P/S and incubated at 37°C with 5% CO_2. RAW264.7 and iRANK cells were plated at 20,000 cells/well in 4-well Nunc™ Lab-Tek™ chamber slides. Four hours after plating, RAW264.7 cells were treated with the media containing 2 nM mouse RANKL with 0 nM, 2 nM, 5 nM or 20 nM anti-mouse RANKL monoclonal antibody (BioLegend) or 20 nM isotype control IgG rat antibody (BioLegend). iRANK cells were treated with the media containing 10 nM CID with 0 nM, 10 nM, 25 nM and 100 nM rat anti-mouse RANKL monoclonal antibody or 100 nM isotype control rat IgG antibody. Cells were cultured for 5 days with media replaced once at day 3. Cells were washed twice with PBS, fixed with 10% buffered formalin for 10 minutes and subjected to TRAP staining following the manufacturer's instructions. Slides were mounted with Aqua-Mount and images were obtained using an upright microscope (Nikon E800). The number of multinucleated TRAP-positive osteoclasts (with ≥ 3 nuclei) were quantified.

6.2.2 *In vivo mouse model of MRONJ*

Since our delivered iRANK cells are allogeneic, we used nude mice lacking T cells to prevent rejection of our engineered cells. First, we confirmed that the absence of T cells in nude mice does not affect wound healing after tooth extraction. We then developed a MRONJ model in these mice as described in previously published works.[45,130] Animals and surgical procedures were handled in accordance with Institutional Animal Care and Use Committee approval (number 2224-09). Six- to ten-week-old nude mice were randomly divided into two groups that

received either intraperitoneal injections of 10 mg/kg of rat anti-mouse RANKL monoclonal antibody or isotype control rat IgG antibody in PBS twice a week for 4 weeks. Under general anesthesia using ketamine/xylazine, the left maxillary first molar was extracted 1 week after the initial injection. A rodent molar luxator (iM3) was used to separate the gingival attachment and a 25-gauge needle was used to gently luxate the tooth. Then, a curved hemostat was used to pull the tooth out. Three weeks after tooth extraction, the mice were euthanized to harvest blood, maxilla and femur. The tissue specimens were immediately fixed in 4% paraformaldehyde in PBS, pH 7.4, at 4°C for 48 hours and stored in 70% EtOH solution. The fixed tissue specimens were first examined by micro-computed tomography (microCT) and a 3D image of the mandible was constructed to quantify changes in alveolar bone structure/architecture and volume. After microCT scanning, these tissues were decalcified with 5% EDTA and 4% sucrose in PBS, pH 7.4 for 4 to 5 weeks at 4°C. The decalcification solution was changed daily. Tissue samples were then processed for paraffin embedding and stained with TRAP solution and hematoxylin and eosin (H&E). Numbers of TRAP-positive multinucleated osteoclasts, amount of empty lacunae and necrotic bone, and new bone formation were recorded and quantified. To examine whether anti-RANKL antibody suppresses the bone remodeling process, including osteoclastic and osteoblastic activity, terminal blood was collected to measure the serum concentration of TRAP-5b and osteocalcin (OCN), biochemical markers for bone resorption and formation, respectively.[45]

6.2.3 *Delivery of iRANK cells in nude mice*

iRANK cells were cultured in α-MEM containing 10% FBS and 100 U/mL of P/S and incubated at 37°C with 5% CO_2. For each treatment, 100,000 cells in 0.5 mg/mL neutralized collagen were delivered to the socket after tooth extraction. The solution was kept on ice until

injection. Following injection, the socket was covered with Gelfoam® (Pfizer Pharmaceutical). Transduced iRANK cells with luciferase were used to visualize cells in the tooth socket.

6.2.4 *Lentiviral production and transduction of luciferase gene*

The packaging plasmids pSL3 (vesicular stomatitis virus G envelope), pSL4 (HIV-1 gag/pol packing genes) and pSL5 (rev gene required for HIV-1 envelope protein expression) were a gift from the Murry Lab and the University of Washington. The transfer plasmid pLEL (luciferase gene) was a gift from the Pun Lab at the University of Washington. The lentiviral vector was packaged in HEK293T cells as previously described[136,137] with the following modifications. Briefly, a total of 5×10^6 of HEK293T cells were seeded in 10-cm dishes treated with poly-D-lysine 24 hours prior to transfection and the culture media was changed just before transfection. A total 20 µg plasmid DNA (7.5 µg pLEL, 2.5 µg pSL3, 6.7 µg pSL4 and 3.3 µg pSL5) was used for the transfection of one dish. The plasmids were added to 4 mL of Opti-MEM (Thermo Fisher Scientific). This was combined with 4 mL of Opti-MEM to which 120 µL of Lipofectamine 2000 has been added (Thermo Fisher Scientific). The solution was added to the cultures and the media was replaced after 14 to 16 hours. The media containing virus was collected after another 48 hours and filtered through a 0.45-µm filter. Various volumes of the media containing virus was applied to the target iRANK cells for overnight incubation. iRANK cells transduced with luciferase gene were allowed to expand before use. Luciferase expression was confirmed and quantified via luminometer.

6.2.5 *In vivo bioluminescence imaging for visualization of iRANK cells*

Bioluminescence is the production and emission of light by a living organism as the result of a chemical reaction during which chemical energy is converted to light energy.[138]

Bioluminescence imaging is based on the sensitive detection of visible light produced during enzyme (luciferase)-mediated oxidation of a molecular substrate (luciferin) when the enzyme is expressed *in viv*o as a molecular reporter.[139] Bioluminescence at the emission wavelength firefly luciferase (560 nm) can be imaged as deep as several centimeters within tissue, which allows at least organ-level resolution.[139] This technology has been applied in studies to monitor transgene expression, progression of infection, tumor growth and metastasis, transplantation, toxicology, viral infections, and gene therapy.[140] For *in vivo* imaging, D-luciferin Firefly potassium salt (PerkinElmer) was prepared at a 15 mg/ml stock in PBS and filtered through a 0.22-μm filter before use. Mice were injected intraperitoneally with 10 μL of stock solution per gram of body weight 10 to 15 minutes before imaging. Mice were then anesthesized by inhalation of isoflurane and were positioned at the nose cones in the Xenogen IVIS imaging system. Images were taken by using the IVIS-200 Imaging System (Xenogen Corporation).

6.2.6 *CID delivery in nude mice*

To induce osteoclast formation of iRANK cells, CID was administered intraperitoneally every day for the first three days after cell delivery, followed by the final injection on day 5. CID was prepared at a 62.5 mg/ml stock in 100% EtOH. A dosing solution at 2.5 mg/ml of CID was then formulated with 10% polyethylene glycol (PEG) 400 and 1.7% Tween 20 according to the manufacturer's protocol (Clontech Laboratories). Animals received 10 mg/kg in a dose volume of 4 ml/kg body weight at each injection. At day 7, animals were euthanized and tissue samples were collected and processed as described previously. Sections were examined for GFP expression and TRAP-positive multinucleated cells.

6.2.7 *MicroCT*

Areas of interest on the maxilla were subjected to microCT scanning (Siemen Inveon micro-PET/CT) using a voxel size of 20 μm^3 and a 0.5-mm aluminum filter. Image analysis was performed using Inveon Research Workplace software. microCT scans were performed at 55 kVp and 145 μA with an integration time of 200 milliseconds using a cylindrical tube (field of view/diameter, 20.48 mm). Resolution was set to medium (1024 × 1024 × 148 pixels). Two-dimensional slices from each maxilla were combined using the built-in software to form a three-dimensional reconstruction. Reconstructions were manipulated so that the viewing angles could provide an accurate representation of bone resorption after 3 weeks of healing. The scanning and analyses of data abide by the published guidelines for assessing bone microstructure in rodents.

6.2.8 *H&E and TRAP staining*

For hematoxylin and eosin (H&E) staining, slides were deparaffinized, rehydrated and placed in Harris hematoxylin solution for 3 minutes before rinsing. This was followed by 40 seconds in ammonium water (0.25% v/v). Finally, slides were dipped in eosin solution 10 times before dehydrating. The slides were mounted with Permount (Thermo Fisher Scientific). For TRAP staining, the slides were deparaffinized, rehydrated and incubated for 30 minutes with TRAP staining solution at 37°C, according to manufacturer's protocol (Acid Phosphatase Kit; Sigma-Aldrich). Nuclei were counterstained with 10.9 μM DAPI Dilactate (Life Technologies) for 5 minutes. Slides were mounted with Aqua-Mount (Thermo Fisher Scientific) and images were obtained using an upright microscope (Nikon E800).

6.2.9 *Immunofluorescence staining of green fluorescent protein (GFP)*

Engineered osteoclasts express GFP so we could visualize and distinguish them from endogenous osteoclasts. To detect GFP expression, slides were deparaffinized and rehydrated with TBS-Tween (TBS-T; 0.05 M Tris buffer, 0.15 M NaCl, 0.1% Tween 20, pH 7.6) before permeabilization with 0.1% Triton X-100 in PBS, pH 7.4. for 10 minutes. Blocking was performed with 4% normal donkey serum (NDS) for 30 minutes before adding the primary antibody. The rabbit anti-GFP polyclonal antibody (A-11122, Thermo Fisher Scientific) was diluted in 2% NDS at a ratio of 1:200 and incubated at room temperature for 1 hour. Slides were rinsed 3 times in TBS-T for 5 minutes each before adding the secondary antibody. Cy3 AffiniPure Donkey Anti-Rabbit IgG (Jackson ImmunoResearch Laboratories, Inc.) was diluted in 2% NDS at a ratio of 1:500 for 30 minutes at room temperature. Slides were rinsed three times in TBS-T for 5 minutes and once in Milli-Q water. Nuclei were counterstained with 10.9 µM DAPI Dilactate (Life Technologies) for 5 minutes. Slides were rinsed with Milli-Q water and PBS before mounting with ProLong Gold Antifade Mountant (Thermo Fisher Scientific). Iimages were obtained using an upright microscope (Nikon E800).

6.2.10 *Blood chemistry*

Serum samples collected from each mouse were stored in −20°C and thawed once. The presence of TRAP-5b was detected by sandwich ELISA using the Mouse TRAP-5b ELISA Kit (Immunodiagnostic Systems). Serum levels of OCN were detected by sandwich ELISA using the Mouse Osteocalcin ELISA Kit (Immunotopics). The procedure was performed according to the manufacturer's protocol, and serum samples were assayed in triplicate.

6.2.11 *Statistical analysis*

Results are expressed as mean ± SEM, n=3 for all experiments unless otherwise indicated. SPSS software v16.0 was used to perform Student's *t*-test to compare means of two individual groups, and one-way ANOVA with post-hoc Tukey test to compare means of three or more individual groups. A value of $p<0.05$ was considered statistically significant.

6.3 RESULTS

6.3.1 *Engineered osteoclasts were resistant to inhibition by anti-RANKL antibody.*

The main feature of our system is that induction of signaling is triggered only by the presence of the small molecule CID, and is not affected by the presence of the endogenous RANK/RANKL inhibitors, such as OPG. We previously showed that iRANK cells were OPG-resistant, which is consistent with the design of our iRANK receptor since it does not possess an extracellular RANKL binding domain and therefore does not require RANKL for signaling. We hypothesized that we would observe a similar pattern with anti-RANKL antibody since anti-RANKL antibody binds to RANKL in a similar manner as OPG. As expected, iRANK cells could form multinucleated TRAP-positive osteoclasts even in the presence of the highest concentration of anti-RANKL antibody (100 nM) (**Figure 6.3**). On the other hand, RANKL-mediated osteoclastogenesis was completely inhibited by anti-RANKL antibody even at the lowest concentration (2 nM) (**Figure 6.3**).

6.3.2 *Nude mice had normal wound healing compared to wild type mice.*

Since iRANK cells are allogeneic and due to the key role of tooth extractions in our study, we first determined if nude mice lacking T-cells have normal wound healing compared to

wild type mice. As shown in **Figure 6.4A**, nude mice (n=5) and wild type mice (n=5) were anesthesized with ketamine/xylazine through intraperitoneal injection and left maxillary first molar was extracted. Typical wound closure after an atraumatic tooth extraction usually occurs within 3 weeks.[45] Clinical presentation of maxilla at 3 weeks after tooth extraction showed that both wild type and nude mice had complete closure of epithelium at the extracted socket (**Figure 6.4B**). H&E staining showed that all mice had connective tissue directly above the bone-filled sockets which indicates normal healing process at the extracted site (**Figure 6.4C**).

6.3.3 *iRANK cells were retained at the extracted socket of nude mice.*

Our lab has previously optimized parameters for the local delivery of iRANK cells in an HO model in nude mice under IACUC protocol # 4223-02 in Dr. Bain's lab. In preliminary studies, we determined that collagen hydrogel makes efficient cell delivery vehicle and retain the engineered cells at the site of HO formation compared to fibrin, Matrigel, and without carrier. Consequently, in this study we used collagen hydrogel as cell delivery vehicles.

To validate cell densities and delivery vehicle after tooth extraction, we used collagen hydrogel as a cell delivery vehicle to localize and retain iRANK cells at the tooth socket of nude mice after tooth extraction. To track the cells *in vivo*, iRANK cells were transfected with luciferase. Luciferase transfected cells with collagen hydrogel were then delivered to the socket and the socket was covered with Gelfoam® dental sponge to help keep the cells in place (**Figure 6.5A**). To visualize luciferase transfected cells, luciferin was injected intraperitoneally 10 to 15 minutes prior to imaging with the Xenogen IVIS imaging system. Cell localization was assessed on the same day as cell delivery (day 0). Additionally, mice were imaged 4 times (day 1, 3, 7 and 10) following injection, at least 24 hours between imaging sessions. At day 10, mice were euthanized to harvest maxilla. The bioluminescence data showed that the signal was detected and

increased over time in all animals that received cells with or without Gelfoam®. As expected, no signal was detected in the animals that did not receive cells but received luciferin. This suggests that iRANK cells were retained at the tooth socket and the cells proliferated, which was expected as the engineered cells were derived from a cell line and were injected into athymic mice (**Figure 6.5B**).

As seen in **Figure 6.5C**, nude mice that received cells with or without Gelfoam® showed an area of inflammation at the extracted socket, while nude mice that did not receive cells showed normal healing at the extracted socket. H&E staining of nude mice that received cells showed complete closure of epithelium and there were areas of proliferating cells underneath (**Figure 6.6A**). We found these cells to be GFP-positive as shown in **Figure 6.6B**. Importantly, adjacent tissue did not stain positive, suggesting these cells were derived from the originally-injected cells. Together, these data suggest that a population of iRANK cells remained at the extracted socket, proliferated, and may have caused inflammation at the tooth socket.

6.3.4 *iRANK cells formed osteoclasts in response to CID in nude mice.*

Our lab has previously optimized CID administration to induce osteoclast formation in HO model in nude mice. We showed that iRANK cells could form TRAP-positive osteoclasts in the collagen hydrogel when activated with CID (**Figure 6.1**). Engineered osteoclasts were also positive to GFP, so we could visualize and distinguish them from endogenous osteoclasts.

The objective of this study was to activate iRANK cells *in vivo* using CID and to determine successful activation using osteoclast staining at the extracted tooth socket in nude mice. **As shown in Figure 6.7A**, mice were anesthetized, and the first molar were extracted as previously described. Cells in combination with collagen hydrogel were delivered to the tooth socket immediately after tooth extraction. Gelfoam® was placed into the extracted socket. CID

was administered intraperitoneally the same day of cell delivery and every day for 3 days then every other day to induce osteoclast differentiation. At day 7, animals were euthanized, and the maxilla was processed as previously described. Clinical presentation of maxilla at day 7 showed complete closure of the epithelium (**Figure 6.7B**). However, epithelium showed irregularity at the extracted area. Most importantly and crucially, we found TRAP-positive multinucleated cells in ~4 areas at the extracted site which were also positive for GFP as shown in **Figure 6.8**. These data suggest that osteoclasts observed were from delivered engineered cells and not endogenous osteoclasts. Moreover, we induced successful osteoclast differentiation of iRANK cells *in vivo*. On the other hand, TRAP-positive multinucleated cells in mice that received iRANK cells without CID were not positive for GFP indicating that they were endogenous osteoclasts (**Figure 6.9**).

6.3.5 *Anti-RANKL antibody induced ONJ-like lesions in nude mice.*

To evaluate the involvement of osteoclasts in MRONJ development, we used anti-RANKL antibody in a tooth extraction mouse model that was previously described.[45] In this study, however, we used nude mice instead of wild type mice. As shown in **Figure 6.10A**, anti-RANKL antibody was administered intraperitoneally two times a week for total 4 weeks. To induce MRONJ, the left maxillary first molar was extracted 1 week after initial anti-RANKL antibody treatment. Clinical presentation at the extracted sites after 3 weeks showed complete epithelial closure in mice treated with control IgG and anti-RANKL antibody (**Figure 6.10B**).

MicroCT scans of the maxilla were shown in **Figure 6.11A**. Bone volume at the extracted sites were analyzed using Inveon Research Workplace software. As seen in **Figure 6.11B**, control IgG antibody-treated mice (n=3) had significantly less bone volume compared to anti-RANKL antibody-treated mice (n=5). This finding indicates that bone remodeling was

inhibited in the anti-RANKL antibody-treated group since there were less osteoclasts present due to the antibody treatment. Therefore, anti-RANKL antibody-treated mice had more bone volume than control IgG antibody-treated mice.

To examine whether anti-RANKL antibody suppressed bone remodeling process, including osteoclastic and osteoblastic activity, we collected terminal blood samples and measured the serum concentration of TRAP-5b and OCN, biochemical markers for bone resorption and formation, respectively. In anti-RANKL antibody-treated mice, TRAP-5b in serum was significantly suppressed compared to the control (**Figure 6.12**). Furthermore, OCN was also decreased significantly in anti-RANKL antibody-treated mice (**Figure 6.13**). These results indicate that bone remodeling was suppressed in anti-RANKL antibody-treated mice.

6.4 DISCUSSION

Denosumab, a class of antiresorptive drug, is a fully human monoclonal antibody that specifically targets RANKL and is known to induce MRONJ.[130] We demonstrated that CID-induced osteoclast differentiation occurred even in the presence of high concentrations of anti-RANKL antibody, a mouse form of denosumab. This result is as expected since the induction of iRANK cells is triggered only by the presence of CID, and not dependent on RANKL.

We proposed to utilize engineered cells (resistant to inhibition by denosumab) to prevent MRONJ *in vivo* and to elucidate the role that osteoclasts play in the development of this disease. We were the first group who developed a MRONJ model in nude mice. Our preliminary data showed that anti-RANKL antibody-treated mice had significantly more bone volume compared to anti-RANKL antibody-treated mice suggesting that bone remodeling was impaired in the antibody-treated group. Moreover, we found that both biochemical markers for bone resorption

(TRAP-5b) and bone formation (OCN) were compromised in anti-RANKL antibody-treated mice. These data are consistent with a recent finding of MRONJ model in wild type mice.[45]

The primary role of mature osteoclasts is to resorb bone matrix. However, roles other than bone resorption have been suggested, such as modulating the differentiation of nearby cells or secreting inflammatory cytokines to induce immune responses.[141] Recent studies suggest that abnormal functions of osteoclasts may contribute to MRONJ development. Woven bone formation is known to occur in two ways: appositional formation from the existing bone surfaces primarily mediated by the osteoclast-osteoblast coupling mechanism, and *de novo* formation without any existing bone surfaces.[142] This dual mode of new bone formation is known to play an important role during healing in the oral cavity after dental interventions, such as implant surgery.[143] In the context of wound healing after tooth extraction, appositional bone formation mandates tight coupling between initial bone resorption mediated by mature osteoclasts and subsequent bone formation by recruiting osteoblasts at the resorbed sites.[144] A defect in this coupling process due to impaired osteoclastic resorptive function in the presence of denosumab may essentially interfere and inhibit appositional woven bone formation, leaving *de novo* bone formation as the only source of new bone formation in the extracted sockets.

These studies represent the first *in vivo* work using CID to induce osteoclast formation *in vivo*. We were able to visualize the cells *in vivo* and verify that they remained at the injection site through the use of collagen hydrogel and Gelfoam®. Most importantly, TRAP-positive multinucleated cells found at the injection site were also positive for GFP indicating they differentiated from engineered cells. We are currently determining whether engineered osteoclasts can prevent MRONJ in nude mice. This study provides a novel paradigm for the mechanism and pathophysiology of MRONJ. Moreover, this study is the first to provide proof of

concept data that osteoclast cell therapy might be a unique strategy for solving this debilitating disease in patients.

The biggest limitation of this study was the use of a cell line, rather than primary cells. These cells proliferated extensively *in vivo* and limited the length of our experiments. The use of this cell line also contributed directly to another limitation, which was the use of athymic mice. These mice were used to minimize immune rejection of the cell line, but these mice have an immune response which differs greatly from wild type mice.

In conclusion, we have developed a mouse model for MRONJ in nude mice and developed a cell and CID delivery method to induce osteoclast formation. We used this model to test our hypothesis that inhibition of osteoclasts by antiresorptive drug, denosumab, plays a direct etiological role in inducing ONJ. However, future experiments that examine the effect of BPs (another type of antiresorptive drug) on osteoclast formation of iRANK cells are still needed. A BP-induced ONJ model would further elucidate the potential therapeutic role of engineered cells and provide insight into future targets.

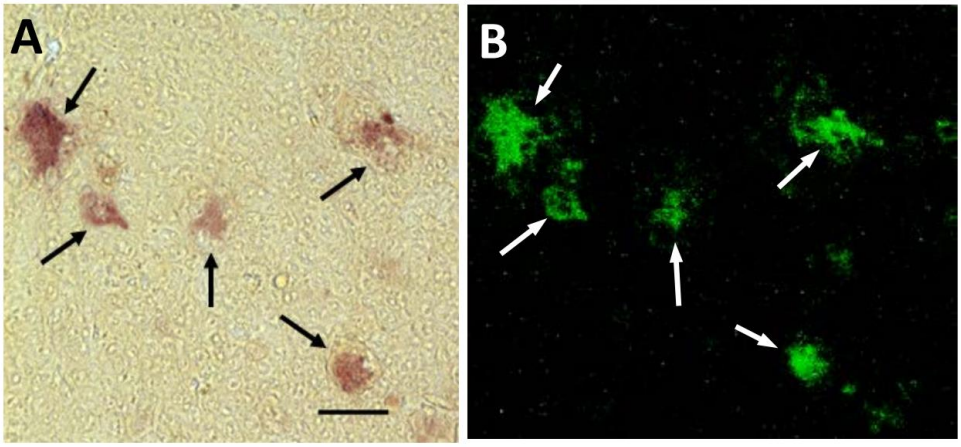

Figure 6.1. iRANK cells formed osteoclasts *in vivo* in response to CID.

BMP-2 was used to induce HO formation in a mouse calf muscle. iRANK cells were delivered in collagen hydrogel carrier one day following BMP-2/matrigel implantation. When cells were activated with CID they fused to form TRAP-positive osteoclasts at the HO site. Arrows indicated TRAP-positive multinucleated cells (A) which were also positive for the iRANK GFP reporter (B). Scale bar = 50 μm

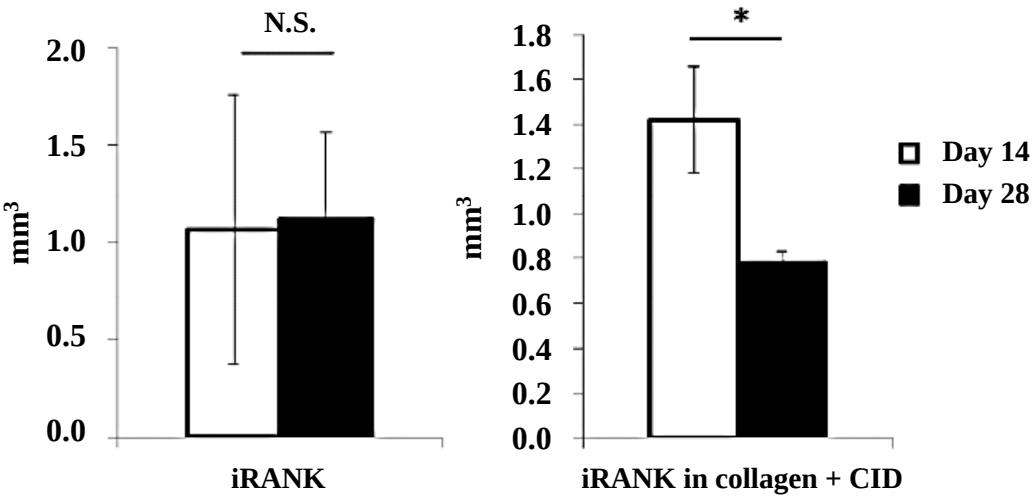

Figure 6.2. HO lesion was reduced in animals that received iRANK cells with CID at week 4 compared to week 2.

HO was induced in nude mice with BMP-2 implantation. The next day iRANK cells were delivered to the site of HO initiation and activated with CID. Cells were delivered again on Days 7, 14, and 21. HO volume was measured at Days 14 and 28. *p<0.05, N.S. = not significant

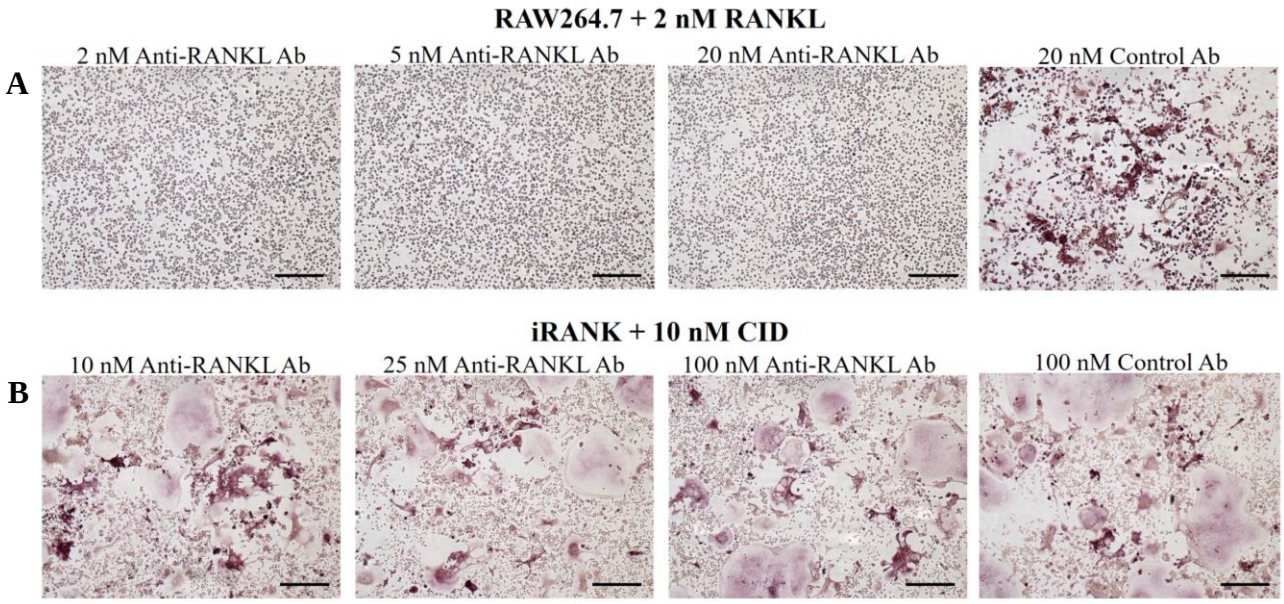

Figure 6.3. CID-induced osteoclastogenesis in iRANK cells was anti-RANKL antibody-independent.

(A) No TRAP-positive multinucleated cell was present after treatment of RAW264.7 cells with 2 nM mouse RANKL in the presence of 2 nM, 5 nM or 20 nM anti-mouse RANKL antibody.

(B) On the other hand, TRAP-positive multinucleated cells were detected after treatment of iRANK cells with 10 nM CID in the presence of 10 nM, 25 nM or 100 nM anti-mouse RANKL antibody. Scale bar = 200 μM

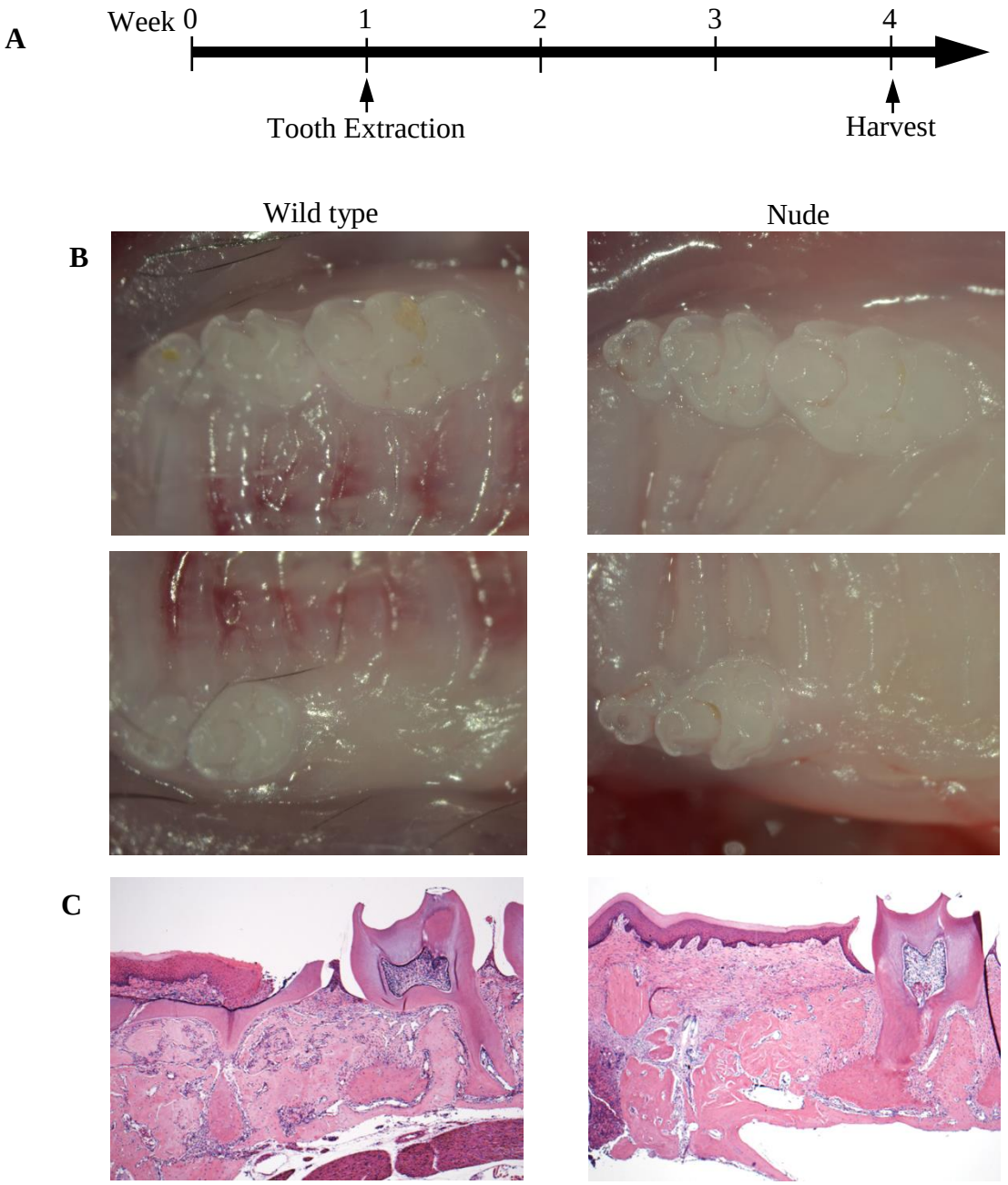

Figure 6.4. Nude mice had normal wound healing of the extracted socket.

(A) Timeline of this animal experiment (B) Clinical presentation showed complete closure of epithelium at the extracted socket in both wild type (WT) (left) and nude mice (right). (C) H&E staining showed normal healing of the extracted socket in both WT (left) and nude mice (right).

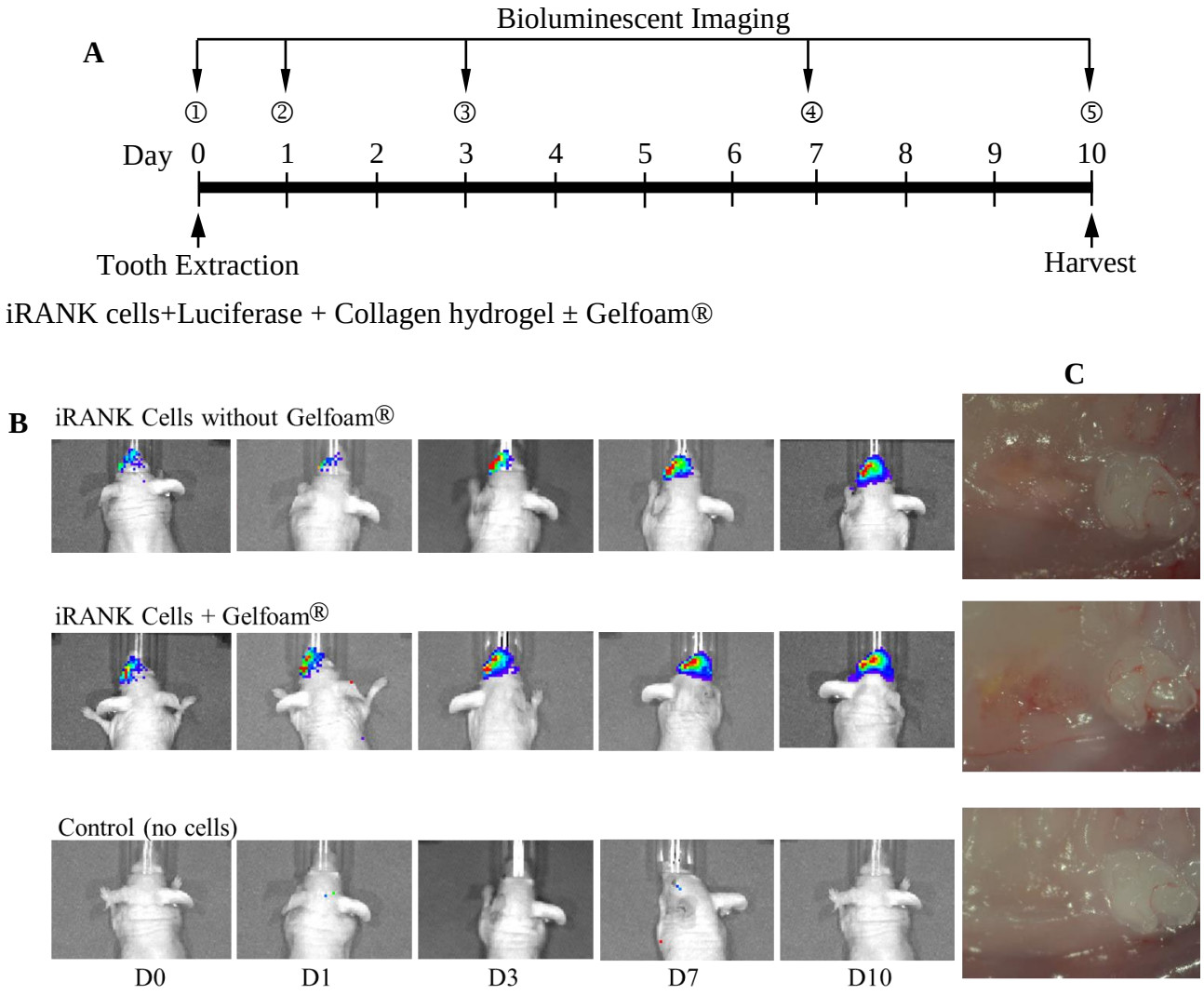

Figure 6.5. iRANK cells could be visualized by bioluminescence.

(A) Timeline of this animal experiment

(B) The bioluminescent signal was detected and increased over time in all animals that received cells with or without Gelfoam®. As expected, no signal was detected in the animals that did not receive cells but received luciferin.

(C) Clinical presentation showed areas of inflammation at the extracted sites in nude mice that received cells with or without Gelfoam®.

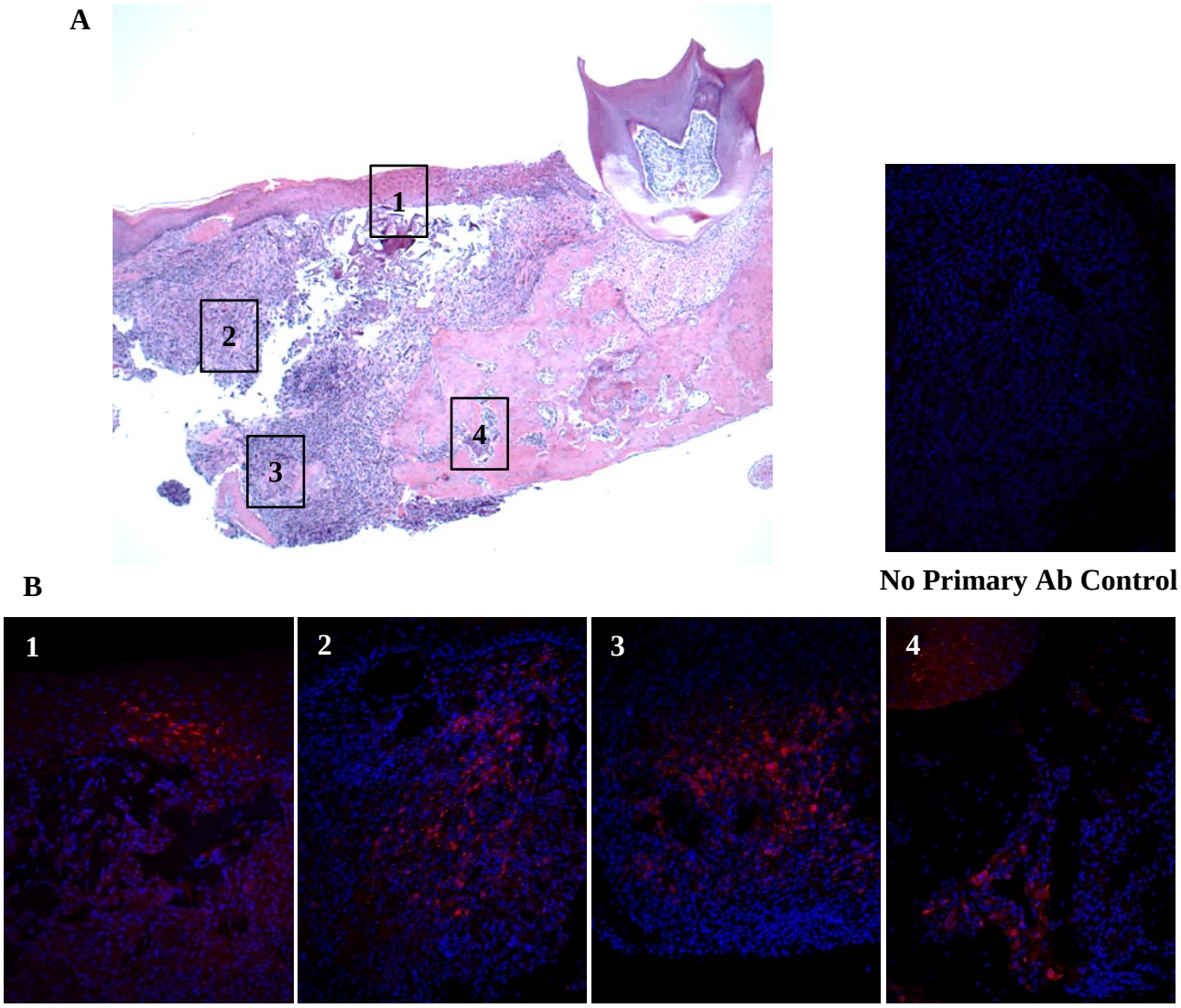

Figure 6.6. iRANK cells were retained in the extracted socket.

(A) H&E staining of nude mice that received cells showed complete closure of epithelium and there were areas of proliferating cells (purple) underneath the epithelium.

(B) GFP-positive cells (red) were detected throughout the area of proliferating cells. DAPI staining of nuclei was shown in blue.

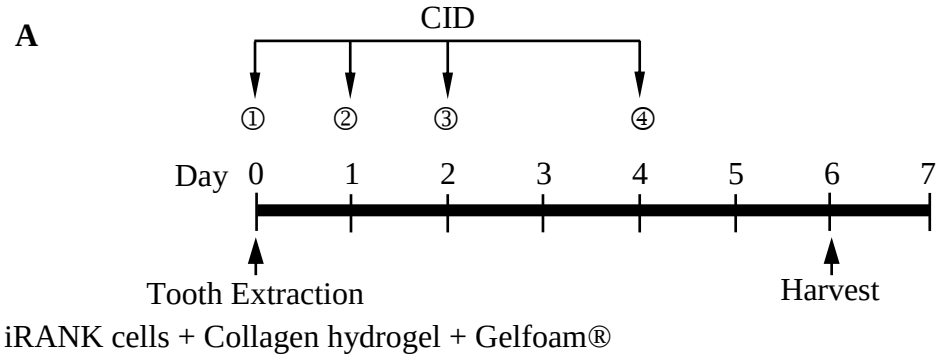

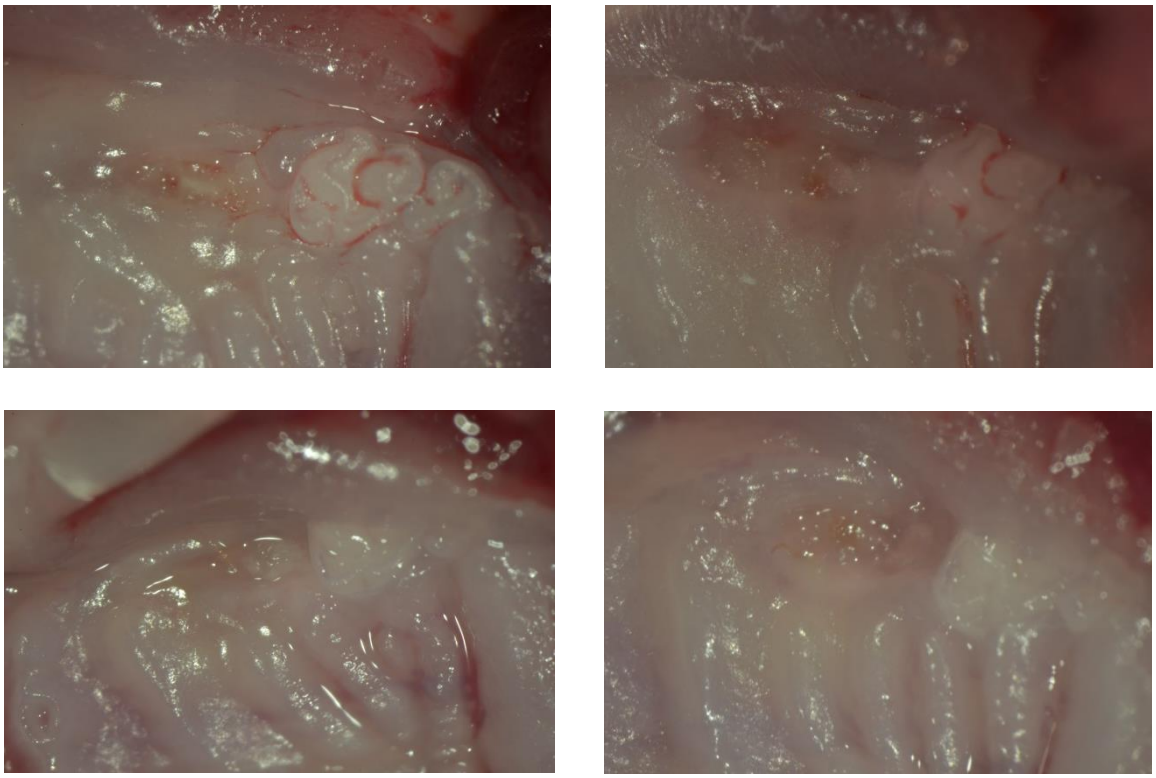

Figure 6.7. Activation of iRANK cells *in vivo* using CID

(A) Timeline of this experiment

(B) Clinical presentation showed complete closure of epithelium at the extracted sockets. However, the epithelium appeared to have irregularity.

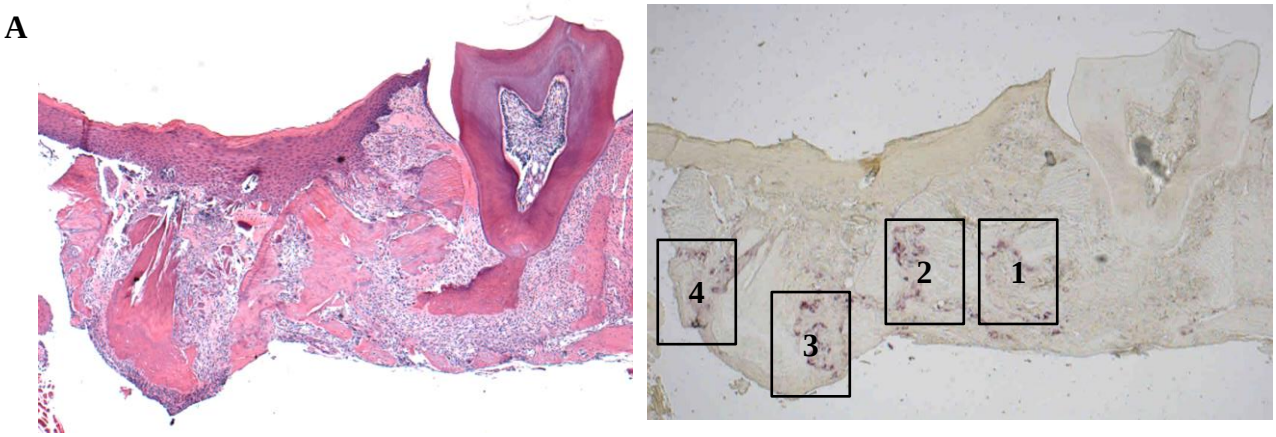
A
4
3
2
1
B
No Primary Ab Control
1
2
1
2

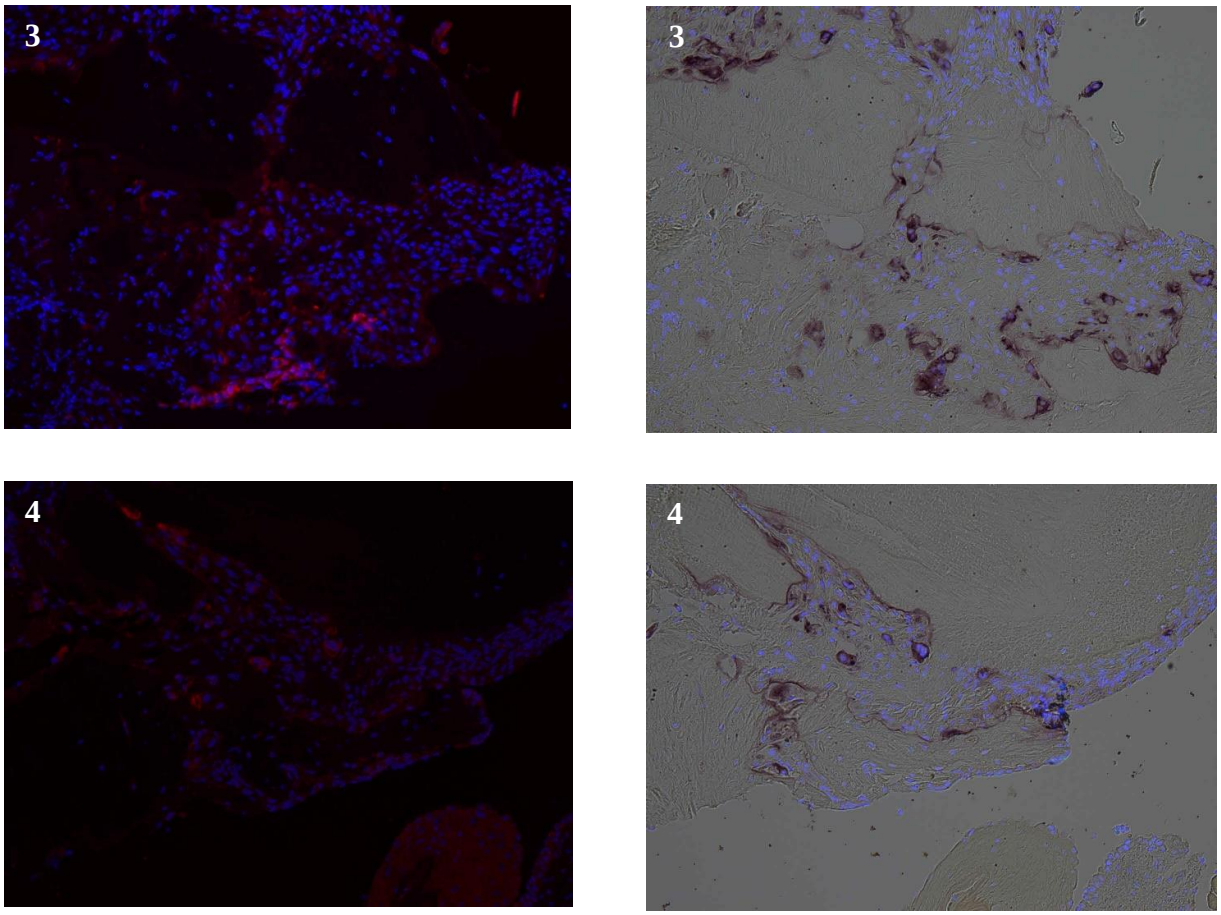

Figure 6.8. iRANK cells formed TRAP-positive multinucleated osteoclasts in response to CID in nude mice.

(A) H&E staining of nude mice that received cells and CID showed normal wound healing of extracted socket (left). TRAP-positive multinucleated cells were observed in ~4 areas (indicated with number in the box) at the extracted site (right).

(B) Each area (1-4) was stained with GFP+DAPI (left panel) and TRAP+DAPI (right panel). TRAP-positive multinucleated cells were also positive for GFP indicating that they differentiated from delivered engineered cells and they were not endogenous osteoclasts.

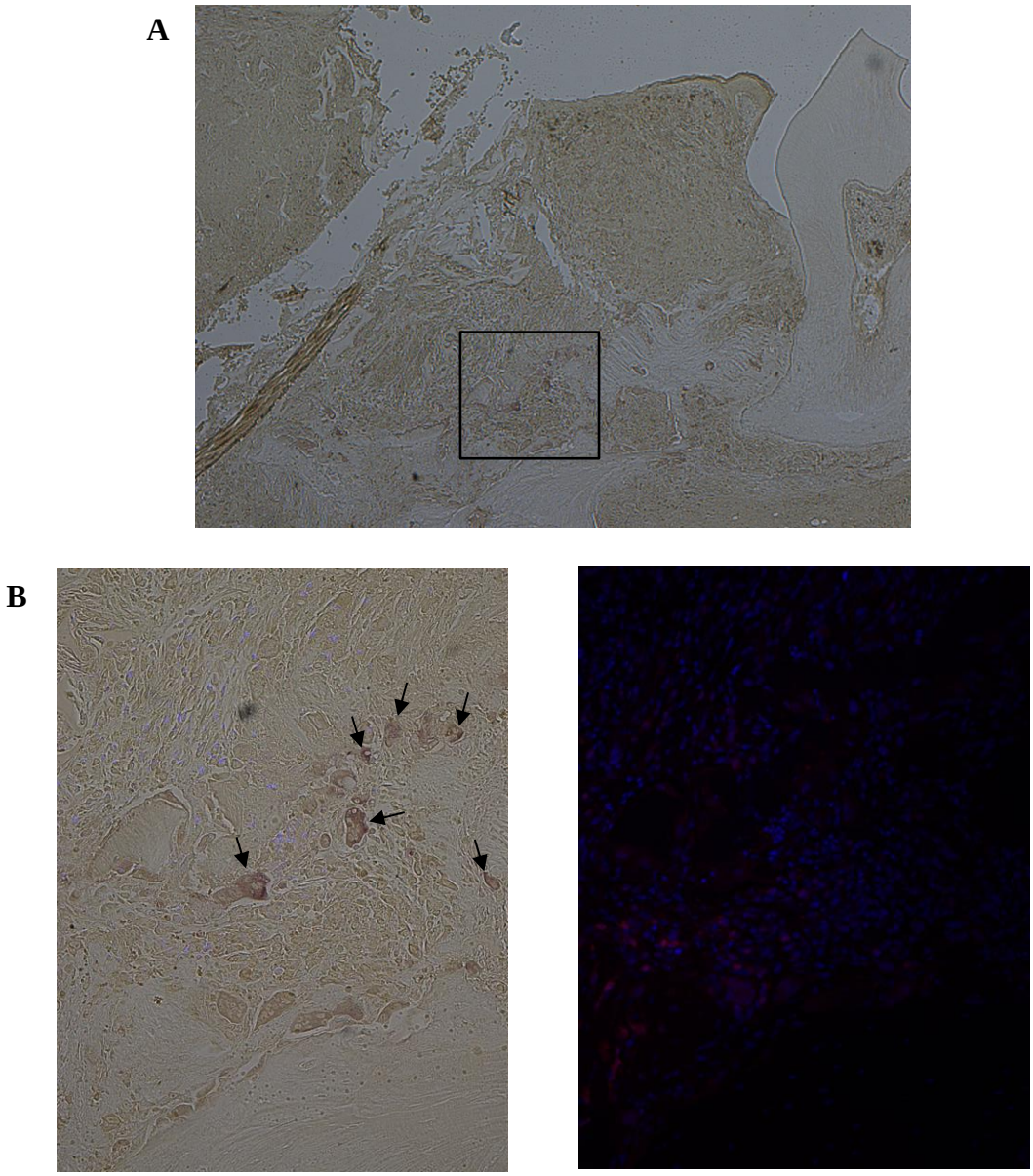

Figure 6.9. Endogenous osteoclasts were detected in nude mice that received iRANK cells without CID.

(A) TRAP-positive multinucleated cells were observed in the extracted site of nude mice that received iRANK cells without CID.

(B) TRAP-positive multinucleated cells (arrows) were not positive for GFP (red) indicating that they were endogenous osteoclasts.

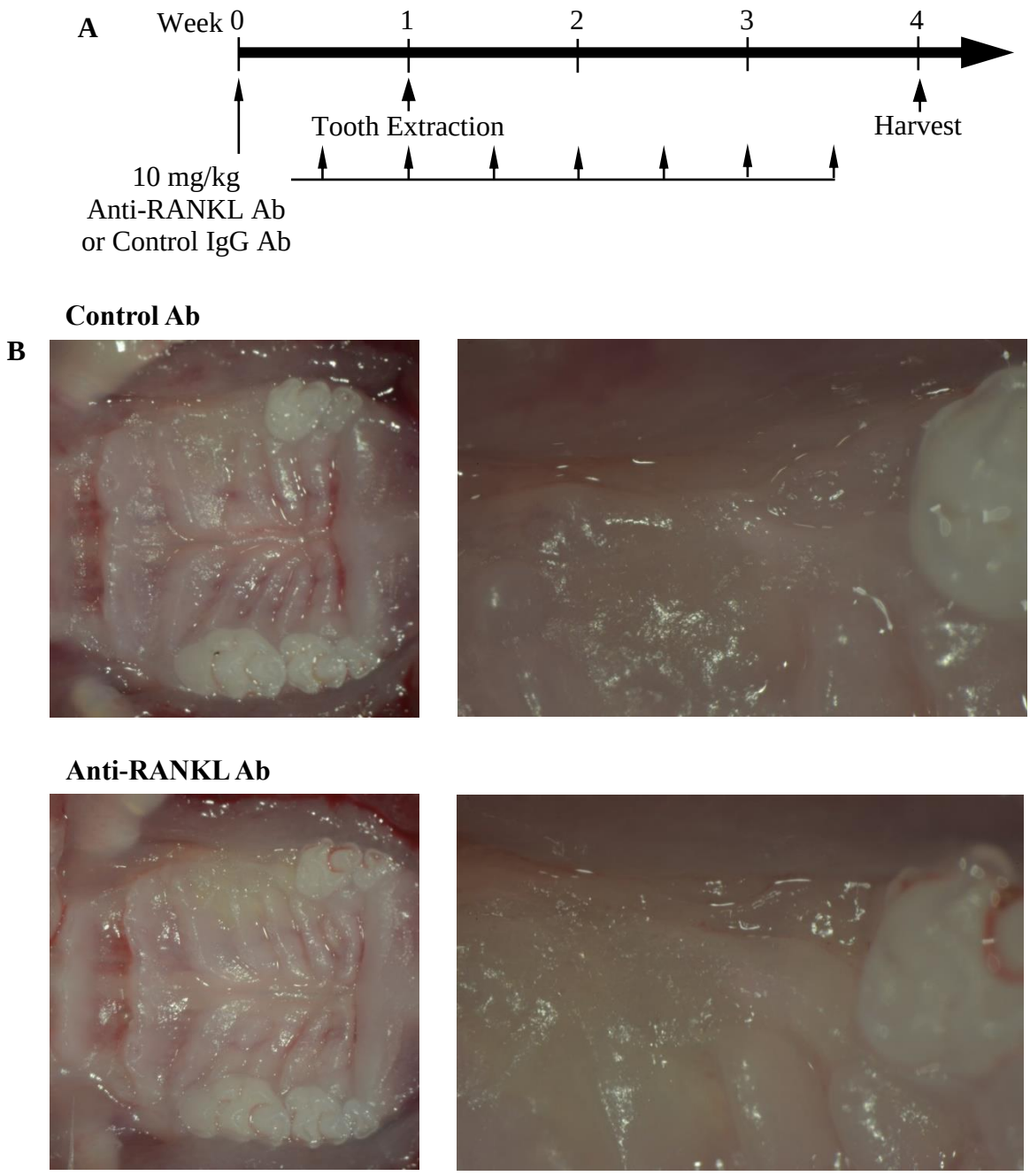

Figure 6.10. Development of MRONJ model in nude mice

(A) Timeline of this experiment

(B) Clinical presentation at the extracted sites after 3 weeks showed complete epithelial closure in mice treated with control IgG and anti-RANKL antibody.

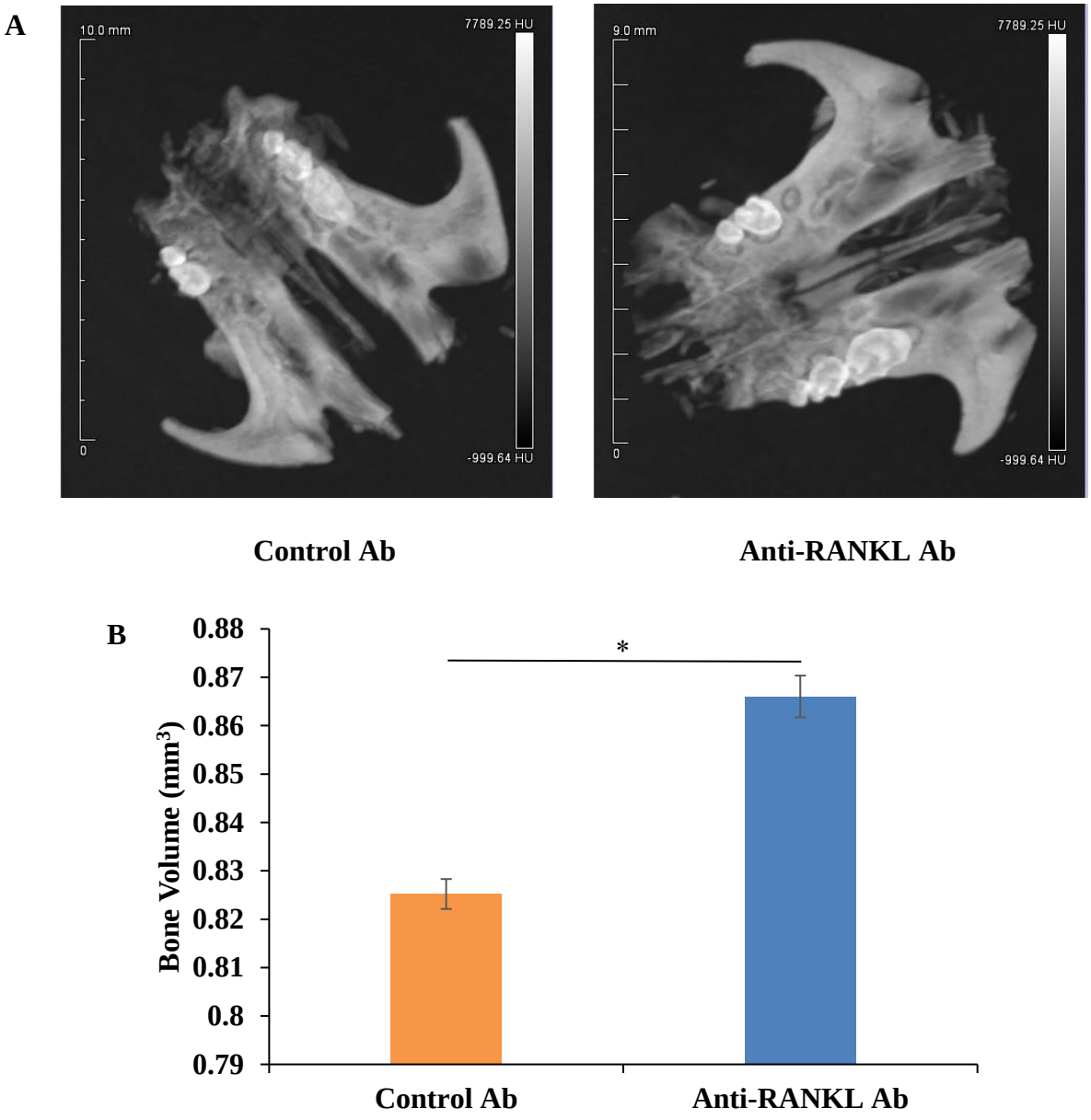

Figure 6.11. MicroCT scans of the maxilla of control antibody-treated mice and anti-RANKL antibody-treated mice

(A) MicroCT scans of the maxilla of control antibody-treated mice (left) and anti-RANKL antibody treated mice (right)

(B) Control antibody-treated mice (n=3) had significantly less bone volume compared to anti-RANKL antibody-treated mice (n=5). *p<0.001

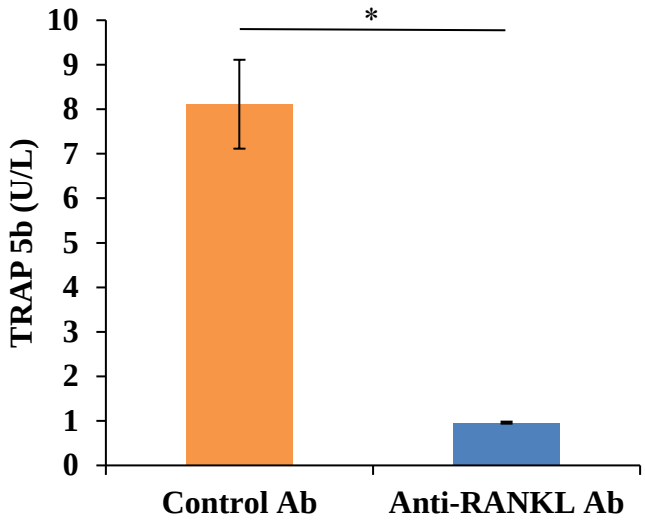

Figure 6.12. Serum TRAP-5b level in anti-RANKL antibody-treated mice was suppressed.

Blood was collected from the control IgG antibody-treated and anti-RANKL antibody-treated mice 4 weeks after initial administration. The serum level of TRAP-5b was significantly reduced in anti-RANKL antibody-treated mice. *$p<0.05$

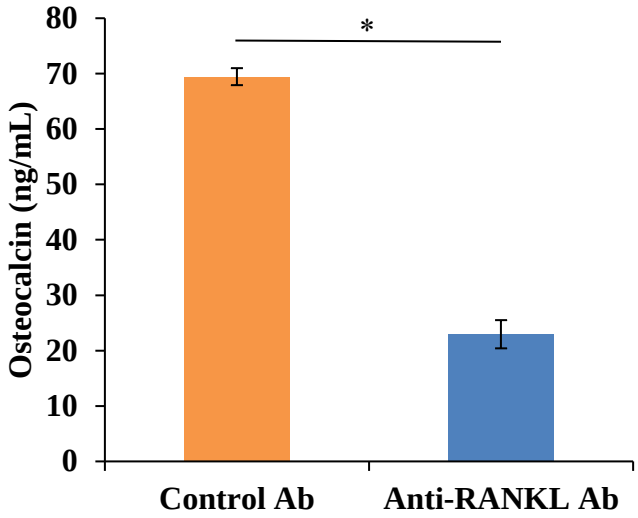

Figure 6.13. Serum OCN level in anti-RANKL antibody-treated mice was decreased.

Blood was collected from the control IgG antibody-treated and anti-RANKL antibody-treated mice 4 weeks after initial administration. The serum level of OCN was significantly decreased in anti-RANKL antibody-treated mice. *$p<0.05$

CHAPTER 7.
CONCLUSIONS

In previous studies, we utilized CID technology to control monocytic precursor differentiation into functional osteoclasts, which is independent of RANKL and M-CSF, and also resistant to OPG, a potent natural inhibitor of osteoclast differentiation. In this thesis, we propose that osteoclasts not only physically resorb bone, but also prevent mineral accumulation by elaborating anticalcific factors. To test this hypothesis, we developed a co-culture system in which engineered osteoclasts were cultured with calcifying cells in media containing high Pi using Transwell inserts. Co-culture of C2C12 cells with engineered osteoclasts significantly reduced calcification of C2C12 cells compared to C2C12 cells cultured alone or co-cultured with iRANK precursor cells. We have been able to reproduce these findings in a traditional cell culture system using media conditioned by engineered osteoclasts and in a second mineralizing cell type, BVICS. To our knowledge, this is the first report to demonstrate the contact-independent ability of osteoclasts to prevent ectopic calcification *in vitro*.

In the present study, we demonstrated that OPN levels secreted from CID-induced osteoclasts were significantly higher than untreated cells. We also showed that OPN plays in an important role in inhibiting cell-mediated calcification, as well as preventing passive mineralization of human HO samples. Moreover, we identified specific forms of OPN present in conditioned media from engineered osteoclasts. Interestingly, a different form of OPN was detected in osteoclast-derived exosomes. Together, these studies point to unique OPN peptides as candidate therapeutic agents to prevent or inhibit calcification and progression of HO. Our studies are the first to suggest that osteoclasts function not only to resorb mineralized matrix

through physical contact, but also to prevent cell-mediated calcification and progression of mineralization of nucleation sites by elaborating OPN, a potent inhibitor for mineral deposition.

We demonstrated that CID-induced osteoclast differentiation occurred in the presence of anti-RANKL antibody which is a mouse form of denosumab, an antiresorptive drug known to cause MRONJ. Therefore, we propose to utilize engineered cells (which are resistant to inhibition by denosumab) to prevent MRONJ *in vivo* and to elucidate the role osteoclasts in the development of this disease. We are the first group who developed a MRONJ model in nude mice and the results were consistent with a recent finding of MRONJ model in wild type mice.[45] We were able to visualize the cells *in vivo* and verify that they remained at the extracted socket through the use of collagen hydrogel and Gelfoam®. Most importantly, we are the first to successfully use CID to induce osteoclast formation of engineered cells *in vivo*.

CHAPTER 8.
FUTURE STUDIES

This study showed that engineered osteoclasts have a contact-independent ability to prevent calcification and we identified osteoclast-derived OPN as one of the factors osteoclasts produce to inhibit calcification. Our data suggest that osteoclasts may be therapeutically useful not only to physically resorb pre-existing mineral but also to actively prevent calcification by elaborating OPN. However, there are further studies that need to be investigated.

1. *Characterization of OPN peptides and their therapeutic use*

We found many forms of OPN present in iRANK osteoclast conditioned media. Therefore, it would be interesting to further identify OPN peptides by using proteomic and biochemical approaches and determine which peptides have inhibitory effects on calcification. We could synthesize the functional OPN peptides to be used as a therapy for EC or HO. OPN has an advantage over cell therapy in that it is easier to manage and does not have immune rejection.

2. *Characterization of engineered osteoclast-derived exosomes and their therapeutic use*

We showed that engineered osteoclasts secreted exosomes. However, specific exosomal markers, such as CD63, EpCAM, TSG10, HSP70 and β-actin, and contamination makers of exosome preparation, such as TFIIB, lamin A/C, calnexin and GP96, need to be verified. Moreover, unique form of OPN found in iRANK osteoclast-derived exosomes need to be further characterize of its inhibitory ability. Ultimately, OPN-loaded exosomes could be used as a therapy for EC or HO.

3. *Effect of bisphosphonates (BPs) on engineered osteoclast formation and the use of these cells to prevent MRONJ caused by BPs*

In this study, we focused on the effect of denosumab on engineered osteoclast differentiation since we have previously shown that iRANK cells could form TRAP-positive multinucleated cells in the presence of OPG, a natural analogue of denosumab. However, it would be interesting to investigate the effect of BPs on engineered osteoclast differentiation. We could then also develop a MRONJ model by using BPs and determine whether engineered osteoclasts could prevent the formation of BPs-related ONJ.

4. *Generation of Csf1r-iRANK transgenic mice as a primary cell source*

The use of iRANK cells has some limitations because they are cell line-derived and can proliferate extensively *in vivo*. Our use of this cell line also requires the use of nude mice, which are immunocompromised and may respond differently compared to wild type mice. Future studies that use primary cells would be a better representative model of the treatment in patients. However, the process to obtain primary cells takes more time and it is more difficult to obtain iRANK transgenic mice.

We are currently generating Csf1r-iRANK transgenic mice by using standard pronuclear injection. These mice are designed to express iRANK and GFP specifically in monocytes, macrophages and osteoclasts. Currently, we are breeding founders to C57BL/6 mice. We will characterize this new mouse line by isolating monocytes from peripheral blood and/or the bone marrow to determine GFP expression levels by FACS analysis as a surrogate for iRANK expression together with markers for monocytes (CD11b and CD115). To determine if the construct is functional, monocytes will be treated with a range of CID concentrations and bone marrow derived- (BMD) stem cells will be treated with CSF-1 and a CID range of concentrations

to generate RANKL-independent osteoclasts. RANKL treatment alone or in combination with CSF-1 will be used as positive control for osteoclast formation. We expect that all these treatments will result in multinucleated TRAP- and GFP-positive osteoclasts. We will then develop an *in vivo* model of MRONJ in these mice instead of nude mice. An advantage of these mice is that they can express the iRANK construct (through which they can differentiate into osteoclasts) without the need for cell delivery. However, this process takes more time and it is more difficult to obtain these mice.

BIBLIOGRAPHY

1. Edwards, J. R. & Weivoda, M. M. Osteoclasts: malefactors of disease and targets for treatment. *Discov. Med.* **13,** 201–10 (2012).
2. Helfrich, M. H. Osteoclast diseases. *Microsc. Res. Tech.* **61,** 514–32 (2003).
3. Ruggiero, S. L. *et al.* American Association of Oral and Maxillofacial Surgeons position paper on medication-related osteonecrosis of the jaw--2014 update. *J. Oral Maxillofac. Surg.* **72,** 1938–56 (2014).
4. Boyle, W. J., Simonet, W. S. & Lacey, D. L. Osteoclast differentiation and activiation. *Nature* **423,** 337–342 (2003).
5. Charles, J. F. & Aliprantis, A. O. Osteoclasts: more than 'bone eaters'. *Trends Mol. Med.* **20,** 449–459 (2014).
6. Rementer, C. W. *et al.* An inducible, ligand-independent receptor activator of NF-kB gene to control osteoclast differentiation from monocytic precursors. *PLoS One* **8,** (2013).
7. Michael Lewiecki, E. Denosumab: An investigational drug for the management of postmenopausal osteoporosis. *Biologics: Targets and Therapy* **2,** 645–653 (2008).
8. Gogakos, A. I., Cheung, M. S., Bassett, J. D. & Williams, G. R. Bone signaling pathways and treatment of osteoporosis. *Expert Rev. Endocrinol. Metab.* **4,** 639–650 (2009).
9. Jackson, M. F., Scatena, M. & Giachelli, C. M. Osteoclast precursors do not express CD68: results from CD68 promoter-driven RANK transgenic mice. *FEBS Lett.* **591,** 728–736 (2017).
10. Xu, F. & Teitelbaum, S. L. Osteoclasts: New Insights. *Bone Res.* **1,** 11–26 (2013).
11. Ikeda, K. & Takeshita, S. The role of osteoclast differentiation and function in skeletal homeostasis. *J. Biochem.* **159,** 1–8 (2016).

12. Novack, D. V. & Teitelbaum, S. L. The Osteoclast: Friend or Foe? *Annu. Rev. Pathol. Mech. Dis.* **3,** 457–484 (2008).

13. Teitelbaum, S. L. & Ross, F. P. Genetic regulation of osteoclast development and function. *Nat. Rev. Genet.* **4,** 638–49 (2003).

14. Tolar, J., Teitelbaum, S. L. & Orchard, P. J. Osteopetrosis. *N. Engl. J. Med.* **351,** 2839–2849 (2004).

15. Väänänen, H. K., Zhao, H., Mulari, M. & Halleen, J. M. The cell biology of osteoclast function. *J. Cell Sci.* **113 (Pt 3,** 377–81 (2000).

16. Giachelli, C. M. Ectopic calcification: gathering hard facts about soft tissue mineralization. *Am. J. Pathol.* **154,** 671–675 (1999).

17. Steitz, S. A. *et al.* Osteopontin inhibits mineral deposition and promotes regression of ectopic calcification. *Am. J. Pathol.* **161,** 2035–2046 (2002).

18. Jono, S. *et al.* Phosphate regulation of vascular smooth muscle cell calcification. *Circ. Res.* **87,** E10–E17 (2000).

19. Forsberg, J. A. & Potter, B. K. Heterotopic ossification in wartime wounds. *J. Surg. Orthop. Adv.* **19,** 54–61 (2010).

20. Freeman, R. V. & Otto, C. M. Spectrum of calcific aortic valve disease: Pathogenesis, disease progression, and treatment strategies. *Circulation* **111,** 3316–3326 (2005).

21. Yutzey, K. E. *et al.* Calcific Aortic Valve Disease: A Consensus Summary From the Alliance of Investigators on Calcific Aortic Valve Disease. *Arterioscler. Thromb. Vasc. Biol.* **34,** 2387–2393 (2014).

22. Nkomo, V. T. *et al.* Burden of valvular heart diseases: a population-based study. *Lancet (London, England)* **368,** 1005–11 (2006).

23. Rajamannan, N. M. *et al.* Calcific Aortic Valve Disease: Not Simply a Degenerative Process: A Review and Agenda for Research From the National Heart and Lung and Blood Institute Aortic Stenosis Working Group * Executive Summary: Calcific Aortic Valve Disease - 2011 Update. *Circulation* **124,** 1783–1791 (2011).

24. Rajamannan, N. M. *et al.* Human aortic valve calcification is associated with an osteoblast phenotype. *Circulation* **107,** 2181–4 (2003).

25. New, S. E. P. & Aikawa, E. Molecular imaging insights into early inflammatory stages of arterial and aortic valve calcification. *Circ. Res.* **108,** 1381–91 (2011).

26. Aikawa, E. *et al.* Osteogenesis associates with inflammation in early-stage atherosclerosis evaluated by molecular imaging in vivo. *Circulation* **116,** 2841–50 (2007).

27. Steiner, I., Kasparová, P., Kohout, A. & Dominik, J. Bone formation in cardiac valves: a histopathological study of 128 cases. *Virchows Arch.* **450,** 653–7 (2007).

28. Lis, G. J. *et al.* Development of mature lamellar bone with a hematopoietic compartment in an aortic valve homograft. *J. Heart Valve Dis.* **18,** 578–80 (2009).

29. Mohler, E. R. *et al.* Bone formation and inflammation in cardiac valves. *Circulation* **103,** 1522–8 (2001).

30. Ueland, T. *et al.* Osteoprotegerin levels predict mortality in patients with symptomatic aortic stenosis. *J. Intern. Med.* **270,** 452–460 (2011).

31. Schoen, F. J. Cardiac valves and valvular pathology: Update on function, disease, repair, and replacement. *Cardiovascular Pathology* **14,** 189–194 (2005).

32. Avogaro, A. & Fadini, G. P. Mechanisms of ectopic calcification: implications for diabetic vasculopathy. *Cardiovasc. Diagn. Ther.* **5,** 343–52 (2015).

33. Wu, M., Rementer, C. & Giachelli, C. M. Vascular calcification: An update on

mechanisms and challenges in treatment. *Calcif. Tissue Int.* **93,** 365–373 (2013).

34. Evrard, S., Delanaye, P., Kamel, S., Cristol, J.-P. & Cavalier, E. Vascular calcification: from pathophysiology to biomarkers. *Clin. Chim. Acta* **438,** 401–414 (2015).

35. Abedin, M., Tintut, Y. & Demer, L. L. Vascular calcification: mechanisms and clinical ramifications. *Arterioscler. Thromb. Vasc. Biol.* **24,** 1161–70 (2004).

36. Demer, L. L. & Tintut, Y. Vascular Calcification: Pathobiology of a Multifaceted Disease. *Circulation* **117,** 2938–2948 (2008).

37. Amann, K. Media Calcification and Intima Calcification Are Distinct Entities in Chronic Kidney Disease. *Clin. J. Am. Soc. Nephrol.* **3,** 1599–1605 (2008).

38. Nicoll, R. & Henein, M. Y. Arterial calcification: friend or foe? *Int. J. Cardiol.* **167,** 322–7 (2013).

39. Viswanathan, S., Sankar, R. & Gowrishankar, K. Genetic disorders with heterotopic ossificans. *Indian J. Orthop.* **49,** 361 (2015).

40. Davies, O. G., Grover, L. M., Eisenstein, N., Lewis, M. P. & Liu, Y. Identifying the Cellular Mechanisms Leading to Heterotopic Ossification. *Calcif. Tissue Int.* **97,** 432–444 (2015).

41. Evans, K. N. *et al.* Inflammatory cytokine and chemokine expression is associated with heterotopic ossification in high-energy penetrating war injuries. *J. Orthop. Trauma* **26,** e204-13 (2012).

42. Forsberg, J. A., Potter, B. K., Polfer, E. M., Safford, S. D. & Elster, E. A. Do inflammatory markers portend heterotopic ossification and wound failure in combat wounds? *Clin. Orthop. Relat. Res.* **472,** 2845–54 (2014).

43. Khan, A., Morrison, A., Cheung, A., Hashem, W. & Compston, J. Osteonecrosis of the

jaw (ONJ): diagnosis and management in 2015. *Osteoporos. Int.* (2015). doi:10.1007/s00198-015-3335-3

44. Allen, M. R. & Ruggiero, S. L. A review of pharmaceutical agents and oral bone health: how osteonecrosis of the jaw has affected the field. *Int. J. Oral Maxillofac. Implants* **29,** e45-57

45. Williams, D. W. *et al.* Impaired bone resorption and woven bone formation are associated with development of osteonecrosis of the jaw-like lesions by bisphosphonate and anti-receptor activator of NF-κB ligand antibody in mice. *Am. J. Pathol.* **184,** 3084–93 (2014).

46. Saad, F. *et al.* Incidence, risk factors, and outcomes of osteonecrosis of the jaw: Integrated analysis from three blinded active-controlled phase III trials in cancer patients with bone metastases. *Ann. Oncol.* **23,** 1341–1347 (2012).

47. Drake, M. T., Clarke, B. L. & Khosla, S. Bisphosphonates: Mechanism of Action and Role in Clinical Practice. *Mayo Clin. Proc.* **83,** 1032–1045 (2008).

48. Hughes, D. E. *et al.* Bisphosphonates promote apoptosis in murine osteoclasts in vitro and in vivo. *J. Bone Miner. Res.* **10,** 1478–87 (1995).

49. Green, J. R. Zoledronic acid: pharmacologic profile of a potent bisphosphonate. *J. Organomet. Chem.* **690,** 2439–2448 (2005).

50. Miller, P. D. Denosumab: Anti-RANKL antibody. *Current Osteoporosis Reports* **7,** 18–22 (2009).

51. Rizzoli, R., Yasothan, U. & Kirkpatrick, P. Denosumab. *Nat. Rev. Drug Discov.* **9,** 591–592 (2010).

52. Katsarelis, H., Shah, N. P., Dhariwal, D. K. & Pazianas, M. Infection and medication-related osteonecrosis of the jaw. *J. Dent. Res.* **94,** 534–9 (2015).

53. Kim, K. M. *et al.* Medication Related Osteonecrosis of the Jaw: 2015 Position Statement of the Korean Society for Bone and Mineral Research and the Korean Association of Oral and Maxillofacial Surgeons. *J. Bone Metab.* **22,** 151 (2015).

54. Chan, K. L. *et al.* Effect of Lipid lowering with rosuvastatin on progression of aortic stenosis: results of the aortic stenosis progression observation: measuring effects of rosuvastatin (ASTRONOMER) trial. *Circulation* **121,** 306–14 (2010).

55. Hashem, R., Tanzer, M., Rene, N., Evans, M. & Souhami, L. Postoperative radiation therapy after hip replacement in high-risk patients for development of heterotopic bone formation. *Cancer radiothérapie J. la Société Fr. radiothérapie Oncol.* **15,** 261–4 (2011).

56. Ota, K. *et al.* Sclerostin is expressed in osteoclasts from aged mice and reduces osteoclast-mediated stimulation of mineralization. *J. Cell. Biochem.* **114,** 1901–7 (2013).

57. Garimella, R. *et al.* Expression and Synthesis of Bone Morphogenetic Proteins by Osteoclasts: A Possible Path to Anabolic Bone Remodeling. *J. Histochem. Cytochem.* **56,** 569–577 (2008).

58. Lund, S. A., Giachelli, C. M. & Scatena, M. The role of osteopontin in inflammatory processes. *Journal of Cell Communication and Signaling* **3,** 311–322 (2009).

59. Rodan, S. B. & Duong, L. T. Cathepsin K – A new molecular target for osteoporosis. *IBMS Bonekey* **5,** 16–24 (2008).

60. Hruska, K., Mathew, S., Lund, R., Fang, Y. & Sugatani, T. Cardiovascular risk factors in chronic kidney disease: does phosphate qualify? *Kidney Int.* **79,** S9–S13 (2011).

61. Chalidis, B., Stengel, D. & Giannoudis, P. V. Early excision and late excision of heterotopic ossification after traumatic brain injury are equivalent: a systematic review of the literature. *J. Neurotrauma* **24,** 1675–86 (2007).

62. Heng, C., Badner, V. M., Vakkas, T. G., Johnson, R. & Yeo, Y. Bisphosphonate-related osteonecrosis of the jaw in patients with osteoporosis. *Am. Fam. Physician* **85,** 1134–41 (2012).

63. Spencer, D. M., Wandless, T. J., Schreiber, S. L. & Crabtree, G. R. Controlling signal transduction with synthetic ligands. *Science* **262,** 1019–24 (1993).

64. Neff, T. & Blau, C. A. Pharmacologically regulated cell therapy. *Blood* **97,** 2535–40 (2001).

65. Blau, C. A., Peterson, K. R., Drachman, J. G. & Spencer, D. M. A proliferation switch for genetically modified cells. *Proc. Natl. Acad. Sci. U. S. A.* **94,** 3076–81 (1997).

66. Jin, L., Asano, H. & Blau, C. A. Stimulating cell proliferation through the pharmacologic activation of c-kit. *Blood* **91,** 890–7 (1998).

67. Jin, L. *et al.* Targeted expansion of genetically modified bone marrow cells. *Proc. Natl. Acad. Sci. U. S. A.* **95,** 8093–7 (1998).

68. Zeng, H. *et al.* Receptor specificity in the self-renewal and differentiation of primary multipotential hemopoietic cells. *Blood* **98,** 328–34 (2001).

69. Whitney, M. L., Otto, K. G., Blau, C. A., Reinecke, H. & Murry, C. E. Control of myoblast proliferation with a synthetic ligand. *J. Biol. Chem.* **276,** 41191–6 (2001).

70. Weinreich, M. A. *et al.* Growth factor receptors as regulators of hematopoiesis. *Blood* **108,** 3713–21 (2006).

71. Tey, S.-K., Dotti, G., Rooney, C. M., Heslop, H. E. & Brenner, M. K. Inducible caspase 9 suicide gene to improve the safety of allodepleted T cells after haploidentical stem cell transplantation. *Biol. Blood Marrow Transplant.* **13,** 913–24 (2007).

72. Clackson, T. *et al.* Redesigning an FKBP-ligand interface to generate chemical dimerizers

with novel specificity. *Proc. Natl. Acad. Sci. U. S. A.* **95,** 10437–42 (1998).

73. Liu, C. *et al.* Structural and functional insights of RANKL-RANK interaction and signaling. *J. Immunol.* **184,** 6910–9 (2010).

74. Iwamoto, K. *et al.* Dimer formation of receptor activator of nuclear factor kappaB induces incomplete osteoclast formation. *Biochem. Biophys. Res. Commun.* **325,** 229–34 (2004).

75. Kubota, K., Wakabayashi, K. & Matsuoka, T. Proteome analysis of secreted proteins during osteoclast differentiation using two different methods: Two-dimensional electrophoresis and isotope-coded affinity tags analysis with two-dimensional chromatography. *Proteomics* **3,** 616–626 (2003).

76. Ranganathan, K. *et al.* Heterotopic Ossification: Basic-Science Principles and Clinical Correlates. *J. Bone Joint Surg. Am.* **97,** 1101–11 (2015).

77. Matsumoto, M. E., Khan, M., Jayabalan, P., Ziebarth, J. & Munin, M. C. Heterotopic ossification in civilians with lower limb amputations. *Arch. Phys. Med. Rehabil.* **95,** 1710–3 (2014).

78. Firoozabadi, R. *et al.* Risk factors for the development of heterotopic ossification after acetabular fracture fixation. *Clin. Orthop. Relat. Res.* **472,** 3383–8 (2014).

79. Cohn, R. M., Schwarzkopf, R. & Jaffe, F. Heterotopic ossification after total hip arthroplasty. *Am. J. Orthop. (Belle Mead. NJ).* **40,** E232-5 (2011).

80. Forsberg, J. A. *et al.* Heterotopic ossification in high-energy wartime extremity injuries: prevalence and risk factors. *J. Bone Joint Surg. Am.* **91,** 1084–91 (2009).

81. Garland, D. E. Clinical observations on fractures and heterotopic ossification in the spinal cord and traumatic brain injured populations. *Clin. Orthop. Relat. Res.* 86–101 (1988).

82. Nandi, S., Maschke, S., Evans, P. J. & Lawton, J. N. The stiff elbow. *Hand (N. Y).* **4,** 368–

79 (2009).

83. Pountos, I., Georgouli, T., Calori, G. M. & Giannoudis, P. V. Do Nonsteroidal Anti-Inflammatory Drugs Affect Bone Healing? A Critical Analysis. *Sci. World J.* **2012,** 1–14 (2012).

84. Shimono, K., Uchibe, K., Kuboki, T. & Iwamoto, M. The pathophysiology of heterotopic ossification: Current treatment considerations in dentistry. *Jpn. Dent. Sci. Rev.* **50,** 1–8 (2014).

85. Mazonakis, M., Berris, T., Lyraraki, E. & Damilakis, J. Cancer risk estimates from radiation therapy for heterotopic ossification prophylaxis after total hip arthroplasty. *Med. Phys.* **40,** 101702 (2013).

86. Genêt, F. *et al.* The impact of preoperative hip heterotopic ossification extent on recurrence in patients with head and spinal cord injury: a case control study. *PLoS One* **6,** e23129 (2011).

87. Ramirez, D. M., Ramirez, M. R., Reginato, A. M. & Medici, D. Molecular and cellular mechanisms of heterotopic ossification. *Histol. Histopathol.* **29,** 1281–5 (2014).

88. Forsberg, J. A., Potter, B. K., Polfer, E. M., Safford, S. D. & Elster, E. A. Do inflammatory markers portend heterotopic ossification and wound failure in combat wounds? *Clin. Orthop. Relat. Res.* **472,** 2845–54 (2014).

89. Isaacson, B. M., Brown, A. A., Brunker, L. B., Higgins, T. F. & Bloebaum, R. D. Clarifying the structure and bone mineral content of heterotopic ossification. *J. Surg. Res.* **167,** e163-70 (2011).

90. Mishra, S., Vaughn, A. D., Devore, D. I. & Roth, C. M. Delivery of siRNA silencing Runx2 using a multifunctional polymer-lipid nanoparticle inhibits osteogenesis in a cell

culture model of heterotopic ossification. *Integr. Biol.* **4,** 1498 (2012).

91. Kikkawa, N. *et al.* Ectopic calcification is caused by elevated levels of serum inorganic phosphate in mdx mice. *Cell Struct. Funct.* **34,** 77–88 (2009).

92. Giachelli, C. M. The emerging role of phosphate in vascular calcification. *Kidney Int.* **75,** 890–897 (2009).

93. Lau, W. L., Pai, A., Moe, S. M. & Giachelli, C. M. Direct Effects of Phosphate on Vascular Cell Function. *Advances in Chronic Kidney Disease* **18,** 105–112 (2011).

94. Chavkin, N. W., Chia, J. J., Crouthamel, M. H. & Giachelli, C. M. Phosphate uptake-independent signaling functions of the type III sodium-dependent phosphate transporter, PiT-1, in vascular smooth muscle cells. *Exp. Cell Res.* **333,** 39–48 (2015).

95. Rattazzi, M. *et al.* Clones of interstitial cells from bovine aortic valve exhibit different calcifying potential when exposed to endotoxin and phosphate. *Arterioscler. Thromb. Vasc. Biol.* **28,** 2165–2172 (2008).

96. Wiester, L. M. & Giachelli, C. M. Expression and function of the integrin alpha9beta1 in bovine aortic valve interstitial cells. *J. Heart Valve Dis.* **12,** 605–616 (2003).

97. Sodek, J., Ganss, B. & McKee, M. D. Osteopontin. *Crit. Rev. Oral Biol. Med.* **11,** 279–303 (2000).

98. Rajachar, R. M., Truong, A. Q. & Giachelli, C. M. The influence of surface mineral and osteopontin on the formation and function of murine bone marrow-derived osteoclasts. *J. Mater. Sci. Mater. Med.* **19,** 3279–3285 (2008).

99. Scatena, M., Liaw, L. & Giachelli, C. M. Osteopontin: A multifunctional molecule regulating chronic inflammation and vascular disease. *Arteriosclerosis, Thrombosis, and Vascular Biology* **27,** 2302–2309 (2007).

100. Giachelli, C. M., Speer, M. Y., Li, X., Rajachar, R. M. & Yang, H. Regulation of vascular calcification: Roles of phosphate and osteopontin. *Circulation Research* **96,** 717–722 (2005).

101. Wada, T., McKee, M. D., Steitz, S. & Giachelli, C. M. Calcification of vascular smooth muscle cell cultures: inhibition by osteopontin. *Circ. Res.* **84,** 166–178 (1999).

102. Jono, S., Peinado, C. & Giachelli, C. M. Phosphorylation of osteopontin is required for inhibition of vascular smooth muscle cell calcification. *J. Biol. Chem.* **275,** 20197–20203 (2000).

103. Speer, M. Y. *et al.* Inactivation of the osteopontin gene enhances vascular calcification of matrix Gla protein-deficient mice: evidence for osteopontin as an inducible inhibitor of vascular calcification in vivo. *J. Exp. Med.* **196,** 1047–1055 (2002).

104. Li, P., Kaslan, M., Lee, S. H., Yao, J. & Gao, Z. Progress in Exosome Isolation Techniques. *Theranostics* **7,** 789–804 (2017).

105. Huynh, N. *et al.* Characterization of Regulatory Extracellular Vesicles from Osteoclasts. *J. Dent. Res.* **95,** 673–9 (2016).

106. Batrakova, E. V & Kim, M. S. Using exosomes, naturally-equipped nanocarriers, for drug delivery. *J. Control. Release* **219,** 396–405 (2015).

107. Holliday, L. S. *et al.* Exosomes: novel regulators of bone remodelling and potential therapeutic agents for orthodontics. *Orthod. Craniofac. Res.* **20 Suppl 1,** 95–99 (2017).

108. Sun, W. *et al.* Osteoclast-derived microRNA-containing exosomes selectively inhibit osteoblast activity. *Cell Discov.* **2,** 16015 (2016).

109. Li, D. *et al.* Osteoclast-derived exosomal miR-214-3p inhibits osteoblastic bone formation. *Nat. Commun.* **7,** 10872 (2016).

110. Koutsopoulos, S. D. E. The calcification of fibrin in vitro. *J. Cryst. Growth* **216,** 450–458 (2000).

111. Yokosaki, Y. *et al.* The Integrin α 9 β 1 Binds to a Novel Recognition Sequence (SVVYGLR) in the Thrombin-cleaved Amino-terminal Fragment of Osteopontin. *J. Biol. Chem.* **274,** 36328–36334 (1999).

112. Senger, D. R., Perruzzi, C. A., Papadopoulos-Sergiou, A. & Van de Water, L. Adhesive properties of osteopontin: regulation by a naturally occurring thrombin-cleavage in close proximity to the GRGDS cell-binding domain. *Mol. Biol. Cell* **5,** 565–574 (1994).

113. Giachelli, C. M., Liaw, L., Murry, C. E., Schwartz, S. M. & Almeida, M. Osteopontin expression in cardiovascular diseases. *Ann. N. Y. Acad. Sci.* **760,** 109–26 (1995).

114. Hou, P. *et al.* Matrix metalloproteinase-12 (MMP-12) in osteoclasts: new lesson on the involvement of MMPs in bone resorption. *Bone* **34,** 37–47 (2004).

115. Agnihotri, R. *et al.* Osteopontin, a novel substrate for matrix metalloproteinase-3 (stromelysin-1) and matrix metalloproteinase-7 (matrilysin). *J. Biol. Chem.* **276,** 28261–7 (2001).

116. Smith, L. L. & Giachelli, C. M. Structural requirements for alpha 9 beta 1-mediated adhesion and migration to thrombin-cleaved osteopontin. *Exp. Cell Res.* **242,** 351–60 (1998).

117. Liaw, L., Almeida, M., Hart, C. E., Schwartz, S. M. & Giachelli, C. M. Osteopontin promotes vascular cell adhesion and spreading and is chemotactic for smooth muscle cells in vitro. *Circ. Res.* **74,** 214–24 (1994).

118. Goncalves DaSilva, A., Liaw, L. & Yong, V. W. Cleavage of Osteopontin by Matrix Metalloproteinase-12 Modulates Experimental Autoimmune Encephalomyelitis Disease in

C57BL/6 Mice. *Am. J. Pathol.* **177,** 1448–1458 (2010).

119. Théry, C., Amigorena, S., Raposo, G. & Clayton, A. Isolation and Characterization of Exosomes from Cell Culture Supernatants and Biological Fluids. in *Current Protocols in Cell Biology* (John Wiley & Sons, Inc., 2006). doi:10.1002/0471143030.cb0322s30

120. Rody, W. J. *et al.* The use of cell culture platforms to identify novel markers of bone and dentin resorption. *Orthod. Craniofac. Res.* **20,** 89–94 (2017).

121. Li, X., Speer, M. Y., Yang, H., Bergen, J. & Giachelli, C. M. Vitamin D receptor activators induce an anticalcific paracrine program in macrophages: Requirement of osteopontin. *Arterioscler. Thromb. Vasc. Biol.* **30,** 321–326 (2010).

122. Brown, K. J. *et al.* Advances in the proteomic investigation of the cell secretome. *Expert Review of Proteomics* **9,** 337–345 (2012).

123. Kostenuik, P. J. *et al.* Denosumab, a fully human monoclonal antibody to RANKL, inhibits bone resorption and increases BMD in knock-in mice that express chimeric (murine/human) RANKL. *J. Bone Miner. Res.* **24,** 182–95 (2009).

124. Russell, R. G. *et al.* The pharmacology of bisphosphonates and new insights into their mechanisms of action. *J. Bone Miner. Res.* **14 Suppl 2,** 53–65 (1999).

125. Colucci, S. *et al.* Alendronate reduces adhesion of human osteoclast-like cells to bone and bone protein-coated surfaces. *Calcif. Tissue Int.* **63,** 230–5 (1998).

126. Heymann, D., Ory, B., Gouin, F., Green, J. R. & Rédini, F. Bisphosphonates: new therapeutic agents for the treatment of bone tumors. *Trends Mol. Med.* **10,** 337–343 (2004).

127. Green, J. R. & Clézardin, P. Mechanisms of Bisphosphonate Effects on Osteoclasts, Tumor Cell Growth, and Metastasis. *Am. J. Clin. Oncol.* **25,** S3–S9 (2002).

128. Viereck, V. *et al.* Bisphosphonates pamidronate and zoledronic acid stimulate osteoprotegerin production by primary human osteoblasts. *Biochem. Biophys. Res. Commun.* **291,** 680–6 (2002).

129. Pan, B. *et al.* The nitrogen-containing bisphosphonate, zoledronic acid, influences RANKL expression in human osteoblast-like cells by activating TNF-alpha converting enzyme (TACE). *J. Bone Miner. Res.* **19,** 147–54 (2004).

130. Aghaloo, T. L. *et al.* RANKL inhibitors induce osteonecrosis of the jaw in mice with periapical disease. *J. Bone Miner. Res.* **29,** 843–54 (2014).

131. Bi, Y. *et al.* Bisphosphonates Cause Osteonecrosis of the Jaw-Like Disease in Mice. *Am. J. Pathol.* **177,** 280–290 (2010).

132. Hokugo, A. *et al.* Increased prevalence of bisphosphonate-related osteonecrosis of the jaw with vitamin D deficiency in rats. *J. Bone Miner. Res.* **25,** 1337–49 (2010).

133. Kang, B. *et al.* Periapical disease and bisphosphonates induce osteonecrosis of the jaws in mice. *J. Bone Miner. Res.* **28,** 1631–40 (2013).

134. Aghaloo, T. L. *et al.* Periodontal disease and bisphosphonates induce osteonecrosis of the jaws in the rat. *J. Bone Miner. Res.* **26,** 1871–82 (2011).

135. Aguirre, J. I. *et al.* Oncologic doses of zoledronic acid induce osteonecrosis of the jaw-like lesions in rice rats (Oryzomys palustris) with periodontitis. *J. Bone Miner. Res.* **27,** 2130–43 (2012).

136. Dull, T. *et al.* A third-generation lentivirus vector with a conditional packaging system. *J. Virol.* **72,** 8463–71 (1998).

137. Tiscornia, G., Singer, O. & Verma, I. M. Production and purification of lentiviral vectors. *Nat. Protoc.* **1,** 241–5 (2006).

138. Davis, M. P., Holcroft, N. I., Wiley, E. O., Sparks, J. S. & Leo Smith, W. Species-specific bioluminescence facilitates speciation in the deep sea. *Mar. Biol.* **161,** 1139–1148 (2014).

139. Sadikot, R. T. Bioluminescence Imaging. *Proc. Am. Thorac. Soc.* **2,** 537–540 (2005).

140. Chen, Z.-Y. *et al.* New Researches and Application Progress of Commonly Used Optical Molecular Imaging Technology. *Biomed Res. Int.* **2014,** 1–22 (2014).

141. Boyce, B. F. *et al.* New roles for osteoclasts in bone. *Ann. N. Y. Acad. Sci.* **1116,** 245–54 (2007).

142. Gorski, J. P. Is all bone the same? Distinctive distributions and properties of non-collagenous matrix proteins in lamellar vs. woven bone imply the existence of different underlying osteogenic mechanisms. *Crit. Rev. Oral Biol. Med.* **9,** 201–23 (1998).

143. Berglundh, T., Abrahamsson, I., Lang, N. P. & Lindhe, J. De novo alveolar bone formation adjacent to endosseous implants. *Clin. Oral Implants Res.* **14,** 251–62 (2003).

144. Feng, X. & McDonald, J. M. Disorders of bone remodeling. *Annu. Rev. Pathol.* **6,** 121–45 (2011).

CURRICULUM VITAE

Worakanya Buranaphatthana

worakanya.b@gmail.com

A. EDUCATION

INSTITUTION AND LOCATION	DEGREE	YEAR	FIELD OF STUDY
University of Washington Seattle, WA, USA	Ph.D.	09/2012 - 12/2017	Oral Biology
Chiang Mai University Chiang Mai, Thailand	D.D.S. (First Class Honours)	06/2004 - 03/2010	Dentistry

B. POSITIONS AND HONORS

Positions and Employment

2010-Present Lecturer, Department of Oral Biology and Diagnostic Sciences**,** Faculty of Dentistry, Chiang Mai University, Thailand

2010-2012 General Dental Practitioner, Chiang Mai University Dental Hospital, Chiang Mai, Thailand

Other Experiences and Professional Memberships

2016-2017 Graduate Student Representative, Department of Oral Health Sciences, University of Washington

2010-Present Member, Dental Council of Thailand

2010-2012 Student Advisory Board, Faculty of Dentistry, Chiang Mai University, Chiang Mai, Thailand

2010-2012 Committee, Department of Oral Biology and Diagnostic Sciences**,** Faculty of Dentistry, Chiang Mai University, Thailand

Academic and Professional Honors

2016-2017 SunStar Preventive Dentistry Award, School of Dentistry, University of Washington

2014-2015 Magnuson Scholar from School of Dentistry, University of Washington

2012 Academic scholarship from Ananda-Mahidol Foundation (King's Scholarship) to pursue PhD studies at the University of Washington, Seattle, Washington

2010 National award for an outstanding dental student who graduated in 2010 from Somdetch Phra Mahitala Dhibesra Adulyadej Vikrom the Prince Father Foundation, given by Crown Princess Maha Chakri Sirindhorn

2005-2010 Outstanding Student of the Year from the Faculty of Dentistry, Chiang Mai University

2009 First place award in the 10th Student Clinician Research Program, organized by the Thai Dental Association and the Dentsply International. The award was a travel prize to attend the 151th Annual Session of the American Dental Association, held in Orlando, Florida from October 7 through October 10, 2010

2009 Ranked the first among all dental students in the class with an overall GPA 3.9

2005 A prize from Professor Dr. Tab Nilanidhi for an overall outstanding result in Dentistry among the freshmen

C. ABSTRACTS AND PRESENTATIONS

2017 **Buranaphatthana W** and Giachelli CM. Engineered Osteoclasts Prevent Cell-Mediated Calcification through Elaboration of Anticalcific Factors. Poster Presentation at the 2017 IADR/AADR/CADR General Session & Exhibition, San Francisco, California, USA from March 22-25, 2017.

2015 **Buranaphatthana W** and Giachelli CM. Engineered Osteoclasts Prevent Bovine Aortic Valve Interstitial Cell Calcification in a Contact-Independent Manner. Poster Presentation at Vascular Biology 2015, the NAVBO (North American Vascular Biology Organization) Annual Meeting, Hyannis, Massachusetts, USA from October 18-22, 2015.

2013 **Buranaphatthana W**, Rementer CW, Scatena M, Giachelli CM. Inducible control of osteoclast differentiation: an engineered cell therapy for heterotopic ossification. Poster presentation at the 2nd meeting of the International Association of Dental Research-Asia Pacific Region (IADR-APR), Plaza Athenee, Bangkok, Thailand from August 21-23, 2013.

2013 **Buranaphatthana W**, Janebodin K, Zheng Y, Ieronimakis N, Reyes M. Angiogenic capacity of pericyte-like murine dental pulp stem cells. Oral presentation at the 2013 IADR/AADR/CADR General Session & Exhibition, Seattle, Washington, USA from March 20-23, 2013.

2011 **Buranaphatthana W**, Chotjumlong P, Bolscher JGM, Nazmi K, Reutrakul V, Krisanaprakornkit S. Up-regulation of cyclooxygenase-2 and prostaglandin E_2 by human β-defensin-3 and LL-37 via distinct signaling pathways. Oral presentation at the 10th Dental Faculty Consortium of Thailand Academic Meeting and Research Presentation, Bangkok, Thailand from October 13-14, 2011.

2010 **Buranaphatthana W**, Satwini S, Maneetham S, Yana P, Mahasantipiya PM and Chompu-inwai P. Effect of human bite forces and bitten object movement on computer aided photogrammetric bite mark analysis. Poster presentation at the 151th Annual

Session of the American Dental Association, Orlando, Florida, USA from October 7-10, 2010.

2009 **Buranaphatthana W**, Satwini S, Maneetham S, Yana P, Mahasantipiya PM and Chompu-inwai P. Effect of human bite forces and bitten object movement on computer aided photogrammetric bite mark analysis. Oral presentation at the 10th Student Clinician Research Program, organized by the Thai Dental Association and the Dentsply International, Bangkok, Thailand from December 16-18, 2009.

D. PUBLICATIONS

1. Rementer CW, Wu M, **Buranaphatthana W**, Yang HL, Scatena M, Giachelli CM. An Inducible, Ligand-Independent Receptor Activator of NF-B Gene to Control Osteoclast Differentiation from Monocytic Precursors. *PLoS One*. 2013 Dec 27;8(12): e84465.
2. Janebodin K, **Buranaphatthana W**, Ieronimakis N, Hays AL, Reyes M. An *in vitro* culture system for long-term expansion of epithelial and mesenchymal salivary gland cells: role of TGF-β1 in salivary gland epithelial and mesenchymal differentiation. *Biomed Res Int*. 2013;2013:815895. Epub 2013 Jun 9.
3. Janebodin K, Zeng Y, **Buranaphatthana W**, Ieronimakis N, Reyes M. VEGFR2-dependent angiogenic capacity of pericyte-like dental pulp stem cells. *J Dent Res*. 2013 Jun;92(6):524-31. Epub 2013 Apr 22.
4. Chotjumlong P, Bolscher JG, Nazmi K, Reutrakul V, Supanchart C, **Buranaphatthana W**, Krisanaprakornkit S. Involvement of the P2X7 purinergic receptor and c-Jun N-terminal and extracellular signal-regulated kinases in cyclooxygenase-2 and prostaglandin E2 induction by LL-37. *J Innate Immun*. 2013;5(1):72-83. Epub 2012 Oct 23.